Temporal Resolution in Time Series and Probabilistic Models of Renewable Power Systems

by

Eric Hoevenaars
B.Sc., Queen's University, 2009

A Thesis Submitted in Partial Fulfillment of the
Requirements for the Degree of

MASTER OF APPLIED SCIENCE

in the Department of Mechanical Engineering

Temporal Resolution in Time Series and Probabilistic Models of Renewable Power Systems

by

Eric Hoevenaars
B.Sc., Queen's University, 2009

Supervisory Committee

Dr. Curran Crawford, Supervisor
(Department of Mechanical Engineering)

Dr. Andrew Rowe, Departmental Member
(Department of Mechanical Engineering)

Supervisory Committee

Dr. Curran Crawford, Supervisor
(Department of Mechanical Engineering)

Dr. Andrew Rowe, Departmental Member
(Department of Mechanical Engineering)

ABSTRACT

There are two main types of logistical models used for long-term performance prediction of autonomous power systems: time series and probabilistic. Time series models are more common and are more accurate for sizing storage systems because they are able to track the state of charge. However, the computational time is usually greater than for probabilistic models. It is common for time series models to perform 1-year simulations with a 1-hour time step. This is likely because of the limited availability of high resolution data and the increase in computation time with a shorter time step. Computation time is particularly important because these types of models are often used for component size optimization which requires many model runs.

This thesis includes a sensitivity analysis examining the effect of the time step on these simulations. The results show that it can be significant, though it depends on the system configuration and site characteristics. Two probabilistic models are developed to estimate the temporal resolution error of a 1-hour simulation: a time series/probabilistic model and a fully probabilistic model. To demonstrate the application of and evaluate the performance of these models, two case studies are analyzed. One is for a typical residential system and one is for a system designed to provide on-site power at an aquaculture site. The results show that the time series/probabilistic model would be a useful tool if accurate distributions of the sub-hour data can be determined. Additionally, the method of cumulant arithmetic is demonstrated to be a useful technique for incorporating multiple non-Gaussian random variables into a probabilistic model, a feature other models such as Hybrid2 currently do not have.

The results from the fully probabilistic model showed that some form of autocorrelation is required to account for seasonal and diurnal trends.

Contents

Supervisory Committee **ii**

Abstract **iii**

Table of Contents **v**

List of Tables **viii**

List of Figures **ix**

Nomenclature **xi**

Acknowledgements **xiv**

1 Introduction **1**

1.1 Model Types 2

1.1.1 Time Series Models 3

1.1.2 Probabilistic Models 4

1.1.3 Review of Literature on Temporal Resolution 5

1.2 Objectives and Key Contributions 5

1.3 Thesis Structure 8

2 Time Series Simulation / Optimization **9**

2.1 Theoretical Basis 10

2.2 Component Models 12

2.2.1 Wind Turbine Model 12

2.2.2 Solar Photovoltaic Model 16

2.2.3 Battery Bank Model 18

2.2.4 Diesel Genset Model 20

2.2.5 Controller Model 21

2.3 Economics Model 21
2.4 Optimization 22

3 Time Step Sensitivity Analysis **24**
3.1 Purpose 25
3.2 Analysis Method 26
3.2.1 Wind Power Analysis 26
3.2.2 Solar Power Analysis 28
3.2.3 Battery Bank Analysis 28
3.2.4 Diesel Genset Analysis 29
3.2.5 Complete System 29
3.3 Problem Set-Up and Parameters 31
3.3.1 Wind Data and Parameters 31
3.3.2 Solar Data and Parameters 32
3.3.3 Battery Bank Parameters 33
3.3.4 Diesel Genset Parameters 33
3.3.5 Component Costs and Economic Parameters 34
3.4 Sensitivity Results 34
3.4.1 Wind Power Sensitivity 35
3.4.2 Battery Bank Sensitivity 36
3.4.3 Diesel Genset Sensitivity 37
3.4.4 Optimization Sensitivity 38
3.4.5 Conclusions and Recommendations 45

4 Time Step Selection Using Probabilistic Models **47**
4.1 Theoretical Basis and Review 47
4.2 Fundamental Equations 49
4.3 Representing Probability Density Functions 50
4.3.1 Wind Power Probability 50
4.3.2 Solar Power Probability 51
4.3.3 Load Power Probability 52
4.4 Calculating Moments and Cumulants from Data 54
4.5 Sum of Independent Random Variables 55
4.5.1 Convolution 55
4.5.2 Method of Cumulants 56

4.6 Reconstructing Probability Density Functions . . . 56
4.6.1 Gram-Charlier Expansion . . . 57
4.6.2 Maximum Entropy . . . 58
4.7 Two-Event Approximation . . . 59
4.7.1 Random Walk . . . 60
4.8 Final Models . . . 62
4.8.1 Time Series/Probabilistic Model . . . 62
4.8.2 Probabilistic Model . . . 66

5 Case Studies **69**
5.1 Model Overview . . . 70
5.2 Off-Grid Residential Power System . . . 71
5.2.1 Battery Backup . . . 71
5.2.2 Diesel Backup . . . 75
5.3 Integrated Multi-Trophic Aquaculture Site . . . 77
5.3.1 Project Background . . . 77
5.3.2 Results . . . 81
5.4 Summary of Findings . . . 83

6 Conclusions **85**
6.1 Future Work . . . 87

Bibliography **89**

Appendix A Photovoltaic Model Calculations **97**
A.1 Tilted Surface Model . . . 97
A.2 Cell Temperature Calculation . . . 100

Appendix B Net Present Cost Calculation **102**

Appendix C Wind Speed Data Synthesis **104**

Appendix D Case Study Results Tables **106**
D.1 Battery Backup . . . 106
D.2 Diesel Backup . . . 108

List of Tables

3.1 Wind turbine parameters 32
3.2 PV parameters 33
3.3 Battery parameters 33
3.4 Diesel genset parameters 34
3.5 Assumed component costs 34
3.6 Total wind kinetic energy over 6-hour simulation 35
3.7 Total turbine energy output over 6-hour simulation 35
3.8 Battery simulation results (continuous charge; 1 kW average charge) 36
3.9 Battery simulation results (combined charge/discharge) 36
3.10 Diesel fuel consumed over 6-hour simulation 37
3.11 System optimization results 39
3.12 Results from 1 month simulation (3 wind turbines, 120 batteries) . . 42
3.13 Results from 1-month simulation (2 wind turbines, 13 kW generator) 43
3.14 Results from 1-month simulation (30 PV modules, 2 wind turbines, 13 kW generator) 43
3.15 Percentage of load met by genset 44

5.1 Battery capacity error (kWh), $E_{b,1\text{hr}} - E_{b,10\text{min}}$ 73
5.2 Fuel consumption error (kL), $V_{f,1\text{hr}} - V_{f,10\text{min}}$ 75
5.3 Battery capacity error relative to 1h optimal configuration 82
5.4 Optimal configuration with different time steps 82

D.1 Battery capacity error (kWh), $E_{b,1\text{hr}} - E_{b,1\text{min}}$ 106
D.2 Battery capacity error (kWh), $E_{b,1\text{hr}} - E_{b,10\text{sec}}$ 107
D.3 Battery capacity error (kWh), $E_{b,1\text{hr}} - E_{b,1\text{sec}}$ 107
D.4 Fuel consumption error (kL), $V_{f,1\text{hr}} - V_{f,1\text{min}}$ 108
D.5 Fuel consumption error (kL), $V_{f,1\text{hr}} - V_{f,10\text{sec}}$ 108
D.6 Fuel consumption error (kL), $V_{f,1\text{hr}} - V_{f,1\text{sec}}$ 108

List of Figures

2.1 System schematic 9
2.2 Fundamental algorithm for the time series method 11
2.3 Wind sub-model 12
2.4 Overview of proportional feedback controller 13
2.5 Pre-controller block diagram 13
2.6 Controller block diagram 14
2.7 Controller blending function 14
2.8 C_p-controller block diagram 15
2.9 Plant block diagram 16
2.10 Solar sub-model 16
2.11 Battery sub-model 18
2.12 Kinetic battery model 19
2.13 Generator sub-model 20
2.14 Controller sub-model 21
2.15 Economics sub-model 21

3.1 Twenty minute sample of synthetic wind speed data 27
3.2 Sample of synthetic load data (March 8) 30
3.3 C_p-λ curve 32
3.4 Genset load and actual power output for part of simulation 38
3.5 Battery SOC on Day 18 (105 PV modules, 80 batteries) 40
3.6 Battery SOC on Days 19-23 (3 wind turbines, 120 batteries) 41
3.7 Battery SOC on Days 18-23 (2 wind turbines, 152 batteries) 41

4.1 Distribution of 1min wind speed data with an hourly mean of 9 m/s 50
4.2 One-minute clearness index histograms (bin width = 0.01) 52
4.3 Standard deviation of one-minute loads given hourly mean 53
4.4 Two-event approximation of the battery power distribution 59
4.5 Fundamental algorithm for time series/probabilistic model 63

4.6 Definition of ψ for determining generator capacity 64
4.7 Determining battery capacity for time series/probabilistic simulation 66
4.8 Fundamental algorithm for probabilistic model 67

5.1 Required battery capacity for a 1h time series simulation 72
5.2 Battery capacity error in time series simulation, $E_{b,1\text{hr}} - E_{b,10\text{min}}$ . . 72
5.3 Annual fuel consumption for a 1h time series simulation 75
5.4 Location of Kyuquot SEAFoods Ltd. 78
5.5 Half-hour sample from load profile 79

Nomenclature

Latin Symbols

A	rotor area
C_p	power coefficient
$C_{p,max}$	maximum power coefficient
c	kinetic battery model Q_1 tank width
F_0	fuel curve intercept
F_1	fuel curve slope
f	frequency
f_{PV}	PV derating factor
G_T	incident solar radiation
$G_{T,STC}$	incident solar radiation at STC
I	rotor inertia
I_{max}	battery maximum charging current
K	proportional gain constant
k	kinetic battery model conductance
n	non-dimensional frequency
P_b	battery charging/discharging power
$P_{c,max}$	battery maximum charging power
P_d	diesel power output
$P_{d,max}$	battery maximum discharging power
$P_{d,r}$	diesel genset rated power
P_l	load
P_n	net power
P_r	renewable power
P_s	solar power
$P_{s,r}$	PV rated power
P_w	wind power
$P_{w,r}$	wind rated power
p^+	positive net load probability
p_{run}	genset forced run probability
Q	kinetic battery model total energy
Q_1	kinetic battery model available energy

Q_2	kinetic battery model bound energy
Q_{max}	kinetic battery model maximum capacity
R	rotor radius
S_u	autospectral density
T_c	cell temperature
$T_{c,NOCT}$	nominal operating cell temperature
$T_{c,STC}$	cell temperature at STC
T_{min}	genset minimum run time
U	mean wind speed
u_*	friction velocity
$u(t)$	wind speed at time, t
V_f	volume of fuel consumption
Z	time zone
z_0	surface roughness height
z_R	rotor height

Greek Symbols

α_P	temperature coefficient of power
β	PV slope
γ	PV azimuth angle
η_c	charging efficiency
η_d	discharging efficiency
η_{gen}	turbine generator efficiency
η_{inv}	inverter efficiency
η_{PV}	cell efficiency at STC
λ	tip speed ratio
λ_d	tip speed ratio demand
ρ_a	air density
ρ_g	ground reflectance / albedo
τ_{aero}	aerodynamic torque
τ_{gen}	turbine generator torque
$\tau_{gen,err}$	turbine generator torque error
$\tau_{gen,lim}$	turbine generator torque limit
$\tau_{gen,r}$	turbine generator torque at rated wind speed

ω	rotational speed
$\dot{\omega}$	rotational acceleration
ω_d	rotational speed demand
ω_{err}	rotational speed error
ω_{lim}	rotational speed limit
ω_r	rotational speed at rated wind speed

Abbreviations

ACS	annualized cost of system
CDF	cumulative distribution function
COE	cost of energy
EENS	expected energy not served
FTS	full time series model
GHG	greenhouse gas
HDKR	Hay-Davies-Klucher-Reindl
HOMER	Hybrid Optimization Model for Electric Renewables
IEC	International Electrotechnical Commission
IMTA	integrated multi-trophic aquaculture
KiBaM	kinetic battery model
LOLP	loss of load probability
LPSP	loss of power supply probability
MPPT	maximum power point tracker
NOCT	nominal operating cell temperature
NPC	net present cost
NREL	National Renewable Energy Laboratory
PDF	probability density function
PGC	probabilistic model using Gram-Charlier expansion
PME	probabilistic model using maximum entropy method
PV	photovoltaic
SOC	state-of-charge
SRRL	Solar Radiation Research Laboratory
STC	standard test conditions
STS	simplified time series model
TMY	typical meteorological year
TSP	time series/probabilistic model

ACKNOWLEDGEMENTS

There are many people that have provided me with invaluable guidance, information, excitement, and love throughout the completion of this thesis.

I would foremost like to thank my supervisor, Dr. Curran Crawford. His respect for and dedication to all of his students is incredible and kept us motivated to deliver the best work we can. He provided encouragement and patience during the uncertain times and knowledge throughout.

Next I want to thank my family. The Skype calls from my parents made me happy and kept me strong. And if I'm going to make this sentimental then I should note that they have always been my greatest inspiration. It truly would have been a struggle without their support. The inspiration thing goes for my brothers too.

I would also like to thank Dr. Stephen Cross. He provided me with very interesting insight into the world of sustainable aquaculture and the opportunity to gain experience with power system design and data acquisition.

To all the office mates who kept me entertained; to the Chillies for bringing me to all the great Victoria restaurants; to the SSDLers for the interesting discussions; to my friends for the love; and to my roommates for not questioning me if I was working late or needed rest: you are the best.

I would finally like to thank the Canadian Integrated Multi-Trophic Aquaculture Network (CIMTAN) and the University of Victoria for providing funding throughout the studies.

"Thinking like ethical people, dressing like ethical people, decorating our homes like ethical people makes not a damn of difference unless we also behave like ethical people."

– George Monbiot

Heat: How to Stop the Planet From Burning

Chapter 1

Introduction

Ever since Samuel Insull began preaching the "gospel of consumption" as CEO of Commonwealth Edison [1], electricity has provided luxuries unheard of in previous generations. But while the electrical grid has continued to expand and electrify more communities ever since, there will always be locations where grid connection is infeasible. These include developing countries and remote locations such as cottages and research laboratories. Typically, diesel fuel is the common energy source as diesel generators have low capital costs and are dispatchable.

However, a diesel generator is not the ideal power source either. Generators are less efficient when partially loaded. Partial loading and multiple start/stop cycles increase wear as well. They are therefore not optimal for supplying unsteady, intermittent loads. These factors, combined with the environmental impact of diesel fuel combustion, mean that renewables-based power systems can often provide an opportunity for cleaner energy at lower cost.

Similarly, green energy incentives such as feed-in tariffs, carbon taxes, and cap-and-trade programs have changed the economics of grid-connected power systems as well. Under some programs, renewables can provide significant return on investment with a payback period under 10 years [2].

Whether grid-connected or stand-alone, proper sizing of the components in a power system is essential in order to ensure reliability and cost-effectiveness. This is made difficult by the variability imposed on the system by unsteady loads, intermittent power sources, and fluctuating storage levels. Simulation is an important design tool and many models (logistical and dynamic) have been developed to aide the system designer.

Logistical models provide long-term performance predictions, economic analyses,

and are useful for component sizing. Dynamic models are primarily for component design and analyses of system stability. They require dynamic mechanical and electrical models of the system components. While dynamic models clearly require fine temporal resolution, logistical models typically ignore the dynamic system behaviour as it is assumed to be unrelated to the long-term performance.

The focus of this thesis is on logistical models developed for component size optimization. The purpose is to identify the effect of temporal resolution on these models. Refer to Section 5.3 for a case study at an integrated multi-trophic aquaculture network that was the original motivation. It is common to model system behaviour with a 1-hour time step and the assumption of quasi-steady-state operation. This thesis challenges this assumption by proposing several questions, such as:

- Is a 1-hour time step precise enough to accurately compute long-term system performance?
- Are wind turbulence and turbine dynamics significant factors not accounted for in these models?
- Is it important to resolve the temporal matching between generated power and the load demand within the hour?
- Are these effects different depending on the source of backup power or the system's location?
- Can the effect of temporal resolution on a particular system be determined from less computationally demanding probabilistic models?

1.1 Model Types

In general, there are two main methods used in logistical models: time series and probabilistic. The time series method is far more common in literature, though the probabilistic method has recently become more popular. The overview of the two methods is given here while more in-depth descriptions are provided in Chapters 2 and 4.

1.1.1 Time Series Models

The time series method assumes quasi-steady-state operation of the power system. A time step is defined and the load and renewable power are assumed to be constant within each step. An energy balance ensures that the total energy produced is equal to the total energy consumed. This type of model requires long-term input data sets for wind speed, solar insolation, and load, with a sample period equal to the time step.

Likely the most widely used time series model for simulating and optimizing renewable power systems is HOMER, developed by the National Renewable Energy Laboratory (NREL) and distributed by HOMER Energy [3, 4]. Many studies have used this tool to examine the feasibility of renewables in locations all around the globe [5–12]. HOMER's optimization procedure uses a full-factorial method that iterates through all possible configurations from the list of "sizes to consider". Many types of energy systems can be modelled with a time series method, such as the coupled wind farm and pumped storage facility analyzed by Wild [13], the solar/tidal/wind system by Niet [14], or the solar/hydro/biogas/biomass/diesel configuration by Gupta *et al.* [15].

This method has many advantages. For one, seasonal and diurnal variations are both accounted for in the input data sets. Also, since the simulation runs chronologically over the year, it can easily track the state-of-charge (SOC) of the storage system. This second feature is very useful for sizing the storage system. Finally, the method is simple and intuitive since it mimicks the actual real-life operation in the time domain.

The fundamental assumption of the time series (quasi-steady-state) method is that the power output from all power sources and the demand from the load can be assumed to be constant within each time step. In reality, the power production and demand are dynamic and continuously changing. Theoretically, the time step could be reduced until the steady-state assumption becomes valid. However, a shorter time step can make the approach infeasible. Obtaining the high frequency data sets required for the simulation can be very difficult. Also, the computational time required to run a full year simulation with fine temporal resolution can restrict the ability to test a large number of configurations for component size optimization.

1.1.2 Probabilistic Models

The pure probabilistic method uses statistical techniques to estimate the probability that the system will be in any particular state. Based on these probabilities, the storage system can be sized to ensure reliability constraints are met. Typically, this method will model wind and load as a stationary processes, thus the mean and standard deviations of wind speed, solar radiation, and power demand are held constant seasonally and diurnally.

The main advantage of the probabilistic method is that it is generally far less computationally demanding. Another advantage is that it does not require short-term wind speed data. Probability density functions (PDF) are used to describe the monthly, seasonal, or even annual distributions of wind speed, solar radiation, and power demand. Though full data sets are not required for probabilistic models, they are often useful for providing more information of the underlying distributions. For instance, the model developed by Barton and Infield [16] and applied by Gassner [17] derives wind speed PDFs by applying filter functions to the frequency spectra of real data. The distribution of wind speeds is assumed to be Weibull over the long-term and Gaussian within each "storage period". Similarly, in Tina *et al.* [18] the distribution shapes are assumed but the parameters are estimated based on real data.

The underlying assumption of stationarity means that synoptic and diurnal variations cannot be considered. Additionally, since the wind and load are modelled as stochastic processes, the order of events is ignored and therefore the SOC of the storage system cannot be tracked. These are the main disadvantages relative to the time series method.

The Hybrid2 model [19] attempts to combine the benefits of the two methods in an approach called the time series/probabilistic method. It uses a technique similar to the time series method in that resource and load data with a sample period of one hour or ten minutes are used to account for the seasonal and diurnal variations. Within each time step, statistical techniques are used to deal with shorter term fluctuations. It can therefore provide higher accuracy without requiring very high resolution data. However, it is more computationally demanding for a given time step choice than the other two methods and therefore has no built-in optimization functionality. Also, the probabilistic part of the method has limitations; for example, wind speed and load distributions must be Gaussian and distributions of solar radiation are not permitted.

1.1.3 Review of Literature on Temporal Resolution

The notion that a model can require finer temporal resolution than 1-hour averages appears to be becoming more widely recognized. In 2007, HOMER added the capability to simulate a system with a time step down to one minute (though it appears there were some bugs along the way since since this capability was later "fixed" in 2010). Despite this, the literature associated with the issue of temporal resolution impacts on energy system sizing is fairly limited.

Notton *et al.* [20] examined the influence of the simulation time step for sizing autonomous photovoltaic (PV) systems. It was found that the use of daily data resulted in significant undersizing but there was a good agreement between the minute and hourly results. When interpreting these results, however, it is important to note that the load profiles that were used varied throughout the day but never within the hour. Incidentally, the daily time step was the only case that was not able to resolve the variability of the load. This likely explains why the minute and hourly results were similar but the daily results tended to undersize the system.

Ambrosone *et al.* [21] compared the fraction of the load covered by a PV-battery system using hourly and daily time steps, referred to as "power analysis" and "energy analysis" respectively. It was found that the size of the battery bank had a greater effect on the agreement between the two methods than the size of the PV array. In particular, there was good agreement for systems with at least two days of storage.

Hawkes and Leach [22] examined the influence of temporal precision in optimizing a micro-combined heat and power system. Five-minute load data was used and results were compared using time steps ranging from one hour to five minutes. In the design optimization (to determine component sizes), the lifetime cost using 5-minute data was 11-16% higher and the optimal generator size was 35-74% lower than when using hourly data. In the dispatch optimization (to determine the optimal dispatch strategy), the life cycle cost using 5-minute data was 3-8% higher and the on-site electricity generation was 60-68% less than when using hourly data.

1.2 Objectives and Key Contributions

One justification of the time series method, despite the increase in computational time, is its ability to chronologically track the state-of-charge of the storage system. This functionality makes the process of sizing a storage system much easier by simply

ensuring that the SOC never drops below a minimum value. Sizing storage systems using the probabilistic method often requires an assumption of some relationship between the standard deviation of the net power in/out of the batteries and the storage size. However, this relationship is not trivial to determine and even depends on the system configuration and component sizes [17]. Since storage systems generally account for a significant portion of the total system cost, this advantage for the time series method is significant.

The large majority of component sizing studies use the time series method and simulate one year of operation with a 1-hour time step. The default step size in HOMER is one hour and many other models in the literature use the same [23–27]. Some authors have mentioned the significance of the time step in time series simulations [19, 28]. However, this author is not aware of any study that has analyzed the impact of temporal resolution on power system simulations with different component configurations (a review of the limited literature available on the subject was provided in the previous section). Therefore, the first objective of this thesis was to perform a sensitivity analysis on the level of temporal resolution in time domain simulations. This study examined the sensitivity on individual components and on the complete system optimization.

One method to resolve the temporal resolution issue in a component sizing study is to first run an optimization using time series simulations with coarse resolution (i.e. a 1-hour time step) and follow this up with a single simulation of the optimal system in a probabilistic framework such as Hybrid2 to account for the high-frequency fluctuations. If the results for the total system cost and reliability are similar, then the temporal resolution used in the time series simulation can be assumed to be sufficient. However, the time step sensitivity could potentially change depending on the configuration and size of the components. To be sure that the time step was valid for the entire range of possible configurations, the Hybrid2 simulation would need to be run for multiple configurations, defeating the purpose of the original time series optimization. Additionally, in Hybrid2 the load can only be assumed to have a Gaussian distribution. If this is not accurately representative of the actual distribution, then it cannot be accurately modelled in Hybrid2. Another problem with this technique is, if the results do not agree, it can be difficult to determine where the error(s) occurred. It could be that the component models had different levels of complexity or it could be that the high frequency fluctuations of one or more components were indeed significant.

Because of these implications, the second objective of this thesis was to develop a new method that successfully uses a probabilistic method to determine the temporal resolution required prior to an optimization procedure run using time series simulations. The intent was not to produce a probabilistic model used to perform the component size optimization because of the drawbacks of probabilistic models described previously (namely the inability to track SOC or account for seasonal and diurnal trends).

The original motivation for this work was from a study attempting to optimize the component sizes for a power system at an aquaculture site on Vancouver Island, British Columbia. The load to be met was very unsteady on short time scales and it was therefore found that a simulation using hourly averages would greatly misrepresent the actual system operation. Therefore, the third objective of this thesis was to use this site as a case study by implementing the probabilistic method developed in this thesis to determine the temporal resolution required for the time series simulation and optimization. Prior to this case study, the effectiveness of the probabilistic models was investigated with a case study of the same system used in the initial time step sensitivity analysis.

In summary, the contributions of this thesis can be divided into four main points:

1. Develop detailed component models including a dynamic wind turbine controller (Chapter 2). Direct comparisons are made to the models of both HOMER and Hybrid2 and key differences are highlighted.

2. Complete a sensitivity analysis of the time step in time series simulations and optimizations (Chapter 3). This includes sensitivity analyses of the individual component performances as well as the component size optimization for a residential power system.

3. Develop a probabilistic model to determine the temporal resolution required prior to a time series simulation (Chapter 4). Two models are developed using a time series/probabilistic method and a fully probabilistic method. By comparing the results from these models with each other and the time series model, the important differences between the time series method and the probabilistic method are identified.

4. Compare the output from the probabilistic models with the output from the time series model for the residential system from the sensitivity analysis. Apply

the models to a case study at the aquaculture site (Chapter 5). The final proposed system design is provided here as well.

1.3 Thesis Structure

The remainder of the thesis is organized as follows:

Chapter 2 details the time series model developed for this work. This includes the component sub-models, the economics model, and the optimization procedure.

Chapter 3 describes the methodology and results from the sensitivity analysis. This work was published in *Renewable Energy* with the title "Implications of temporal resolution for modeling renewables-based power systems" [29].

Chapter 4 provides details of the probabilistic models developed for this work. This includes the statistical methods used in both the time series/probabilistic model and the fully probabilistic model.

Chapter 5 gives the results from two case studies. The first is for the same system as in the sensitivity analysis in order to compare the results from the probabilistic and time series models. The second is for the IMTA aquaculture site that was the initial inspiration for this work. Preliminary findings for the second case study were presented at the *CSME Forum 2010* with the title "Renewable energy feasibility and optimization at an aquaculture site" [30].

Chapter 6 concludes the thesis and provides recommendations for future work.

Chapter 2

Time Series Simulation / Optimization

To complete the objectives of this thesis, a time series model was developed in Matlab using the quasi-steady-state assumption to model the electrical flow of power in the system and optimize the sizes of the system components. A new model was necessary to allow the full capability to add and edit components to the model. In particular, because the aim was to examine time steps down to one second, a dynamic wind turbine model was required.

The two-bus electrical system configuration is shown in Figure 2.1. Renewable power sources include wind turbines and PV modules, both of which are assumed to produce DC power. Batteries and AC diesel generators can be included for storage and backup power to meet an AC load. The model could easily be modified to include a DC load (and the appropriate AC-DC rectifier) if necessary. Though a grid model was developed and can be included as part of the overall system model, it was ignored in this thesis which deals with only stand-alone systems.

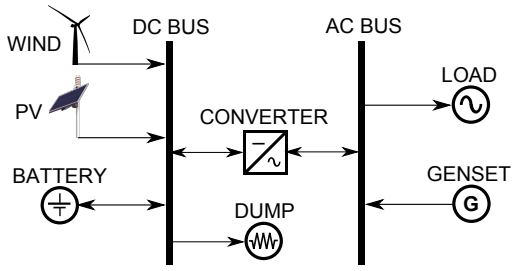

Figure 2.1: System schematic

This chapter will provide a more detailed explanation of the underlying equations in the time series method as well as a description of the optimization method and component sub-models used in this thesis. Most time series models in the literature use the same basic framework for the simulations. The differences lie in the optimization method, objective function, types of components included in the system, and the component models themselves. Therefore, the review of the literature on the subject will be distributed throughout this chapter in the relevant sections below.

2.1 Theoretical Basis

The time series method requires data sets for the load and renewable resources over the entire length of the simulation period with a sample period equal to the time step. In each time interval, t, the component sub-models calculate the average wind and solar power production. The sum of the two is then the average total renewable power, P_r, over the time step:

$$P_r(t) = P_w(t) + P_s(t) \tag{2.1}$$

where P_w and P_s are the average wind and solar power over the time step, respectively. The renewable power production is treated as a "negative load", resulting in the net power, P_n:

$$P_n(t) = P_r(t) - P_l(t) \tag{2.2}$$

where P_l is the average load over the time step. If positive, this net power represents the average power that can be used to charge the batteries or must be sent to the dump load. If negative, it represents the average power that must be met by the backup power sources. The control strategy of the system controller determines how the backup sources are dispatched. The generator model calculates the fuel consumption based on the average power output of the genset. Finally, the total system cost is calculated based on the fuel consumption, component costs, and economic paramaters.

The fundamental algorithm is shown in Figure 2.2. This figure represents the case where wind and solar are the renewable sources. If other renewables such as run-of-river hydro are included, the basic structure remains the same. The generator here is assumed to run on diesel, though it could easily be modelled with any other type of fuel, including biodiesel. Finally, in this model, the final output is the net

present cost (NPC). Often, a system reliability metric is also output which is later used as a constraint to the optimization. Examples of such metrics are described in the next section. The resource data is generally obtained from meteorological data or synthetically derived.

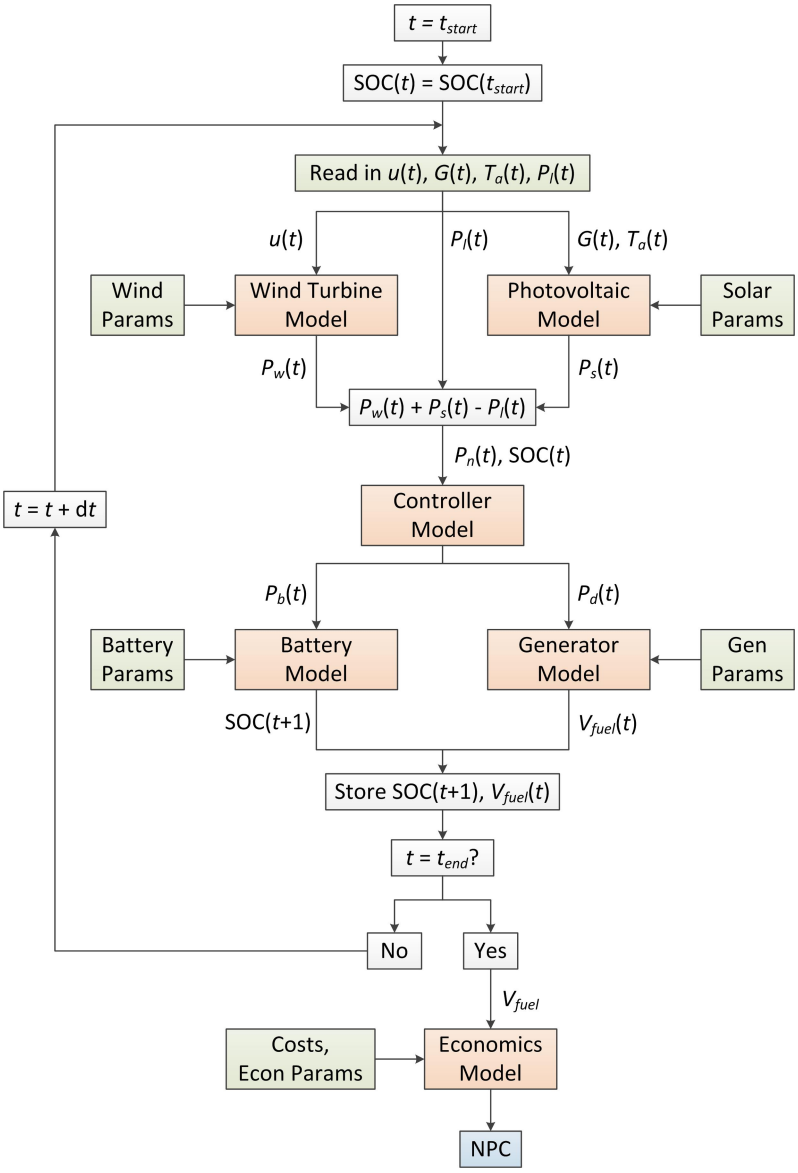

Figure 2.2: Fundamental algorithm for the time series method

2.2 Component Models

The algorithms of the component sub-models in Figure 2.2 are detailed in this section along with a brief review of the models used by other authors.

2.2.1 Wind Turbine Model

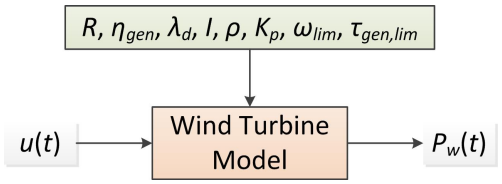

Figure 2.3: Wind sub-model

The simplest method for moelling a wind turbine is to assume a constant power coefficient [24, 31], thus reducing the model down to a single equation relating wind power to wind speed:

$$P_w(t) = \frac{1}{2}\rho_a A C_p u(t)^3 \eta_{gen} \tag{2.3}$$

where ρ_a is the air density, A is the rotor area, C_p is the power coefficient, $u(t)$ is the wind speed at time t, and η_{gen} is the generator efficiency. Mechanical efficiency is usually described by a turbine's C_p-λ curve where λ is the tip speed ratio. Simple wind turbine models assume a constant C_p value equal to the maximum of this curve. However, this is an ideal model that is not generally accurate. It also assumes that the power output will continue to rise with wind speed. In reality, a turbine's output is limited to its rated power by stall or pitch control.

Instead, the output power of the wind turbine is often interpolated from the turbine's power curve. This curve can be obtained directly from a turbine manufacturer's technical specifications [4, 25, 32, 33]. Alternatively, the curve can be scaled to reflect a "generic" turbine [27] or its shape can be represented by a polynomial [23, 34–36].

As specified by the International Electrotechnical Commission (IEC) standard [37], these curves are typically based on 10-minute averages and are therefore not applicable for high frequency wind data. Since an objective of this thesis was to perform a sensitivity analysis on the time step down to one second, the turbine's inertia had to be accounted for in the model.

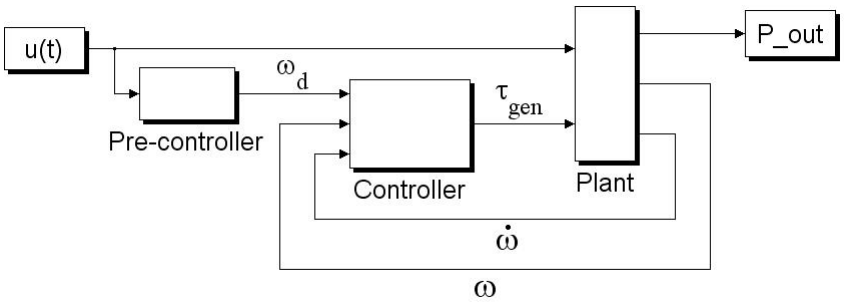

Figure 2.4: Overview of proportional feedback controller

A dynamic model was created in Simulink with variable speed C_p and stall control. The purpose was not to design an optimal controller but only to ensure that the turbine power output in the simulation was realistic in accounting for the response time of the turbine. The design is divided into the pre-controller, controller, and plant as shown in Figure 2.4. The digitilization of a feedback controller can lead to instabilities in the model [38]. To prevent these instabilities, the dynamics are solved using a variable time step. This time step is given an upper limit of one second but no lower limit.

A constant tip speed ratio demand, λ_d, is defined as the point at which the turbine has its highest mechanical efficiency, corresponding to $C_{p,max}$. It is noted that while this maximizes aerodynamic efficiency, it does not necessarily optimize electrical power generation since the generator efficiency varies with rotational speed. However, a constant generator efficiency is assumed in this thesis. The pre-controller shown in Figure 2.5 calculates the rotational speed demand and applies a rotational speed limit, ω_{lim}:

$$\omega_d = \begin{cases} \lambda_d u(t)/R & : u(t) < \omega_{lim} R/\lambda_d \\ \omega_{lim} & : u(t) \geq \omega_{lim} R/\lambda_d \end{cases} \tag{2.4}$$

It should be noted that real controllers do not have knowledge of the instantaneous wind speed and therefore this model assumes an ideal controller. This was suitable for this study since it was not the design of the controller that was of concern.

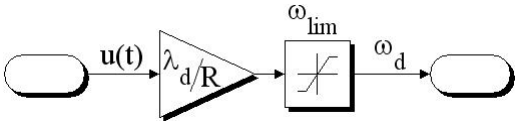

Figure 2.5: Pre-controller block diagram

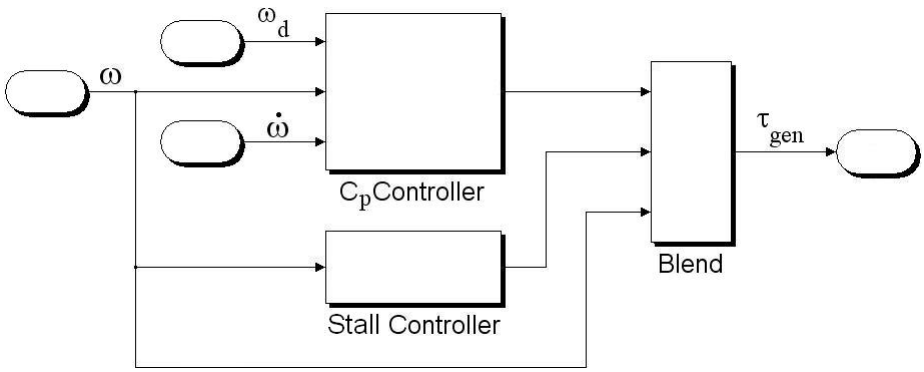

Figure 2.6: Controller block diagram

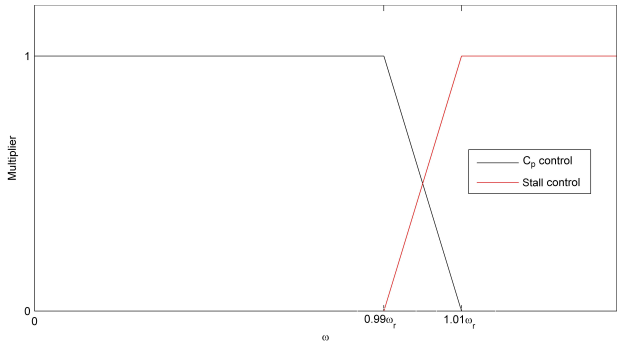

Figure 2.7: Controller blending function

In this model, a variable-speed turbine is operated with two types of control: C_p-control when the rotational speed is below the rated speed and stall control when it is above the rated speed. To prevent instabilities at near rated wind speeds, the outputs from both controllers are blended. Figure 2.6 shows the overall controller block diagram and Figure 2.7 describes the blending function. The blend occurs for wind speeds between 99% and 101% of the rated wind speed, ω_r.

The C_p controller uses generator torque control to command the generator torque demand in order to keep the tip speed ratio close to λ_d which increases C_p. This is based on the controller from McIntosh [38]. Figure 2.8 shows the block diagram. Rotor dynamics are modelled by the relationship:

$$\tau_{aero} + \tau_{gen} = \dot{\omega} I \tag{2.5}$$

where τ_{aero} is the aerodynamic torque, τ_{gen} is the generator (control) torque, $\dot{\omega}$ is the rotor acceleration, and I is the rotor inertia. The direction of the generator torque

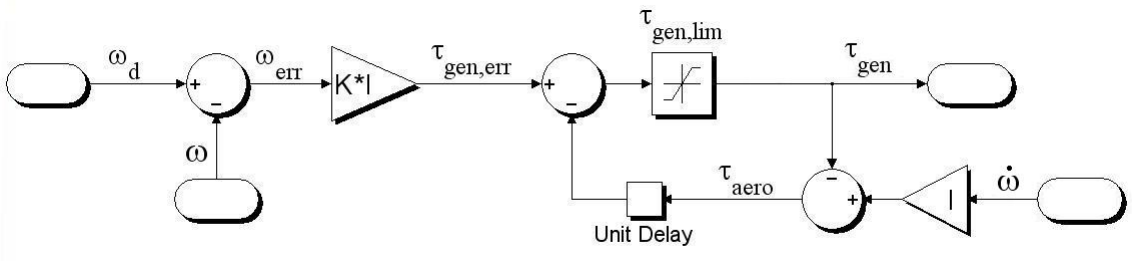

Figure 2.8: C_p-controller block diagram

is opposite to the aerodynamic torque and is always negative. The C_p-controller calculates the generator torque adjustment required ($\tau_{gen,err}$) from the rotational speed error (ω_{err}) and the proportional gain constant (K). The aerodynamic torque is estimated from Equation 2.5 by rearranging for τ_{aero}. The controller then adjusts the generator torque to ($-\tau_{aero} + \tau_{gen,err}$) and limits this to the generator torque limit, $\tau_{gen,lim}$.

The variable-speed stall controller is included to prevent overspeed and reduce damage and wear during periods of high wind speeds. The turbine is prevented from following the C_p-λ curve and instead is forced to operate at a lower tip speed ratio and C_p. The generator torque limit is removed and an applied generator torque causes the rotor speed to decrease while keeping the power output constant. The generator responds to the torque command almost instantaneously [39]. In the model, the torque is calculated by:

$$\tau_{gen} = \frac{\omega_r \tau_{gen,r}}{\omega} \tag{2.6}$$

where ω_r and $\tau_{gen,r}$ are the rotational speed and generator torque at rated wind speed.

The turbine dynamics are calculated in the Plant subsystem, as shown in Figure 2.9. The actual aerodynamic torque is calculated using the C_p value (interpolated from an assumed C_p-λ curve at the current rotor speed) and the instantaneous wind speed. Assuming a C_p curve, which represents steady-state operation, is an approximation in a dynamic model. McIntosh [38] showed that for smaller rotors ($R < 3$ m), the quasi-steady model with an assumed C_p curve has a similar accuracy in predicting a rotor's integral unsteady energy performance as a more complex unsteady gust model. Therefore, unsteady aerodynamics are ignored in the model developed here. The aerodynamic torque is then added to the generator torque demanded from the controller to determine the total torque on the drive shaft. Rotor acceleration is

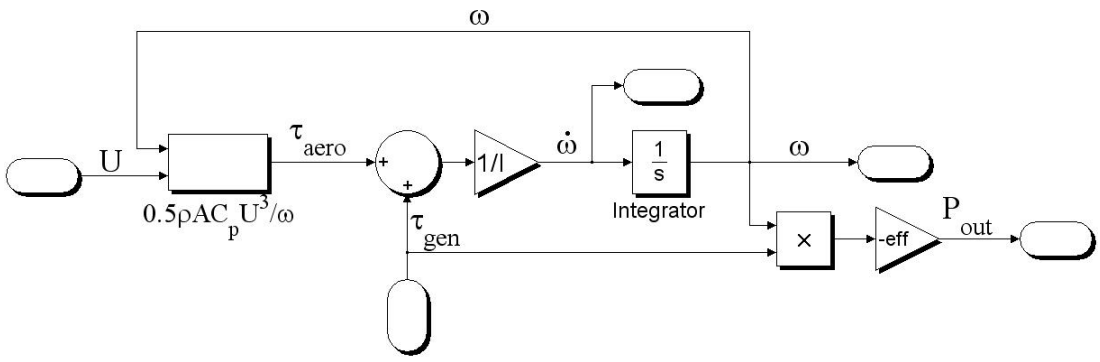

Figure 2.9: Plant block diagram

calculated from Equation 2.5 and integrated to determine the rotor speed using a fourth-order Runge-Kutta method. Finally, the turbine power output is calculated by:

$$P_w = -\eta_{gen}\tau_{gen}\omega \tag{2.7}$$

where η_{gen} is the generator efficiency, assumed to be constant. Variability of the turbine power output would be exaggerated further if the efficiency changed with variation in torque and speed. The negative sign is because τ_{gen} is negative by definition.

2.2.2 Solar Photovoltaic Model

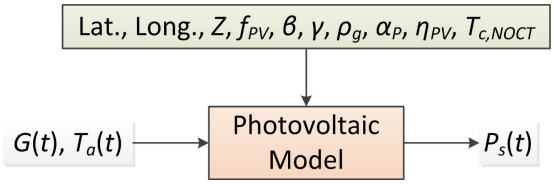

Figure 2.10: Solar sub-model

Complex models of PV cells can be useful for component design, though they are generally not necessary for long-term performance models that are only concerned with the output power from the PV cell. Nevertheless, some authors choose to model an equivalent circuit, incorporating such PV characteristics as the short circuit current and open circuit voltage [33, 35].

However, the model can be simplified if it is assumed that a maximum power point

tracker (MPPT) is included in the system. An MPPT is a type of battery charger or grid tie inverter that applies a resistance to the PV circuit in order to ensure that the operating point of the cell on its I-V curve is such that it outputs the maximum power given the environmental conditions (irradiation and temperature). The result is that the relationship between incident radiation and output power becomes approximately linear [4]. The linear approximation is supported by Perpiñan *et al.* [40], who showed that the energy produced by a PV grid-connected system follows a quasi-linear relation with irradiation on the generator surface, and Gansler *et al.* [41], who found that the estimate of total energy production from a PV system with an MPPT is similar regardless of the data resolution used.

Because of the simplicity and validity of the linear assumption, several authors have made this assumption in their models [4,23–27,31,34,36]. The same assumption is made in this thesis. The power output is then adjusted based on the cell temperature and the cell's temperature coefficient of power, α_P, resulting in a PV output calculated by:

$$P_s(t) = P_{s,r} f_{PV} \frac{\bar{G}_T(t)}{\bar{G}_{T,STC}} [1 + \alpha_P (T_c(t) - T_{c,STC})] \tag{2.8}$$

where $P_{s,r}$ is the PV rated power, $\bar{G}_T$ is the incident solar radiation, and f_{PV} is the derating factor to account for the reduced power output in real world applications. $\bar{G}_{T,STC}$ and $T_{c,STC}$ are the incident solar radiation (1 kW/m^2) and cell temperature (25°C) at standard test conditions. The cell temperature, T_c, is calculated at each time step as shown in Appendix A.2.

Prior to applying Equation 2.8, the horizontal surface radiation from the input data set must be converted to the radiation on the tilted PV surface. The tilted surface model used here was developed by Reindl *et al.* [42] and is referred to as the HDKR model [43]. Detailed calculations are provided in Appendix A.1. First, the diffuse fraction was estimated using Erbs' empirical regression [44]. Vijayakumar *et al.* [45] compared the results of this regression with actual diffuse radiation data. The general trend was followed but there was significant scatter, suggesting the possibility of inaccuracies on short time scales. However, these errors appear to cancel out over the long run. Using Erbs' regression and the Perez model [46], the difference in monthly average radiation on a tilted surface using hourly data and 1 minute data was found to be within 1% for most months and 2% for some winter months. Therefore, the inaccuracies for the tilted surface calculations are likely to be less significant for systems with storage. Since the HDKR model is similar to the Perez model as they

are both anisotropic sky models that account for circumsolar diffuse radiation and horizon brightening [43], it is assumed to be valid for any resolution of input radiation data. The author is unaware of any tilted surface models or diffuse fraction regressions that are better suited for short-term data.

Inverter Model

The power produced from both wind and solar is assumed to be DC, which is typical of PV and small wind technologies. In order to supply the load, this power must be converted to AC power with an inverter. It is assumed that this inverter has a constant efficiency, η_{inv}.

2.2.3 Battery Bank Model

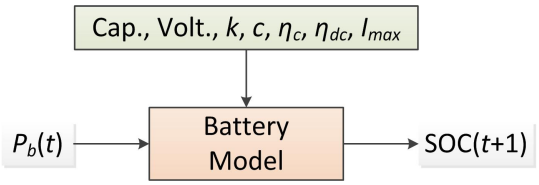

Figure 2.11: Battery sub-model

The battery sub-model is run once the controller has already determined what portion of the net load must be met by the batteries or what portion of the excess power is sent to charge the batteries. The battery and controller models are somewhat interactive since the controller must know the maximum charge or discharge that can be sustained from the battery at any point in time (which is calculated in the battery model).

The simplest method for modelling a battery bank is to assume constant charging and discharging efficiencies. Many authors have made this assumption [27, 31, 34], some with constraints imposed by a maximum depth of discharge [23, 26, 35, 36].

However, this simple model does not account for phenomena that are generally observed in lead acid batteries such as the change in capacity with state-of-charge and the change in voltage with charging current. To account for these, Yang *et al.* [33] model the flow of current in the battery, including a self-discharge rate, and track the floating charge voltage based on the state-of-charge.

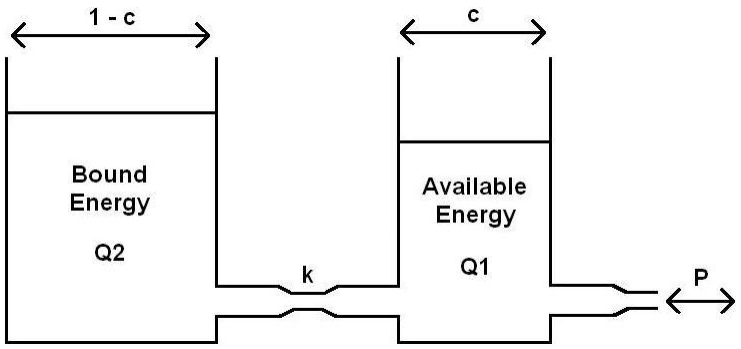

Figure 2.12: Kinetic battery model, modified from [47]

For quasi-steady time series models, Manwell and McGowan [47] found that it is desirable to assume the power to and from the battery is constant over each time step. Therefore, the requirement of the model is to describe the flow of power rather than the voltage characteristics. The kinetic battery model (KiBaM) they developed uses an analogous model of two tanks storing "available energy" and "bound energy" with conductance between the two (Figure 2.12). This model has been used in other time series models [4, 32] and was used for this thesis since it can accurately mimick the dynamic processes of lead acid batteries.

The resulting equations from the KiBaM model are used to calculate the maximum possible charging and discharging powers, $P_{c,max}$ and $P_{d,max}$, at any point in time:

$$P_{c,max} = \frac{kQ_1e^{-k\Delta t} + Qkc(1 - e^{-k\Delta t})}{1 - e^{-k\Delta t} + c(k\Delta t - 1 + e^{-k\Delta t})} \tag{2.9}$$

$$P_{d,max} = \frac{-kcQ_{max} + kQ_1e^{-k\Delta t} + Qkc(1 - e^{-k\Delta t})}{1 - e^{-k\Delta t} + c(k\Delta t - 1 + e^{-k\Delta t})} \tag{2.10}$$

where k and c are the kinetic battery model parameters shown in Figure 2.12, Δt is the time step length, Q_{max} is the maximum capacity of the battery bank, and Q_1 and Q are the available and total energy in the battery bank at the beginning of the time step. These maximum charge rates are sent to the controller which then determines how much power will flow into or out of the batteries. The available and bound energy tanks are then updated by:

$$Q_{1,end} = Q_1e^{-k\Delta t} + \frac{(Qkc - P_b)(1 - e^{-k\Delta t})}{k} + \frac{P_bc(k\Delta t - 1 + e^{-k\Delta t})}{k} \tag{2.11}$$

$$Q_{2,end} = Q_2 e^{-k\Delta t} + Q(1-c)(1-e^{-k\Delta t}) + \frac{P_b(1-c)(k\Delta t - 1 + e^{-k\Delta t})}{k} \quad (2.12)$$

where Q_2 is the bound energy and P_b is the charging/discharging power.

In this way, the effect of the state-of-charge and floating charge voltage of the battery bank are accounted for by the KiBaM model. In this thesis, a maximum charging current, I_{max}, is also imposed on the battery model. This is multiplied by the nominal voltage to calculate the maximum charging power to prevent overcharging issues.

2.2.4 Diesel Genset Model

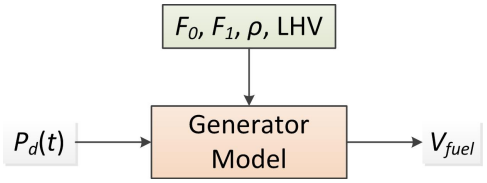

Figure 2.13: Generator sub-model

The simplest method of modelling the genset is to assume a constant efficiency [36]. However, it is well known that the genset will be less efficient when partially loaded. Instead, a linear relationship between fuel consumption and power output is often used [4, 26, 32]. In fact, this is an accurate description of the actual relationship of real generators [48].

Since diesel gensets typically have constant speed operation, a dynamic model was considered to be unnecessary. Starts and stops are not modelled explicitly but frequent start/stop cycles are reduced by the minimum run time imposed on the model. The fuel consumption is calculated in this thesis by:

$$V_f(t) = F_0 P_{d,r} + F_1 P_d(t) \quad (2.13)$$

where F is the fuel consumption (L/h), $P_{d,r}$ is the rated capacity (kW), P_d is the instantaneous power output (kW), and F_0 and F_1 are the fuel curve intercept (L/h·kW$_\mathrm{r}$) and slope (L/h·kW$_\mathrm{o}$). The intercept represents the fuel consumed while the generator runs idle.

A high number of generator start/stop cycles and significant partial loading will cause long term maintenance problems [48, 49]. Therefore, an additional minimum

run time, T_{min}, and minimum power output, P_{min}, are imposed on the model.

2.2.5 Controller Model

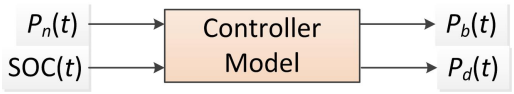

Figure 2.14: Controller sub-model

When a system includes dispatchable components, such as a genset, a dispatch strategy must be implemented by the system controller. If there is only one dispatchable component and no storage, the strategy is simple: output whatever power is required to meet the load once all of the renewable energy has been consumed. When a system includes storage or multiple dispatchable generators, the strategy can become more complicated. Two of the most common strategies will be used in this thesis for systems with a genset and battery bank: load-following and cycle-charging.

In both strategies, the generator only runs when the renewables and batteries cannot meet the load on their own. With load-following control, the generator only outputs enough power to meet the instantaneous load (unless it is below the minimum power output). The advantage is that it maximizes the amount of energy supplied by the renewable sources. With cycle-charging control, whenever generator power is required, it operates at its rated power and excess energy is stored in the batteries. The advantage is that the genset always operates at its maximum efficiency. Both strategies are considered in later chapters.

2.3 Economics Model

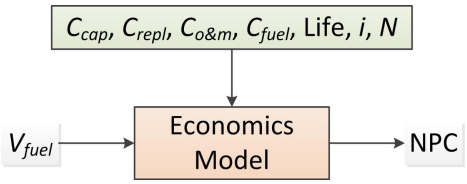

Figure 2.15: Economics sub-model

The metric used to calculate the total system cost is the NPC, which is the present value of all costs over the project lifetime minus the present value of all revenues. Costs include capital, replacement, operation, maintenance, and fuel. Emissions and grid power costs can also be added to the model but were not considered in this thesis. Revenues include grid sales in grid-tied systems and component salvage values. The systems investigated in this work are not connected to the grid and therefore the only revenues are from salvage values at the end of the project lifetime. Each simulation is run for one year and it is assumed that each year is the same over the entire project. See Appendix B for details on the NPC calculation.

2.4 Optimization

The most important factors determining the feasibility of a power system are its cost, reliability, and emissions. Optimization procedures generally aim to minimize cost while maximizing reliability. Some minimize emissions as well. The most common metrics for measuring the cost of a system are the levelized cost of energy (COE) [23,26,34,50] and the NPC [4,32,51]. The annualized cost of system (ACS) is another possible metric as well [33].

Several reliability metrics can be used depending on what the system designer deems to be most important:

- Loss of load probability (LOLP): the percentage of time intervals with some unmet load [27]
- Loss of power supply probability (LPSP): the ratio of all energy deficits to total energy demand [23, 24, 33, 35]
- Expected energy not served (EENS): the maximum percentage of load in any time step that is left unmet [34]
- Autonomous system: the system must successfully meet the load at all time steps in the simulation [4, 26]

Considering the importance of both cost and reliability, the component sizing process becomes a multi-objective optimization. Typically, the objective function is to minimize the cost metric while a constraint function ensures that a reliability metric is kept below a certain value. Additional constraints on the total emissions can also be included [32].

Several different optimization algorithms have also been applied to the component sizing process. The graphical method used in Borowy and Salameh [35] is simple but is only applicable provided there are only two component sizes to be optimized. If the components can all be represented by linear models, a linear programming technique can be applied as in Chedid and Saliba [34]. However, more complex systems with more than two components and non-linear models require more complex optimization routines.

Standard non-linear optimization algorithms, such as Matlab's *fmincon* function, can easily get stuck in a local minimum. For example, in a component size optimization, an algorithm might find that a marginal increase in wind and storage capacities does not lower the required generator capacity because the peak demand is at a time when there is no wind and the battery is empty. There would be some fuel savings throughout the year but they might be outweighed by the increase in wind and battery capital costs. The NPC of this system would be a local minimum. However, it might be true that a larger increase in wind and battery capacity would result in some available energy in the battery at the time of the peak demand. Therefore, the generator capacity could be lowered. Fuel savings would then be even greater because a lower generator rated capacity would be more efficient at meeting partial loads. This new system might have a lower NPC than the other local minimum but would not be identified by some optimization algorithms.

Some authors have applied genetic algorithms [32,33,51] and a simulated annealing technique [31] though these still do not ensure a global minimum. This can only be done with a full-factorial search of the entire feasible range of component sizes at the cost of additional computation time. This full-factorial optimization procedure was used in several studies [23, 26, 27] as well as in HOMER.

Since the full-factorial approach was sufficiently fast for running the optimizations in this thesis, it was implemented here. The objective function is to minimize the NPC of the system over a 25-year project lifetime. The reliability constraint is that the system must be completely autonomous, therefore meeting the load during all time steps.

Chapter 3

Time Step Sensitivity Analysis

The time series method described in Chapter 2 assumes quasi-steady-state system operation. In other words, the various components are assumed to operate at steady-state within each time step but the steady-state operation point varies between time steps. Since energy systems are in fact continuously dynamic, it stands to reason that a shorter time step will provide greater temporal resolution and more accurately describe the actual operation of the system (provided the model accounts for any component dynamics that might become significant with a shorter time step).

The inaccuracy caused by using low temporal resolution can be broken down into several factors. Generally, the operation of each component in a simulation will be affected by the time step of the model. A wind turbine's inertia will cause dynamic effects that can only be resolved with a time step on the order of seconds or less. Additionally, the available energy in the wind will change depending on the amount of variability in the input wind speeds that is accounted for. This is because of the cubic relationship between wind speed and power. Similarly, if the power output from a PV panel is non-linear to the incident radiation, then the total energy output will depend on the resolution of the radiation data provided to the model.

The effects of the inaccuracies caused by the individual components are not independent. Increasing the temporal resolution of the input data will more accurately show how well the power available from the renewable sources aligns with the load power distribution in the time domain. Since the operation of the backup power source is determined by the net power at all times, the choice of time step will also affect the battery and diesel genset operation.

Clearly, there are incentives to use as short a time step as possible. Realistically, however, there is a limit to what level of resolution is feasible. Most wind speed

data sets contain sample averages of one hour or ten minutes. It is rare to find data sets more temporally precise than this for wind speed, solar radiation, or load data. Even if it is possible to find high resolution data for all of the resources and load, the computation time for a simulation will increase significantly. Particularly if a large number of iterations are required for an optimization, the total computational time can be significantly longer with high temporal resolution.

3.1 Purpose

For the reasons stated above, it is therefore important in time domain simulations to choose a time step that provides sufficient accuracy but keeps the computational time and required data resolution as low as possible. This is especially important for system design optimization. However, many studies assume that a 1-hour time step will provide accurate results without justifying the selection. Despite being a common choice, it cannot be assumed to be generally applicable to any energy system. Most likely, this step size is often used because data sets with this resolution are widely available. The author is not aware of any study that has determined this step size to provide accurate results for all systems. In fact, it would be expected that a model's sensitivity to its time step will vary from system to system, depending largely on the configuration, location, and nature of the load.

The sensitivity would likely be affected by system configuration because each of the individual components will have its own sensitivity. The components that are included in the system will affect the overall sensitivity. The location will also have an effect because the variability of the resources will change. For instance, some locations will have more turbulent winds or cloudier days. Also, the variability of the load will affect the sensitivity.

The purpose here was to investigate the efficacy of the common 1-hour time step. The components were analyzed individually and as complete systems with many different configurations. A hypothetical scenario was considered to determine how significant temporal resolution is and which components and configurations are most sensitive. The same framework could then be used for any other system as well.

3.2 Analysis Method

The system components included in this sensitivity analysis were the load, renewable sources (wind and solar), diesel genset, and battery bank. These components were first analyzed individually in order to pinpoint the possible sources of sensitivity. They were then combined and simulated as complete hybrid systems, including component optimization, to determine how these sensitivities interact in the overall system.

The systems in this analysis were designed to meet the load of a single off-grid house. The same model could be used to simulate and optimize larger systems for entire rural communities or grid-connected systems (in which case the diesel generator would be unnecessary). In the larger systems, the short-term load fluctuations would likely be less pronounced due to spatial averaging. Therefore, the effect of temporal resolution would likely be less than for the single house scenario but could be analyzed using the same procedure.

The results were compared using time steps of one second, ten seconds, one minute, ten minutes, and one hour. Since a shorter time step is able to more closely represent the continuous system dynamics, the "errors" referred to in the results were calculated by comparing with the 1-second results.

3.2.1 Wind Power Analysis

The theoretical power available in the wind is proportional to the cube of the hub-height wind speed, resulting in a non-linear power curve. Therefore, by averaging the wind speed values over an extended period, the energy available in the wind will be underestimated. Much of the kinetic energy in the wind occurs at high frequencies in the form of turbulence and this information can be lost by averaging.

However, for the purposes of sizing a power system, it is not the available energy in the wind that is important but rather the energy output from the turbine. Inertial effects and turbine operational limits restrict its ability to extract the energy contained in the turbulence. Therefore, the question here is whether it is necessary to model the turbine with enough temporal precision to account for the wind turbulence and machine inertia.

Here, the goal was to isolate the sensitivity of the wind component from the system. This was accomplished by comparing the total energy output from the turbine model using the various time steps. Since this required wind speed data sets at 1-second intervals which are not readily available, the data used here were synthesized

from the Kaimal spectrum as described below. Nine data sets were created (each with 6 hours worth of data). The mean wind speeds were set to 6, 9, and 12 m/s with three unique data sets generated for each because of the random process of determining the Fourier coefficients. For calculating the friction velocity, the height and surface roughness were assumed to be 15 m and 0.1 m, respectively.

Generating Wind Speed Data

The Kaimal spectrum has been shown to provide a good empirical description of the observed spectra in the atmosphere [52]. The expression of the normalized Kaimal spectrum is as follows [53]:

$$\frac{fS_u(f)}{u_*^2} = \frac{52.5n}{(1+33n)^{5/3}} \tag{3.1}$$

where $S_u(f)$ is the autospectral density of the wind speed, f is the frequency (Hz), u_* is the friction velocity (m/s), $n = fz/U$ is a non-dimensional frequency, and z is the height.

Given a particular mean wind speed, Matlab's *ifft* function was used to perform an inverse fast fourier transform based on the method from Branlard [54]. An overview of the method is provided in Appendix C. The fundamental basis is that the Fourier coefficients are generated randomly using a normal distribution with mean 0 and standard deviation determined by the spectrum.

This method has the ability to synthesize data in the time domain with any time

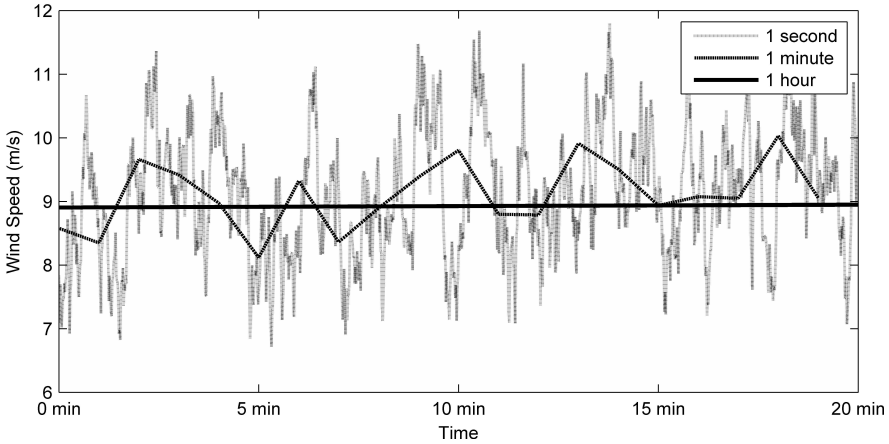

Figure 3.1: Twenty minute sample of synthetic wind speed data

step. In this case, a data set with 0.1-second intervals was created and these values were then aggregated to create separate datasets for the various time steps being considered in this work (1 second, 10 seconds, 1 minute, 10 minutes, and 1 hour). A 20-minute sample is shown in Figure 3.1 for time steps of 1 second, 1 minute, and 1 hour. The effect of temporal smoothing over longer time steps is clearly illustrated.

3.2.2 Solar Power Analysis

The PV model assumes a linear relationship between power output and incident radiation as described and justified in Section 2.2.2 because it is assumed to be installed with an MPPT. This means that the estimate of total energy production should be similar regardless of the data resolution used, as shown by Gansler *et al.* [41] for a PV system with an MPPT. For this reason, the PV component was not analyzed individually. It was included in the "Complete system" analysis because the sub-hour fluctuations could affect system operation depending on how it matched with the load.

3.2.3 Battery Bank Analysis

A battery's performance is determined by how much energy it can store and how much power it can charge or discharge. Both the energy and power capabilities are affected by several battery parameters and depend also on the state of charge. The kinetic battery model described in Section 2.2.3 accounts for most of these influences. As mentioned previously, the model treats the battery as a set of two tanks storing "available energy" and "bound energy" with conductance between the two. The maximum allowable charge rate, in kW, at any time is determined by the amount of available energy. Similarly, the max discharge rate is determined by the unfilled capacity in the available energy tank.

Additionally, these max charge rates depend on the model's time step. Given a particular state of charge in the available energy tank, a shorter time step will allow for larger charge and discharge rates. This is because the model recognizes that any charge rate must only be maintained for the length of the next time step. Nevertheless, a very high charge rate cannot be sustained even with a short time step because the available energy tank will fill up fast and the max charge rate in subsequent time steps will drop very low. Because of this, the average max power

over an extended length of time will be approximately equal regardless of the time step, provided the battery does not switch between charge and discharge modes.

If a battery switches between charge and discharge mode within an hour, then averaging the net power to the battery over an hour will cause a loss of information. The battery losses will be lower since the charge and discharge powers will cancel each other out.

To determine the battery bank's sensitivity to the time step, two scenarios were analyzed: continuous charge and combined charge/discharge. In both cases the total battery capacity was set to 10 kWh and the system was simulated for 6 hours. A wind power data set was taken from the wind power analysis and scaled to a mean of 1 kW. For the discharge scenario, a 1 kW constant load was also included so that the battery would alternate between charge and discharge modes. The initial state of charge was set to 40% for the continuous charge scenario and 70% for the combined charge/discharge scenario.

3.2.4 Diesel Genset Analysis

A diesel generator's efficiency depends on the power level, with maximum efficiency at its rated power output and lower efficiency when partly loaded. As mentioned in Section 2.2.4, the relationship between fuel consumption and power output is nearly linear as was assumed in this model. Because of this linear relationship, the total fuel consumption over a given period will be the same regardless of the time step, provided the generator does not shut off. However, the fuel consumption will change if the generator cycles through starts and stops throughout the period.

To isolate the sensitivity of the generator, a simulation was run with a constant 10 kW load and varying levels of wind penetration to add variability to the generator's output power. Again, a wind power data set was taken from the wind power analysis but this time it was scaled to means of 0, 3, and 6 kW.

3.2.5 Complete System

The sensitivities of the individual components are not independent in the complete system. For example, an increase in wind or solar energy output will reduce the demand on the battery bank or genset. Additionally, it is essential that the load is met at all times and therefore it is important how well the power generation from the renewables matches the load in the time domain.

For the sensitivity analysis of the complete system, a load profile for an individual household was sythesized as described below. For each combination of solar, wind, battery, and diesel components, an optimization procedure was run to compare the optimal component sizes (in order to minimize NPC) for temporal resolution values of one hour, ten minutes, and one minute. The computation time required to run a complete optimization with even finer resolution proved to be infeasible for this study. Some of the optimal configurations were then simulated for one month with very high temporal resolution (1-second and 10-second) in order to compare the results and also determine the source of the sensitivities.

Generating Load Data

The load profile was synthesized for a typical residence using GridLAB-D [55] for 1-minute intervals over the course of a year. The load included a heat pump and various household appliances. The heat pump demand was calculated with a building heat model that accounted for the ambient and internal temperatures as well as the temperature set point. The program used typical weather data from Seattle, WA. The on/off schedules for the appliances were input based on reasonable estimates of a typical residential household. Figure 3.2 shows a typical day taken from the load profile used in the "Complete system" section of the analysis. The smoothing effect is evident when the load was averaged over an hourly time step. For the high frequency data sets (1-second and 10-second), the load was held constant within each minute.

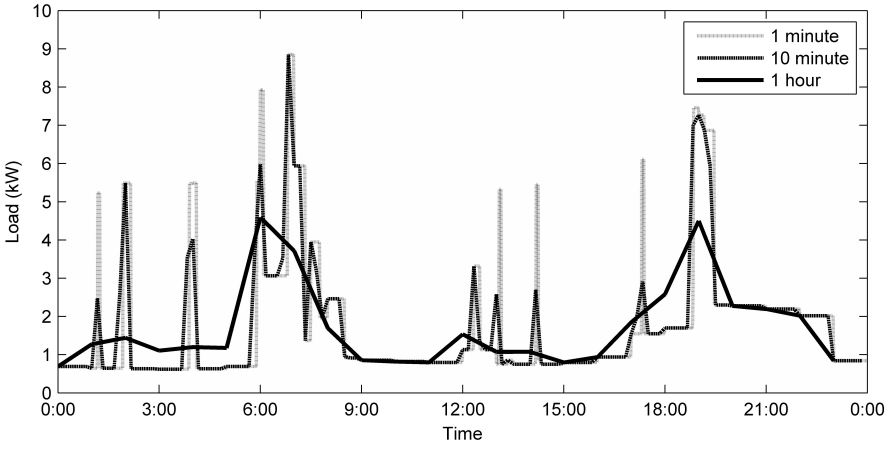

Figure 3.2: Sample of synthetic load data (March 8)

3.3 Problem Set-Up and Parameters

The component models used for this analysis were shown in Chapter 2 to depend on several technical parameters. Generally, these parameters are provided by the manufacturer as part of its technical specifications. For this work, it was desired that the parameters would reflect typical off-the-shelf components. Therefore, most of the technical parameters were taken from components in the catalogue of a distributor of renewable energy components in Victoria, BC.

It was assumed that all of the components were modular. The PV array consisted of Day4 Energy's 175 W '48MC' PV modules. The wind turbine considered was the 4.5 kW model described in Section 3.3.1. The diesel generator rated power was limited to multiples of 1 kW. The battery bank consisted of East Penn's 370 Ah '8L16P' models (2.22 kWh at 6V) and only strings of 8 batteries were considered as they could be connected in series to ensure a 48 V system. The inverter was sized to meet the maximum output from the PV or wind components. For the optimizations, a constraint ensured that the load was met at all time steps throughout the year. A load-following control strategy was implemented for configurations that included both a battery bank and a diesel genset.

3.3.1 Wind Data and Parameters

The wind turbine sensitivity analysis involved 6-hour simulations and required data sets with 1-second resolution. As mentioned in Section 3.2.1, these data were sythesized from the Kaimal spectrum using the method from Branlard [54] with mean wind speeds of 6, 9, and 12 m/s.

For the sensitivity analysis of the complete system, a full year of data were required. Van der Hoven's classic study [56] observed a spectral gap in the wind spectrum between the high frequency turbulence components and lower frequency synoptic/diurnal components at Brookhaven National Laboratory. This observation demonstrated that the short- and long-term wind speed variations can be treated separately [57]. In this study, low frequency variances in the wind were accounted for by using 1-minute wind data, at a height of 12.8 m, for all of 2010 at NREL's Solar Radiation Research Laboratory (SRRL) [58]. The high frequency data were then synthesized using the 1-minute mean wind speeds as inputs. The final values were then blended between the minutes to smooth out the abrupt changes at each minute and scaled by a factor of 2 so that the wind regime was more viable for power

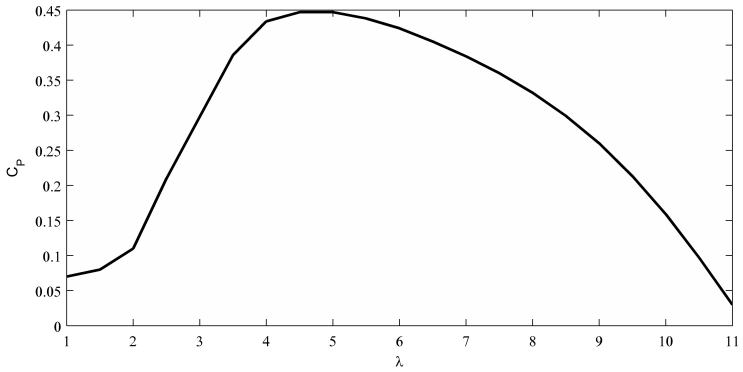

Figure 3.3: C_p-λ curve

production in the hypothetical scenario.

The turbine parameters used in this work are shown in Table 3.1. The assumed C_p-λ curve (Figure 3.3) and the rotor inertia, I, were derived by performing a blade optimization procedure in the ExcelBEM model from Crawford [59]. The tip speed ratio demand, λ_d, was defined as the point at which the turbine operates most efficiently, corresponding to $C_{p,max}$. The rotational speed limit, ω_{lim}, and generator torque limit, $\tau_{gen,lim}$, along with the generator efficiency, η_{gen}, resulted in a maximum output of 4.5 kW. For system sizing purposes, this was assumed to be the rated power.

Table 3.1: Wind turbine parameters

λ_d	R	ω_{lim}	$\tau_{gen,lim}$	I	K	ρ^*	η_{gen}
5	2 m	25 rad/s	-200 N·m	8.2 kg·m^2	0.6	1.225 kg/m^3	90%

* Assuming the standard atmosphere at sea level [60]

3.3.2 Solar Data and Parameters

Section 3.2.2 detailed why it was not necessary to complete an analysis isolating the sensitivity of the solar power output. Therefore, the only data set required was for the complete system sensitivity analysis. Similar to the wind data, 1-minute global horizontal surface radiation was obtained from the SRRL database for 2010 [58]. For sub-minute data, these values were held constant within the minute.

The PV input parameters are shown in Table 3.2. The location and time zone, Z, were chosen to represent NREL's solar laboratory from where the wind, solar,

and temperature data were obtained. The slope, β, was set equal to the latitude and the azimuth angle, γ, was set to zero so that the panel faced due south. The ground reflectance, ρ_g, was assumed. The temperature coefficient of power, α_P, the nominal operating cell temperature, $T_{c,NOCT}$, and the cell efficiency at standard test conditions, η_{PV}, were based on the specifications of the 175 W '48MC' PV model manufactured by Day4 Energy.

Table 3.2: PV parameters

f_{PV}	Lat.	Long.	Z	β	γ	ρ_g	α_P	$T_{c,NOCT}$	η_{PV}	Life
0.8	39.7°N	105.2°W	MST	39.7°	0°	0.2	-0.44 %/°C	46.9°C	14.7	25 yr

3.3.3 Battery Bank Parameters

Table 3.3 shows the battery parameters used in this study. The capacity, voltage, and kinetic battery parameters, k and c, were chosen to represent East Penn's '8L16P' battery model. Both k and c were estimated by a least squares fit of the capacity curve, as described by Manwell and McGowan [47]. The charging and discharging efficiencies, η_c and η_d, were chosen to provide a round-trip efficiency of 85%. Finally, to reduce wear on the batteries, a minimum allowable state of charge of 30% was applied.

Table 3.3: Battery parameters

Capacity	Voltage	k	c	η_c	η_d	I_{max}	Life
370 Ah	6 V	0.630 hr^{-1}	0.347	92.2%	92.2%	75 A	10 yr

3.3.4 Diesel Genset Parameters

The diesel generator parameters used in this work are shown in Table 3.4. The fuel curve coefficients, F_0 and F_1, were assumed based on Barley and Winn [61]. The diesel fuel density, ρ_d, and lower heating value were assumed based on Edwards *et al.* [62]. Additionally, since repeated on/off cycling of a genset will increase maintenance issues, a minimum run time of 10 minutes was assumed. Finally, because partial loading

lowers the fuel efficiency and increases wear, a minimum diesel load of 30% of the rated power was enforced.

Table 3.4: Diesel genset parameters

F_0	F_1	ρ_d	LHV	Life
0.08 L/h·kW$_r$	0.25 L/h·kW$_o$	832 kg/m^3	43.1 MJ/kg	20 000 hr

3.3.5 Component Costs and Economic Parameters

The costs used in this work are shown in Table 3.5. Capital and replacement costs were obtained from a local distributor of renewables. Annual wind O&M costs were assumed to be 2.3% of the total invested cost [63]. The fuel cost was simply an estimate based on current diesel prices and considering the extra expenses associated with its transport to a remote location. Additionally, an annual real interest rate of 5% was assumed over a 25-year project lifetime.

Table 3.5: Assumed component costs

	Capital	**Replacement**	**O&M**	**Fuel**
Solar (175 W)	$1,000	$785	$0	-
Wind (4.5 kW)	$21,750	$20,000	$500/yr	-
Diesel (1 kW)	$500	$500	$0.10/hr	$1.50/L
Battery (370 Ah)	$375	$375	$0	-
Inverter (1 kW)	$500	$500	$0	-

3.4 Sensitivity Results

This section details the results from the sensitivity analysis described above for the individual components and for the complete system optimization. The "errors" referred to correspond to the difference from the 1-second results as it is assumed that the shortest time step best represents the actual system operation.

3.4.1 Wind Power Sensitivity

The total available kinetic energy in the wind and the ability of the turbine to extract this energy are both affected by the temporal resolution of a simulation. The former is affected because of the non-linear relationship between wind speed and power and the latter is caused by the inertia of the turbine. Table 3.6 shows the kinetic energy in the wind and Table 3.7 shows the resulting power output from the turbine model over the 6-hour simulations. Note that these are the averaged results since three data sets were created for each of the mean wind speeds.

As expected, the total kinetic energy in the wind was lower for the longer time steps because the wind speed fluctuations were smoothed out. Since the available energy is proportional to the cube of the wind speed, these fluctuations contain extra energy that is not captured in low resolution data. The results show that the error in the estimate of available kinetic energy for 1-hour data is typically around 4%.

The error in total energy output was very similar for the lower mean wind speeds of 6 and 9 m/s. The smoothing effect caused the energy input to decrease and the turbine's inertia had little influence on its ability to capture the energy in the turbulence (this may be not be the case for larger turbines with greater inertia than the one modelled here).

At the higher wind speed of 12 m/s, the extra energy in the wind input to the turbine did not cause the power output to increase as well. In fact, the output was

Table 3.6: Total wind kinetic energy, in kWh, over 6h sim (% error from 1s results)

U (m/s)*	**1 Second**	**10 Second**	**1 Minute**	**10 Minute**	**1 Hour**
6	10.4	10.4 (0.7%)	10.2 (2.1%)	10.0 (3.8%)	10.0 (4.3%)
9	35.0	34.7 (0.9%)	34.2 (2.3%)	34.8 (3.6%)	33.7 (3.8%)
12	83.2	82.3 (1.1%)	81.2 (2.5%)	80.1 (3.8%)	79.9 (4.0%)

* Results are averaged using three synthetic wind speed data sets for each mean speed

Table 3.7: Total turbine energy output, in kWh, over 6h sim (% error from 1s results)

U (m/s)*	**1 Second**	**10 Second**	**1 Minute**	**10 Minute**	**1 Hour**
6	4.2	4.2 (0.7%)	4.1 (2.1%)	4.0 (3.8%)	4.0 (4.3%)
9	14.1	14.0 (0.9%)	13.8 (2.3%)	13.6 (3.6%)	13.6 (3.8%)
12	25.2	25.6 (1.4%)	26.2 (3.9%)	27.0 (6.8%)	27.0 (7.0%)

* Results are averaged using three synthetic wind speed data sets for each mean speed

greater for the lower resolution simulations. The reason for this is that the turbine was operating at its limits and was not able to take advantage of the extra energy available in the high frequency components of the wind. It would slow down as the input wind speed dropped but it could not speed up as the wind blew faster than its rated speed. By smoothing out the wind profile, the turbine was able to operate at its maximum power output for a longer period of time. The magnitude of the error was larger as well. Instead of having a power output that was 4% lower using a 1-hour step compared with a 1-second time step, the output was 7% higher. This suggests that, using this control approach, the turbine is most sensitive to temporal resolution if the input wind speed is close to its rated speed.

3.4.2 Battery Bank Sensitivity

For the continuous charge scenario, the initial state of charge was set to 40%. Table 3.8 shows the final state of charge, the total charge absorbed by the battery, the amount of energy sent to the dump load because the battery could not handle it, and the overall efficiency (defined as the ratio of energy absorbed by the battery to the energy generated by the wind). There is a clear agreement between the results of the simulations using different time steps, confirming that the kinetic battery model can be used for any level of temporal precision.

In the combined charge/discharge scenario, the initial state of charge was set to 70%. The final state of charge and the total loss of charge for the 6-hour simulation

Table 3.8: Battery simulation results (continuous charge; 1 kW average charge)

	1 Second	**10 Second**	**1 Minute**	**10 Minute**	**1 Hour**
Final SOC	84.6%	84.6%	84.6%	84.7%	84.6%
Charge (kWh)	4.46	4.46	4.46	4.47	4.46
Dump (kWh)	1.16	1.16	1.16	1.16	1.17
Efficiency	74.4%	74.4%	74.4%	74.4%	74.3%

Table 3.9: Battery simulation results (combined charge/discharge)

	1 Second	**10 Second**	**1 Minute**	**10 Minute**	**1 Hour**
Final SOC	68.7%	68.9%	69.3%	69.8%	69.9%
Charge Loss (kWh)	0.13	0.11	0.07	0.02	0.01

are shown in Table 3.9. Since the average wind power and average load were equal (1 kW), the only cause of the battery's loss of charge was from its charge and discharge efficiencies. In the low resolution simulations, the fluctuations were filtered out and so the net load was consistently near zero. This meant that the flow of charge into and out of the battery was small and therefore the battery losses were negligible. However, with higher resolution, the battery losses increased since the wind and load fluctuations did not necessarily match up. Even still, the total loss of 0.131 kWh with a 1-second time step was only 2.2% of the load that was met over the simulation (6 kWh). This suggests that the battery is less sensitive to temporal resolution than some of the other components.

3.4.3 Diesel Genset Sensitivity

The time step sensitivity of the genset depends on the variability of its power output. Table 3.10 shows the fuel consumption of the generator over the 6-hour simulation with varying wind penetration levels and time steps. As wind penetration increased, the variability of the generator power output increased and the mean output decreased. With no variability, the time step does not affect the model output. This is represented by the 0% wind scenario where the genset is used to meet a constant 10 kW load. In this case, the generator constantly operated at its rated power and the fuel consumption was the same regardless of the time step.

With 30% wind penetration, the mean generator output was lowered to 7 kW. The generator efficiency dropped as well since it is less efficient at meeting partial loads. In the low resolution simulations, the added variability was not properly accounted for and so the power output and efficiency remained fairly smooth. With higher resolution, the power output and efficiency fluctuated around the mean but since the relationship between fuel consumption and power output was assumed to be the linear, the total fuel usage did not change.

At 60% wind penetration, the mean load on the generator was reduced to 4 kW

Table 3.10: Diesel fuel consumed, in L, over 6h sim (% error from 1s results)

Wind (%)	**1 Second**	**10 Second**	**1 Minute**	**10 Minute**	**1 Hour**
0	19.8	19.8 (0%)	19.8 (0%)	19.8 (0%)	19.8 (0%)
30	15.3	15.3 (0.0%)	15.3 (0.0%)	15.3 (0.0%)	15.3 (0.0%)
60	11.4	11.2 (1.8%)	11.0 (4.0%)	10.8 (5.6%)	10.8 (5.6%)

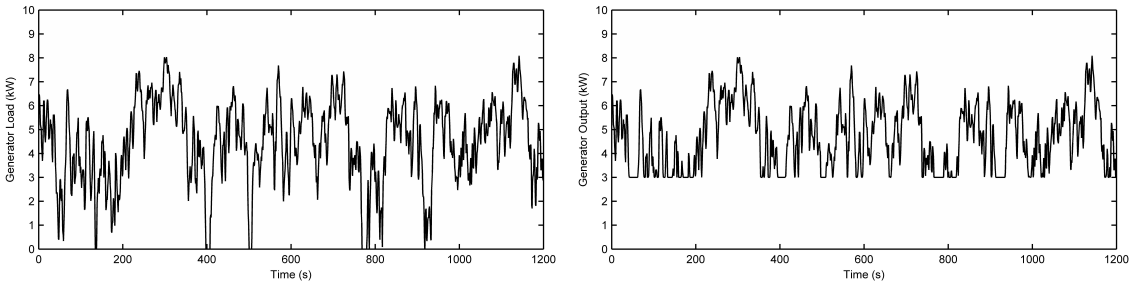

(a) Load (b) Output power

Figure 3.4: Genset load and actual power output for part of simulation (1s step)

which was only slightly higher than the 3 kW minimum allowable output. With the variability from the wind, the instantaneous net load frequently dropped below 3 kW (Figure 3.4a), meaning the generator was not able to continuously follow the load (Figure 3.4b). Because the generator was forced to operate at the minimum power output even when the load dropped lower, the total fuel consumption increased. Since the low resolution simulations did not realize the added variability, the power output did not drop below the minimum and therefore the fuel consumption was nearly 6% lower. Therefore, the genset model is clearly more sensitive to the time step when it operates near its minimum allowable output.

3.4.4 Optimization Sensitivity

Using the costs, parameters, and components from Section 3.3.5, the optimal component sizes for each of the possible configurations were found and are shown in Tables 3.11a-3.11c.

The optimal configuration consisted of a combination of wind and solar with both a battery bank and a diesel genset for backup. The batteries allowed more of the wind and solar energy to be used to meet the load and the generator ensured that the load could be met during long periods with poor wind and little sunshine. However, it was the relative results using various time steps, not the specific results for this scenario, that were important for this study.

Table 3.11: System optimization results

(a) 1 hour

Config.	S	W	D	B	NPC
D	-	-	7	-	$324,956
S-D	39	-	7	-	$276,414
S-B	101	-	-	80	$169,056
W-D	-	2	6	-	$200,675
W-B	-	3	-	120	$202,524
D-B	-	-	7	8	$261,997
S-W-D	26	1	6	-	$190,094
S-W-B	46	1	-	96	$154,548
S-D-B	63	-	6	32	$120,932
W-D-B	-	2	6	24	$121,953
S-W-D-B	27	1	5	16	$99,630

(b) 10 minute

S	W	D	B	NPC
-	-	14	-	$629,546
65	-	14	-	$488,583
104	-	-	80	$172,438
-	2	12	-	$297,634
-	2	-	160	$190,222
-	-	13	8	$292,847
29	2	12	-	$265,241
45	1	-	88	$147,900
66	-	12	32	$127,946
-	2	13	24	$121,013
26	1	12	24	$102,426

(c) 1 minute

S	W	D	B	NPC
-	-	14	-	$631,560
65	-	14	-	$498,599
105	-	-	80	$173,565
-	2	13	-	$340,338
-	2	-	152	$184,702
-	-	14	8	$292,271
30	2	13	-	$301,170
44	1	-	88	$146,773
66	-	14	32	$129,996
-	2	13	24	$118,692
25	1	11	40	$105,720

S - 175 W solar modules; W - 4.5 kW wind turbines; D - 1 kW diesel gen*; B - 370 Ah batteries
* Assuming a load-following control strategy

As the size of the time step changed, the NPC over the 25-year project lifetime changed as well and this change was more significant for certain configurations. Three main factors were identified that affected the results as the level of temporal resolution varied:

- Wind turbulence energy: An increase in wind energy using shorter time steps
- Load smoothing: Averaging data over longer time steps
- Temporal matching: Alignment in time between renewable power and load

The increase in wind energy is evident from the results of the wind-battery configuration. It is the only explanation for why the NPC decreased as the temporal resolution increased. The other two factors are related since it is the smoothing of the load over longer time steps that causes the model to ignore the temporal matching between the renewable sources and the load. However, they affect the results separately. Load-smoothing mostly affects the genset and is the reason why its rated power tends to be higher with a shorter time step. While the size of a battery bank represents its energy capacity, the size of a generator represents its power capacity. Since load averaging affects only the power distribution of the load, and not the total energy required, it affects the size of the generator much more than the size of the battery bank.

The third factor, temporal matching, is most significant for configurations that do not have a battery bank and was the main reason why the NPC was significantly underestimated when using a 1-hour time step for these configurations. This makes sense since, with a higher degree of temporal resolution, the wind and solar power

must line up with the load at the sub-hour level. Without a battery bank, any excess wind and solar energy would be lost, meaning the diesel generator must be used to fill in the gaps. Combined with the fact that the generator is sized much larger than with lower temporal resolution (because of load-smoothing), much more generator fuel and maintenance is required to supplement the wind and solar energy.

Analysis: Battery Backup

In Tables 3.11a-3.11c, it is clear that configurations with only batteries for backup (S-B, W-B, and S-W-B) were far less sensitive to temporal resolution than those with diesel backup. This supports the results from Section 3.4.2 that showed that the battery bank was not very sensitive to the time step.

The total NPC of the solar-battery configuration was only 2.6% higher with a 1-minute step size than with a 1-hour step and the PV array was 3.8% larger. Figure 3.5 shows the change in the battery SOC over the course of a typical day. More or less, by the end of the day, they all converge to a final state of charge. Small differences in battery losses exist because of temporal matching between the solar resource and the load. It is this temporal matching that caused the PV array size to be slightly larger with a shorter time step.

For the wind-battery and solar-wind-battery configurations, the system cost was slightly overestimated using coarser temporal resolution. This was simply because of the additional energy available in the high frequency components of the wind. Tracking the battery SOC as shown in Figure 3.6 clearly shows the influence of the

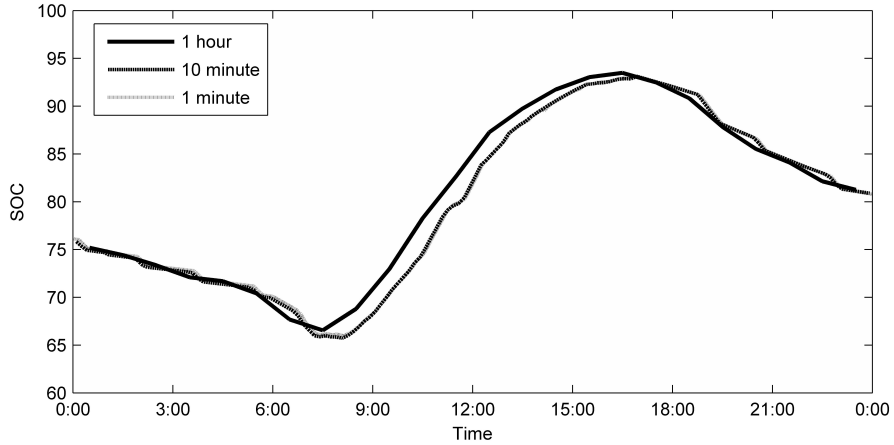

Figure 3.5: Battery SOC on Day 18 (105 PV modules, 80 batteries)

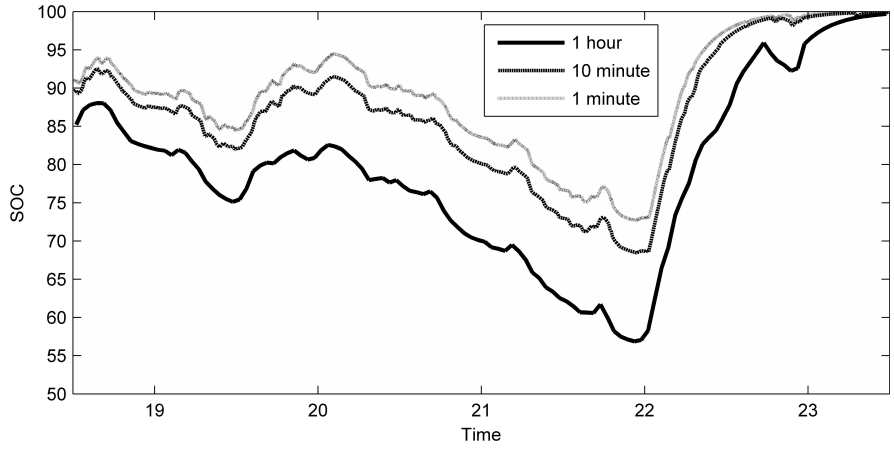

Figure 3.6: Battery SOC on Days 19-23 (3 wind turbines, 120 batteries)

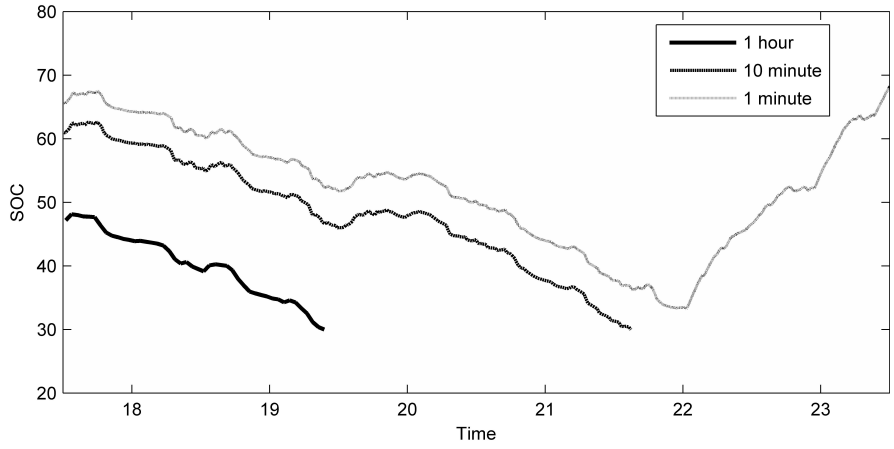

Figure 3.7: Battery SOC on Days 18-23 (2 wind turbines, 152 batteries)

Table 3.12: Results from 1 month simulation (3 wind turbines, 120 batteries)

	1 Second	10 Second	1 Minute	10 Minute	1 Hour
Min SOC (%)	62.4	62.3	62.3	61.2	56.9
Final SOC (%)	89.3	89.3	89.3	88.8	87.8

extra wind energy on the simulation. Figure 3.7 demonstrates why the optimal system using a 1-minute time step was not feasible when less temporal precision was used, since the SOC dropped below the 30% minimum. Looking at the minimum and final SOC of a 1-month simulation shown in Table 3.12, it is clear that using a time step shorter than 1 minute would not affect the results. This analysis suggests that a 1-hour step is acceptable but will lead to a slightly oversized system design. Better temporal resolution will bring the system costs down and is recommended if possible.

In general, two of the main factors affecting the sensitivity are far less significant with battery backup: load smoothing and temporal matching. Smoothing out the load by averaging reduces the peak load but this is less significant with battery backup. Provided the net power into or out of the battery does not exceed its max power constraints (which is usually the case in a properly sized system), the size of the battery required is determined by how much energy it must store, not how much power it can output. Similarly, the battery can easily handle the fluctuating net loads caused by poor temporal matching within an hour. In this case, the only additional losses are due to the battery's charging and discharging efficiencies.

Analysis: Diesel Backup

The simulations of systems with only diesel for backup (D, S-D, W-D, S-W-D) were far more susceptible to error using coarser temporal resolution. Both load smoothing and temporal matching have a far greater impact on system error than in the battery backup configurations.

Without a battery, the genset's rated power output must be greater than the net load at all times. Since both solar and wind power are not reliable on their own, the maximum net load is generally equal to the peak load. Averaging the load reduces this peak load and leads to significant undersizing of the genset. This also leads to an underestimate of the total fuel consumption as well. Since the rated power is lower, the average net load on the genset is closer to its rated output and it is therefore more efficient. The minimum output, which was defined as 30% of the rated power,

Table 3.13: Results from 1-month simulation (2 wind turbines, 13 kW generator)

	1 Second	10 Second	1 Minute	10 Minute	1 Hour
Wind (kWh)	2020	2017	2016	1970	1858
Fuel (L)	993	921	860	800	839
Gen Hours	479	443	413	386	415

Table 3.14: Results from 1-month simulation (30 PV modules, 2 wind turbines, 13 kW generator)

	1 Second	10 Second	1 Minute	10 Minute	1 Hour
Wind (kWh)	2020	2017	2016	1970	1858
Fuel (L)	778	715	661	603	617
Gen Hrs	373	342	315	289	305

is also lower. With a lower minimum and less variability, the generator output is rarely under the minimum, making it less wasteful as well.

Additionally, when there is poor temporal matching between the sources and the load, the genset must fill in the gaps. In many cases, the power required to fill a gap is fairly small and inefficient to be met by the genset. Finally, because of the minimum run time of the genset, whenever it is required to fill in a gap, it must remain on for at least 10 minutes, leading to further losses that would not be captured with coarser temporal resolution.

All of these factors resulted in large errors in the component sizing and system cost estimation. In the most basic case, diesel-only, a 10-minute time step proved to be sufficient in eliminating load smoothing and therefore giving accurate results. A similar result was found for the solar-diesel configuration. For wind-diesel, the results were slightly different. Unlike solar power which is inherently unreliable and will never be available outside of daytime hours, the non-operational time of a wind turbine is far less in a good wind regime. In this case, the peak net load on the genset was reduced by the wind but was not fully captured by any time step longer than 1 minute. Table 3.13 shows the total wind production and fuel consumption over a 1-month simulation. Despite the extra energy from the wind with shorter time steps, fuel consumption increased because of the poor temporal matching between the wind and the load caused by the wind turbulence and load variability. This mismatch meant that the genset had to turn on for brief periods and also had to stay

on for the 10-minute minimum run time. As Table 3.14 shows, the solar-wind-diesel configuration is affected by the time step in the same way.

Analysis: Diesel / Battery Backup

For configurations with both deisel and battery for backup (D-B, S-D-B, W-D-B, S-W-D-B), the sensitivity is somewhat higher than for battery-backup systems and somewhat lower than for diesel-backup systems. Similar to the diesel-backup systems, load smoothing leads to undersizing of the genset. However, the battery can reduce this error if it is able to store enough energy at the right time to reduce the peak net load on the genset. Additionally, if the load on the genset is below its minimum allowable output power, the excess power generated can be stored in the batteries instead of being sent to the dump load. The issue of temporal matching within the hour is far less significant than with diesel-backup configurations because it is almost always handled by the battery.

In the simplest diesel-battery configuration without solar and wind, the error with a 1-hour time step was much smaller than in the diesel-only configuration. However, the ultimate result was the same in that a 10-minute time step was required for accurate results. The main role of the battery bank in this system was to store the excess power from the genset when it is required to output more than what is needed to meet the load (i.e. the net load was below the minimum allowable output). Only a small level of storage was required.

With the addition of solar and/or wind power, most of the load was met by the renewable sources because of the high cost of fuel. Table 3.15 lists the percentage of the load met by the genset in the optimal system simulations. Though load smoothing affected the fuel consumption calculations, since the contribution of the genset was smaller, the impact on the overall system cost was also much smaller.

Table 3.15: Percentage of load met by genset, based on optimal system simulations

	1 Minute	**10 Minute**	**1 Hour**
S-D-B	12.3	11.6	11.7
W-D-B	7.6	8.7	10.3
S-W-D-B	4.1	6.6	9.2

3.4.5 Conclusions and Recommendations

Systems with battery backup were found to have far less sensitivity to the simulation time step. A 1-hour time step appears to be sufficient for a solar-battery system, as long as both the PV array size and the NPC are scaled up by roughly 5%. System costs for configurations that included wind as well were overestimated with coarser resolution. A 1-hour time step could be used though finer resolution would provide a slightly lower overall cost.

For systems with diesel backup, finer resolution was clearly required. When choosing a time step, the user must be sure that load-smoothing does not allow the generator to be undersized. Since solar and wind power are unreliable, it is often necessary that the genset be sized to meet the peak load. Additionally, the large number of start/stop cycles and partial loading of the generator in a wind-diesel system suggest that a high temporal resolution is required. This also suggests that these systems are not suitable for this application. Unacceptably high numbers of stop/start cycles and prolonged low-load running of the generator will cause increased wear and reduce its lifetime [49]. Also, without a battery bank and charge controller, short term fluctuations from wind turbulence will cause variations in the system voltage and frequency [49]. Attempting to meet a highly fluctuating load with unpredictable and fluctuating energy resources without a battery bank for storage will inevitably lead to all of these issues and should be avoided.

Systems with both diesel and batteries for backup had so many factors affecting the results that it was difficult to develop a simple recommendation for the choice of time step when sizing a generic renewable power system. Small flucuations within the simulation can be the difference between a feasible and an infeasible system.

The most obvious example of this is with the solar-wind-diesel-battery configuration. Despite the fairly similar results for total NPC, the optimal system sizes were found to be significantly different. To determine the reason for this, the three optimal configurations were simulated with each time step in an attempt to compare the component costs. As expected, the "1-hour optimal" configuration was infeasible with a 10-minute and 1-minute time step. This was obviously because the 5 kW genset was unable to meet spikes in the load when it was not smoothed out. The "10-minute optimal" was also found infeasible with a 1-minute time step. Investigating where the failure occurred, it was clear that load-smoothing was again the reason. An unexpected result was that the "1-minute optimal" configuration was infeasible

when using a 10-minute time step. In this case, it was the extra energy in the high frequency components of the wind that made the system feasible with a 1-minute step but infeasible with a 10-minute step.

What this example shows is that there are several factors affecting the results, sometimes competing against each other in determining whether a system is feasible and often depending on the choice of time step. Identifying beforehand which of these factors will affect the results is evidently not a simple task.

Chapter 4

Time Step Selection Using Probabilistic Models

In this chapter, two models are developed transitioning from the time series method described in Chapter 2 towards a fully probabilistic method, including a combined time series/probabilistic model. The purpose is to identify the differences between the time series and probabilistic methods that are most significant in system design and attempt to develop a model that can be used as a tool for determining the temporal resolution required for a particular time series simulation. A priori knowledge of the requisite time step based on the energy sources, load data, and possible system configurations would allow for the best choice of time step to use in subsequent optimizations. The underlying theory and examples from the literature are provided first, followed by a description of the statistical methods used, and finally the details of the individual models.

4.1 Theoretical Basis and Review

The fundamental basis for the probabilistic method is the assumption that the power from the renewable resources and the load power are random variables with specific probability density functions. For example, it is common to model wind speeds with a Weibull distribution since it has been found to accurately represent the variation in hourly wind speeds over a year [57]. Typically, these functions are assumed to be representative over the entire simulation period, though some authors have used different functions for each hour of the year [18]. Using these distribution functions

and statistical techniques, new probability density functions can be calculated for the net power, battery charge/discharge power, and diesel power output. From these, various methods can be used to estimate the storage capacity required and evaluate the total system cost and reliability metrics. The simulation is typically faster than a time series simulation and does not require high resolution resource and load data.

Bucciarelli [64] developed a method to represent a known probability density function of the energy flow in and out of storage as an equivalent distribution allowing only two events: an increase in stored energy by amount Δ, with probability p, or a decrease in stored energy by amount Δ, with probability q. This two-event approximation simplifies the problem and keeps the mean and variance of the daily net power distribution the same. However, it can only be used to model one random variable (in this case, PV power). Bagul *et al.* [65] extended the method to a three-event approximation that is suitable for two random variables (wind and solar power) and includes a probability that the storage level does not change over a discrete time period.

Barton and Infield [16] derived wind speed and solar insolation probability density functions by applying filter functions to the frequency spectra of real data. Integrating across all phases for each harmonic component, the mean and variance of wind speed and irradiance were calculated and added in quadrature to determine the variance in the change in SOC over a discrete time period. For sizing the storage system, the required energy storage capacity was empirically found to be approximately twice the standard deviation of the change in SOC. Gassner [17] applied this method to wind systems designed to meet a specified firm power commitment.

Tina *et al.* [18] grouped real data by hour of the day for each month and derived separate probability density functions for wind speed and solar insolation at each hour. Density functions for wind and solar power were calculated from the resource distributions and added together by convolution with the assumption that they are statistically independent. This assumption is reasonable since the density functions are representative of a particular hour of the year and therefore correlation between the two is not strong. This system is assumed to be grid-connected and has no method for sizing an auxhiliary storage system.

The above models do not account for the chronological sequence of events. Accuracy, particularly in terms of the required storage capacity, is lower than with the time series method and therefore the time series method remains useful to ensure that the system design will perform as intended. They also all assume a steady or

quasi-steady load, making them less applicable for systems with highly variable loads.

4.2 Fundamental Equations

In the probabilistic models developed in this section, it will be assumed that wind power, solar power, and load are independent random variables each with a unique probability density function (PDF). The validity of the assumption of statistical independence between these variables depends on the time scale over which the distributions are representative. This is an important point that will be developed further in this chapter and analyzed using the results provided in the next chapter.

With this assumption, the main equations of the probabilistic model are:

$$\boldsymbol{R} = \boldsymbol{W} + \boldsymbol{S} \tag{4.1}$$

$$\boldsymbol{N} = \eta_i \boldsymbol{R} - \boldsymbol{L} \tag{4.2}$$

$$\mathrm{E}[\boldsymbol{B}] = \frac{1}{\sqrt{\eta_b}} \int_{-\infty}^{0} P_n f_N(P_n)\,\mathrm{d}P_n + \sqrt{\eta_b} \int_{0}^{\infty} P_n f_N(P_n)\,\mathrm{d}P_n \tag{4.3}$$

$$\mathrm{E}[\boldsymbol{D}] = -\int_{-\infty}^{-P_{min}} P_n f_N(P_n)\,\mathrm{d}P_n - P_{min} \int_{-Pmin}^{0} f_N(P_n)\,\mathrm{d}P_n \tag{4.4}$$

In the notation used for this thesis, random variables are represented by bold-faced letters and probability density functions are represented by $f_X(x)$. $\mathrm{E}[\boldsymbol{X}]$ is the expected value. The variables $\boldsymbol{R}$, $\boldsymbol{W}$, $\boldsymbol{S}$, $\boldsymbol{N}$, $\boldsymbol{L}$, $\boldsymbol{B}$, and $\boldsymbol{D}$ are the renewable, wind, solar, net, load, battery, and diesel powers (generally all dealt with in kW).

It is evident from these equations that the inverter efficiency is applied to all of the generated renewable power even if it is being used to charge the batteries but it is not applied to any power output from the batteries. This is slightly different from the time series model which applied the inverter efficiency only to the fraction of renewable power being used to meet the load and any power discharged from the batteries in a particular time step. The correct method would depend on whether the renewable components are set up simply as battery charging components or to serve the load directly. For the purposes of a probabilistic model, the difference is likely negligible if the simulation covers an adequately long enough period of time and a 1-year simulation would appear to be adequate.

4.3 Representing Probability Density Functions

This section will describe some statistical models for wind, solar, and load distributions and identify reasons why they are not ideal. Instead, it is proposed that, in this work, they be represented by moments calculated directly from data.

4.3.1 Wind Power Probability

The distribution of hourly mean wind speeds over a year has been found to be well represented by the Weibull distribution. However, since hourly mean wind speeds are often measured, it is the sub-hour distribution of speeds that is more important here. It is common to describe a wind regime based on its turbulence intensity:

$$I_T = \frac{\sigma_u}{U} \tag{4.5}$$

where U is the mean wind speed and σ_u is the standard deviation of speeds within an interval (typically ten minutes or one hour). Since it is based on only the first two statistical moments, this method assumes a Gaussian distribution. Generally, wind speeds within a 1-hour or 10-minute interval are roughly Gaussian [57]. Unfortunately, the tail-regions of wind speed distributions have been found to be quite non-Gaussian. Morales *et al.* [66] showed that higher-order moments of turbulent fluctuations are required for an accurate description of the more extreme fluctuations.

The data from the SRRL database used in Chapter 3 were analyzed to determine

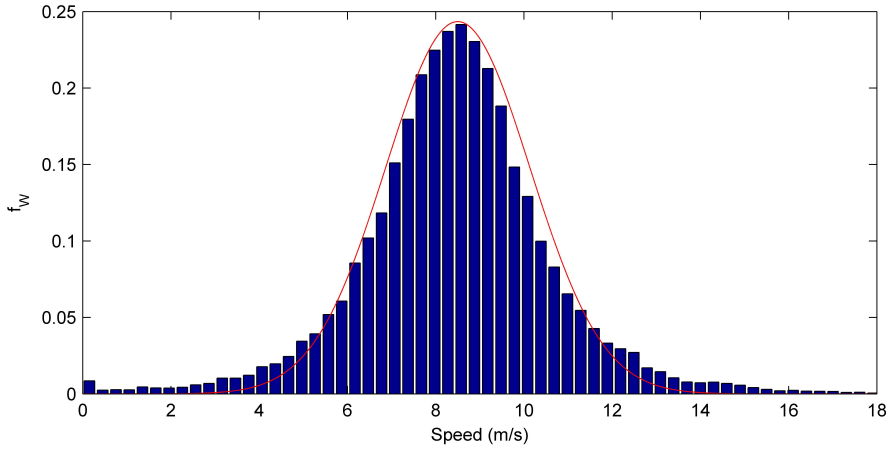

Figure 4.1: Distribution of 1min wind speed data with an hourly mean of 9 m/s

the "Gaussianity". The 1-minute wind speed data were binned according to the mean wind speed of the hour in which each measurement was taken. Figure 4.1 shows the distribution of actual 1-minute data in the bin centered at 9 m/s as well as a Gaussian distribution for comparison. Though it seems like a reasonably good fit, the Gaussian curve clearly underestimates the tail regions. Since the available wind power is proportional to the cube of the wind speed, the underestimate of power is even worse. For this reason, Gaussianity is not assumed in this thesis. Instead the PDF is represented by higher-order moments calculated directly from the data as will be described later.

4.3.2 Solar Power Probability

The distribution of solar power is somewhat more complicated than wind because the power output depends on the location, the time of day/year, and the sky clarity. The location is constant, of course, but the time and clarity are variable. The effects of location and time are both accounted for by the air mass – the ratio of the mass of atmosphere that beam radiation must pass through to the mass it would pass through if the sun were at the zenith (directly overhead):

$$m_a = \frac{1}{\cos\theta_z} \tag{4.6}$$

where θ_z is the zenith angle. The sky clarity is measured by the clearness index – the ratio of horizontal radiation on the Earth's surface to the horizontal extraterrestrial radiation at that location and time:

$$k_t = \frac{G_h}{G_o} \tag{4.7}$$

Tovar *et al.* [67] derived an empirical function to determine the distribution of 1-minute clearness indices for any air mass using data from Granada, Spain. The assumed form was the Boltzmann statistic and the resulting distribution was bimodal, indicating two main states: cloudy and not cloudy. However, this distribution assumes the hourly mean clearness index, k_t^H, is unknown. In a similar study, Tovar *et al.* [68] used the same assumed function form but instead of binning the data by air mass, it was binned by the hourly mean clearness index. The resulting distribution was unimodal. This method ignores the influence of the air mass but is likely a better representation of the distribution if k_t^H is known. Similarly, Hollands and Huget [69]

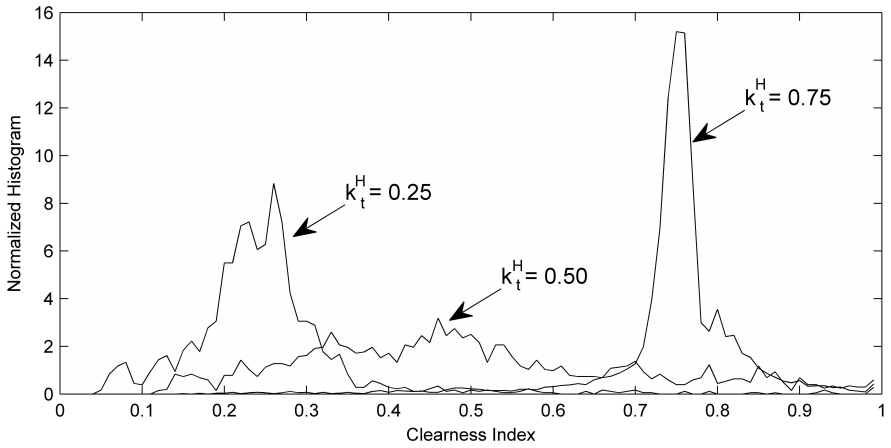

Figure 4.2: One-minute clearness index histograms (bin width = 0.01)

empirically derived a distribution of clearness indices given a mean clearness index with an assumed form of a modified Gamma distribution.

The SRRL solar data were analyzed to determine how well the data agreed with the Tovar method based on hourly clearness indices. First, the 1-minute clearness indices were binned by k_t^H. To avoid errors that arise near sunset and sunrise, data with a solar zenith angle greater than 85° were ignored. The histograms, normalized for a total probability of one, for three different hourly mean clearness indices are shown in Figure 4.2.

The most noteworthy result is that the distribution for midrange k_t^H values is very broad. This is contrary to what was found in [68]. Analyzing the data, this result appears to make sense. The midrange hourly averages tended to occur in transition periods from clear to cloudy skies or vice versa. Therefore, both high and low k_t values would be expected within the hour.

Overall, there was a poor agreement using the coefficients derived empirically in the paper. Also, using the same general function for the distribution shape, the parameters could not be adjusted to give a good description of the shape across the entire range of hourly clearness indices. Further work would need to be completed to identify a distribution that better represents actual short term solar radiation data.

4.3.3 Load Power Probability

The load is assumed to be constant in many probabilistic models. For example, Gassner [17] developed a model to design systems that provide a firm power com-

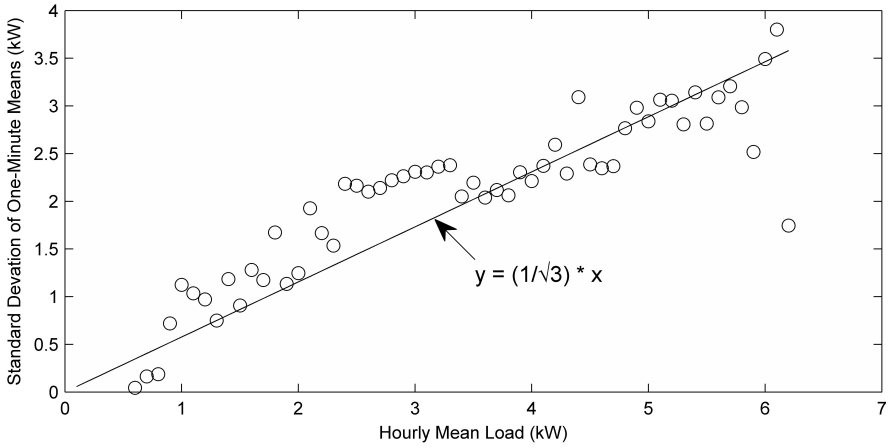

Figure 4.3: Standard deviation of one-minute loads given hourly mean

mitment. Tina *et al.* [18] assumed a constant "local load" within each hour. It is important for this thesis that load variation is considered and therefore a density function must be assumed. In Hybrid2, a Gaussian distribution is assumed, though this is not always representative of actual loads. For instance, the residential load profile in the sensitivity analysis of Chapter 3 exhibits on/off characteristics that would not be well-represented by a Gaussian distribution.

A binomial distribution might be effective for the residential load to better represent the on/off cycles of various appliances. However, it would likely be fairly complicated given the number of appliances and that the heat pump load often varied significantly with time of day and year. Instead, the data were binned by hourly mean load and the histograms were analyzed to observe any trends. No clear trends were found and it did not appear any more likely for the 1-minute averages to be close to the hourly mean. There was, however, a trend in the standard deviation of 1-minute load data binned by the hourly mean, shown in Figure 4.3.

The general trend appears to be similar to a hyberbolic function. However, an exact distribution is not required for this model so a simpler fit is sufficient. The relationship is approximately linear and a least squares regression gives a slope of 0.5797. With this information, it seems reasonable to assume a continuous uniform distribution over a range of load values with a standard deviation roughly equal to $0.5797 P_l^H$, where P_l^H is the hourly mean load. In fact, it can be shown that the standard deviation of a uniform distribution from 0 to $2P_l^H$ is equal to $\frac{1}{\sqrt{3}} P_l^H$, or $0.5774 P_l^H$. This is the slope of the line in Figure 4.3. For convenience, therefore, a

uniform distribution could be assumed from $2P_l^H$ to 0. To ensure a total probability of 1, the constant density distribution is given by:

$$f_l(P) = \begin{cases} 1/(2P_l^H) & : 0 \leq P \leq 2P_l^H \\ 0 & : \text{otherwise} \end{cases} \tag{4.8}$$

Though the method outlined here is a fairly reasonable way to approximate the distribution given its non-standard characteristics, it is clearly not a perfect representation of the actual load data that is more spiky because of the on/off cycles of the appliances.

4.4 Calculating Moments and Cumulants from Data

As shown in the previous sections, it was difficult to develop accurate analytic functions defining the sub-hour distributions of wind, solar, and load power. Another way of approximating the PDF of a data set is to calculate several of its moments. The moments are a set of constants that define the shape of a PDF. Every distribution has an infinite number of moments though higher order moments are less significant. Often, no more than the first four moments are sufficient for an accurate representation of a distribution.

The first moment represents the arithmetic mean, or the expected value:

$$\mu_1 = \frac{1}{N} \sum_{i=1}^{N} x_i \tag{4.9}$$

where N is the number of values in the data set.

Higher order moments are often calculated relative to the mean such that the r^{th} central moment is:

$$\mu_r = \frac{1}{N} \sum_{i=1}^{N} (x_i - \mu_1)^r \tag{4.10}$$

Some of these have special meanings. The second central moment defines the variance, the third is the skew, and the fourth is the kurtosis.

Alternatively, the moments can be calculated relative to the origin and are then labelled the raw moments:

$$\mu'_r = \frac{1}{N} \sum_{i=1}^{N} x_i^r \tag{4.11}$$

A property of all distributions is that the moment of order 0 must be equal to 1.

Another set of constants, called cumulants, also define a distribution and are often more useful from a practical standpoint. They can be determined from the raw moments (or vice versa) using the recursive formula [70]:

$$\kappa_r = \mu'_r - \sum_{j=1}^{r-1} \binom{r-1}{j} \mu'_j \kappa_{r-j} \quad : \quad r > 1 \tag{4.12}$$

where the first cumulant, κ_1, is equal to the first moment, μ'_1.

As will be seen in the next section, an advantage of representing a random variable by its cumulants is the ease with which they can be added together using cumulant arithmetic.

4.5 Sum of Independent Random Variables

Given Equations 4.1 and 4.2, it is clear that an important concept for the probabilistic models is the addition of independent random variables. Two methods are described here for this calculation and it is demonstrated why the method of cumulants is best for this application.

4.5.1 Convolution

If the PDFs of two random variables are known, the PDF of their sum is found by convolution. Let

$$\boldsymbol{Z} = \boldsymbol{X} + \boldsymbol{Y} \tag{4.13}$$

Then

$$f_Z(z) = \int_{-\infty}^{\infty} f_X(x) f_Y(z-x)\,\mathrm{d}x \tag{4.14}$$

This can be extended to a weighted sum as well. Let

$$\boldsymbol{Z} = a\boldsymbol{X} + \boldsymbol{Y} \tag{4.15}$$

Then

$$f_Z(z) = \int_{-\infty}^{\infty} f_{aX}(ax) f_Y(z-ax)\,\mathrm{d}(ax) \tag{4.16}$$

Since $f_{aX}(ax) = f_X(x)/a$ and $\mathrm{d}(ax) = a\mathrm{d}x$, then

$$f_Z(z) = \int_{-\infty}^{\infty} f_X(x) f_Y(z - ax)\,\mathrm{d}x \tag{4.17}$$

Applying this concept to the models being developed here, it can be seen that solving Equation 4.3 or 4.4 would require a triple integral. If analytic expressions of the wind and solar power PDFs are not known or are not easily integrated, then this would have to be solved numerically and would be very computationally expensive. This was the first approach for the probabilistic models developed in this chapter. Despite attempts to implement numerical integration techniques including adaptive quadrature and double integration functions in Matlab, the method proved to be computationally impractical.

4.5.2 Method of Cumulants

Alternatively, if the distributions are approximated by its cumulants as described in Section 4.4, the cumulants of the sum of two independent random variables (Equation 4.13) are simply equal to the sum of the individual cumulants:

$$\kappa_{Z,r} = \kappa_{X,r} + \kappa_{Y,r} \tag{4.18}$$

For the weighted sum in Equation 4.15, the cumulants are [71]:

$$\kappa_{Z,r} = a^r \kappa_{X,r} + \kappa_{Y,r} \tag{4.19}$$

Clearly, this is a far simpler calculation than for convolution. The following section will describe how a distribution can be reconstructed from a finite set of its cumulants.

4.6 Reconstructing Probability Density Functions

If a number of cumulants of a PDF are known, it can be approximated using various techniques. Two of these are described here: Gram-Charlier expansion and the maximum entropy method. Each has advantages and disadvantages.

4.6.1 Gram-Charlier Expansion

The goal of Gram-Charlier expansion is to define a distribution as an expansion of a series of derivatives of a reference PDF, $\alpha(x)$:

$$f_X(x) = \sum_{r=0}^{\infty} (-1)^r \, \frac{c_r}{r!} \, \alpha^{(r)}(x) \tag{4.20}$$

where $\alpha^{(r)}(x) = (\mathrm{d}/\mathrm{d}x)^r \, \alpha(x)$.

For the Gram-Charlier series of Type A, the reference PDF is defined by the standard Gaussian distribution [72]:

$$\alpha(x) = \frac{1}{\sqrt{2\pi}} e^{-\frac{1}{2}x^2} \tag{4.21}$$

In this case, Equation 4.20 becomes:

$$f_X(x) = \sum_{r=0}^{\infty} c_r H_r(x) \alpha(x) \tag{4.22}$$

where H_r are the Hermite polynomials [72]:

$$H_r = r! \sum_{j=0}^{\lfloor r/2 \rfloor} \frac{(-1)^j \, x^{r-2j}}{j! \, (r-2j)! \, 2^j} \tag{4.23}$$

where $\lfloor \, \rfloor$ represents the "floor" function. Finally, the vector of coefficients c_r can be easily calculated from the known moments [71]:

$$c_r = \sum_{j=0}^{\lfloor r/2 \rfloor} \frac{(-1)^j \, \beta_{r-2j}}{j! \, (r-2j)! \, 2^j} \tag{4.24}$$

where $\beta_r = \mu_r / \sigma^r$ are the standardized central moments.

The advantages of this method are its simplicity and speed. However, it is only accurate for distributions that resemble a Gaussian distribution. If this is not true, the resulting distribution is not guaranteed to be positive definite over the entire domain [73].

4.6.2 Maximum Entropy

Van Erp and van Gelder [74] provide an overview of entropy distributions and how they can be calculated from a finite set of raw moments. The objective is to maximize the information entropy of a distribution defined as:

$$H = -\int_{-\infty}^{\infty} f_X(x) \ln f_X(x) \, \mathrm{d}x \tag{4.25}$$

The constraints of this optimization are that the moments of the distribution must equal the known values:

$$\int_{-\infty}^{\infty} x^i f_X(x) \, \mathrm{d}x = \mu'_i \quad : \quad i = 0, 1, ..., m \tag{4.26}$$

where m is the highest order of the known raw moments. The distribution that satisfies the objective and constraint functions will always take the Pearsonian form [74]:

$$f_X(x) = \exp(-\lambda_0) \exp\left(-\sum_{i=1}^{m} \lambda_i x^i \right) \tag{4.27}$$

Rockinger and Jondeau [75] show that this procedure can be solved by numerically minimizing:

$$Q(\lambda) = \int_{D_x} \exp\left[\sum_{i=1}^{m} \lambda_i (x^i - \mu'_{X,i}) \right] \mathrm{d}x \tag{4.28}$$

where D_x is the assumed domain of possible x values (e.g. $\pm\, 6\sigma$).

The informational entropy is a measure of the uncertainty of a random variable. There is not a unique distribution function given only a set of moments to match as a constraint. An advantage of the maximum entropy method is that the output distribution is the one that maximizes the uncertainty given the limited information from the moments. This makes better theoretical sense than other methods that ignore some uncertainty by assuming a particular form, as in the Gram-Charlier expansion. Another advantage is that the resulting distribution is guaranteed to be positive over the entire domain.

The disadvantages of this method are speed and robustness. Speed is, of course, made worse by the optimization portion of the algorithm, particularly since the objective function requires numerical integration. The method is also less robust because it tends to give errors when higher order moments (greater than 3 or 4) are included. Van

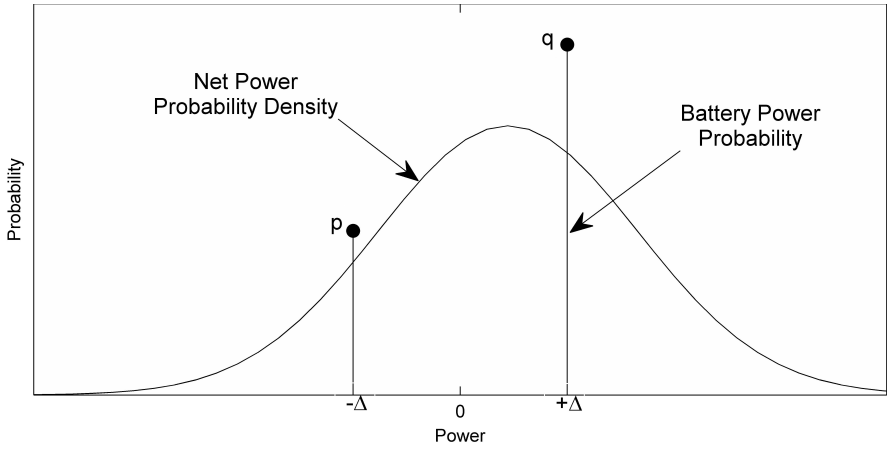

Figure 4.4: Two-event approximation of the battery power distribution (not to scale)

Erp and van Gelder [74] mention that the minimization package in Matlab "breaks down" at five or more moments. Based on experience from the work in this thesis, the value of the objective function in Equation 4.28 can grow very large because it is an integral of an exponential function. With higher order moments, the function often reaches the point where it surpasses Matlab's largest floating-point number.

4.7 Two-Event Approximation

Two-event approximation is used to represent the battery power distribution, $\boldsymbol{B}$, as illustrated in Figure 4.4. The method is based on that of Bucciarelli [64] in which the daily net power PDF was represented by two events with discrete probabilities. The probabilities, p and q, and the magnitude of Δ were chosen in order to keep the 0^{th}, 1^{st}, and 2^{nd} moments the same as in the actual distribution.

A slightly different method for calculating p, q, and Δ is used in this thesis because it is desired to have a two-point approximated distribution of battery power instead of net power. Given a PDF of net power reconstructed from the moments using a method from the previous section, in order to approximate the battery power distribution, all of the battery losses must be properly accounted for. Therefore, Equation 4.3 must be satisfied. This is true if the following equations are satisfied:

$$p \cdot (-\Delta) = \frac{1}{\sqrt{\eta_b}} \int_{-\infty}^{0} P f_N(P)\, \mathrm{d}P \tag{4.29}$$

$$q \cdot \Delta = \sqrt{\eta_b} \int_0^\infty P f_N(P)\, \mathrm{d}P \tag{4.30}$$

$$p + q = 1 \tag{4.31}$$

These three equations are solved for the three unknowns.

4.7.1 Random Walk

The advantage of the two-event approximation is that random walk theory can be applied to estimate the required battery capacity. The probabilistic models assume a stationary process and therefore random walk theory provides the basis for calculating the probability of being in any of the discrete levels of battery charge.

The fluctuating battery stored energy can be modelled as a Markov process since the battery charge state depends only on the previous state and the change in stored energy in the current time step. With two-event approximation for the battery power distribution, the change in stored energy is either $(-\Delta \cdot \mathrm{d}t)$ with probability p or $(+\Delta \cdot \mathrm{d}t)$ with probability q. Here, $\mathrm{d}t$ is the time step of each step in the Markov process.

Defining the process in this way means the entire storage capacity is divided into N discrete levels where:

$$N = \frac{E_{cap}}{\Delta \cdot \mathrm{d}t} \tag{4.32}$$

and the transition matrix, M, for the N storage states is shown in Equation 4.33 along with the vector π containing the probability of being in each of the states assuming a stationary process.

$$M = \begin{bmatrix} p & q & 0 & \cdots & \cdots & \cdots & 0 \\ p & 0 & q & 0 & & & \vdots \\ 0 & p & 0 & \ddots & \ddots & & \vdots \\ \vdots & 0 & \ddots & \ddots & \ddots & 0 & \vdots \\ \vdots & & \ddots & \ddots & 0 & q & 0 \\ \vdots & & & 0 & p & 0 & q \\ 0 & \cdots & \cdots & \cdots & 0 & p & q \end{bmatrix}; \quad \pi = \begin{bmatrix} \pi_1 \\ \pi_2 \\ \vdots \\ \pi_i \\ \vdots \\ \pi_{N-1} \\ \pi_N \end{bmatrix} \tag{4.33}$$

The only possibility for the battery state to stay the same between time steps is if it is fully charged and there is excess energy or if it is empty and there is an energy

deficit.

Under steady state (since stationarity is assumed), the following relationship is true:

$$M \cdot \pi = \pi \tag{4.34}$$

In this case, the solution is [64]:

$$\pi_i = a^{i-1} \frac{1-a}{1-a^N} \quad : \quad i = 1, 2, ..., N \tag{4.35}$$

where $a = q/p$. The loss of load probability (LOLP) for a system without diesel is therefore equal to the product of the probability that the battery charge is in the lowest possible state and the probability that the battery is currently discharging:

$$\text{LOLP}_t = \pi_1 p \tag{4.36}$$

This is the probability of not meeting the load in a single time step, thus the subscript t. Manipulating these equations, the required battery capacity for a particular LOLP_t is [64]:

$$E_{cap} = \frac{\ln\left[1 + \frac{p(a-1)}{\text{LOLP}_t}\right]}{\ln\left[a\right]} \cdot \Delta \cdot \mathrm{d}t \tag{4.37}$$

There is one condition for it to be possible to calculate the numerator in the above equation:

$$p < q + \text{LOLP}_t \tag{4.38}$$

This makes sense since the battery charge cannot be sustained if the probability of discharging is greater than the probability of charging by more than the allowable LOLP.

It is desired that the LOLP be prescribed as the probability that the load is not met in *any* time step over the entire year. The LOLP_t in each time step is calculated by:

$$\text{LOLP}_t = 1 - (1 - \text{LOLP})^{\mathrm{d}t/8760} \tag{4.39}$$

where $\mathrm{d}t$ is in hours.

4.8 Final Models

The combined time series/probabilistic model and the fully probabilistic model are both described here. It was previously mentioned that probabilistic methods have significant disadvantages when compared with time series models, such as the inability to track the state of charge with time. Additionally, it is often necessary to run a time series simulation in order to confirm the results from a probabilistic model or "calibrate" its parameters [17]. Therefore, the objective here is not to develop a probabilistic model to be used on its own for sizing the components of a power system. Rather, it is to create a probabilistic model that can predict the error to be expected from a time series simulation based on hourly means. From this, the goal is to deduce the level of temporal resolution necessary for sufficient accuracy in a time series simulation or optimization. The models are described here and compared with the time series model for two case studies in the next chapter.

4.8.1 Time Series/Probabilistic Model

The overall algorithm for the time series/probabilistic model is shown in Figure 4.5. More detailed descriptions of the individual steps are provided in this section.

1. Read in u, G, P_l: High resolution arrays of wind speed, solar radiation, and load data are read in, spanning the entire year.

2. Bin: These data are binned by hourly mean wind speed, solar radiation, and load. In this thesis, 50 equally spaced bins are used for each data set.

3. Calculate P_w, P_s: High resolution wind data is converted to wind power values by:

$$P_w = \begin{cases} \frac{1}{2}\rho A C_{P,max} u^3 \eta_{gen} & : u < U_r \\ P_{w,r} & : u \geq U_r \end{cases} \tag{4.40}$$

   where U_r and $P_{w,r}$ are the rated wind speed and power. Therefore, this results in sets of wind powers binned by hourly mean speed. It ignores turbine dynamics. For solar, the horizontal radiation data is converted to radiation on the tilted surface as shown in Appendix A.1 and converted to power values by:

$$P_s = P_{s,r} f_{PV} \frac{G_T^H}{G_{T,STC}} \tag{4.41}$$

which ignores cell temperature effects.

4. Calculate μ'_w, μ'_s, μ'_l: The first m raw moments are calculated in each bin for the resource and load distributions.

5. Run time series: In each hour, wind, solar, and load powers are represented by the statistical moments calculated previously in the corresponding bin based on the hourly mean wind speed, solar radiation, and load in that time step. Nearest point interpolation is used to identify the correct bin. The wind, solar, and load cumulants are calculated using Equation 4.12. The net power cumulants are calculated based on Equation 4.19. After this step, the net power cumulants are known for each hour.

6. Estimate required $P_{d,r}$: To estimate the required genset capacity, first the hour with the lowest net power expected value, κ_1, is identified. The capacity is then

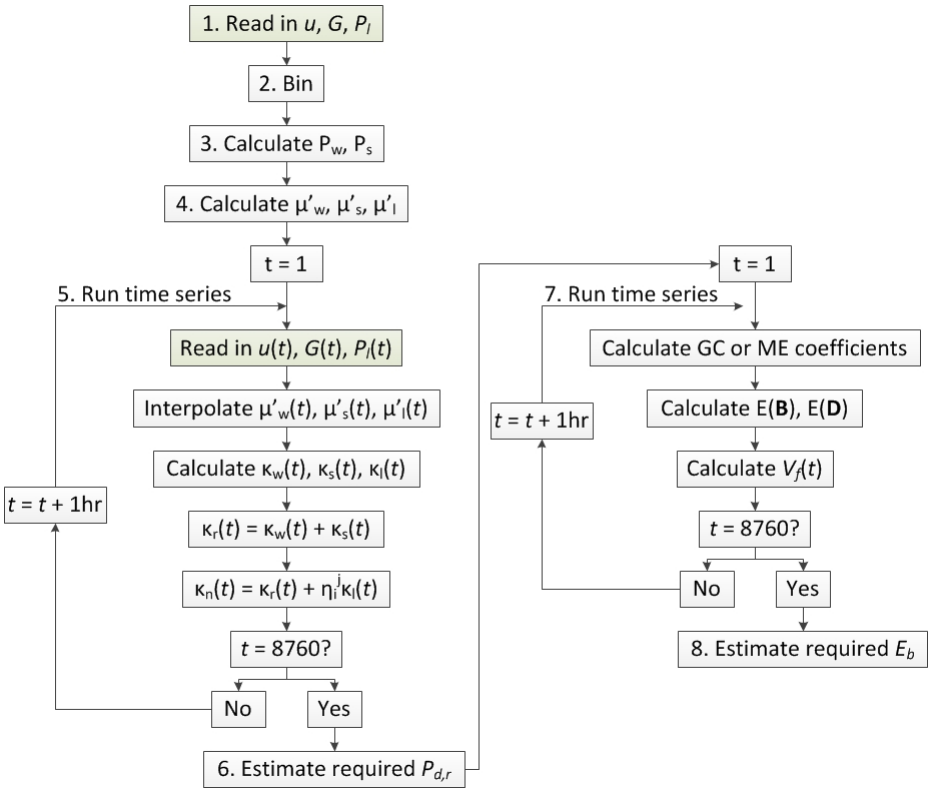

Figure 4.5: Fundamental algorithm for time series/probabilistic model

estimated by solving the following optimization:

$$\begin{aligned} \underset{P}{\text{maximize}} \quad & P \\ \text{subject to} \quad & \psi \leq \text{LOLP}_t \\ & P \leq 0 \end{aligned} \tag{4.42}$$

where LOLP_t is the loss-of-load probability in each sub-hour time step and ψ is an integral of the net power distribution as shown in Figure 4.6. The genset capacity, $P_{d,r}$, is the absolute value of the solution to this optimization and the minimum power output is 30% of this. The user-prescribed LOLP is the probability of not meeting the load at *any* time within the hour. One can be determined from the other by:

$$\text{LOLP}_t = 1 - (1 - \text{LOLP})^{T_{hr}} \tag{4.43}$$

where T_{hr} is the high resolution time step in hours.

7. Run time series: Again the time series is run. This time, the generator capacity is known; therefore the minimum power output is also known (30% of rated power). In each hour, Equations 4.3–4.4 are solved, though the generator equation is adjusted for the minimum run time as described shortly. Gram-Charlier expansion is used to define f_N since the maximum entropy method proved to be too time consuming in this model. Since Gram-Charlier expansion can result in

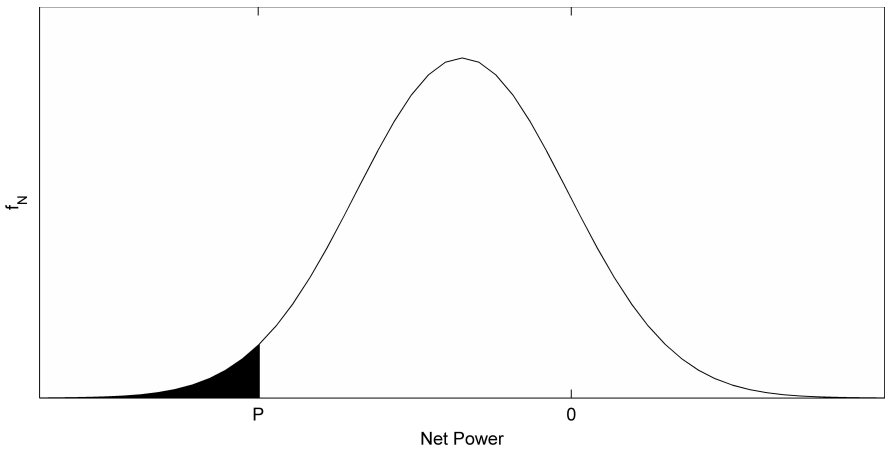

Figure 4.6: Definition of ψ for determining generator capacity

negative probabilities, a check is added and the number of moments calculated is reduced if necessary until an acceptable distribution is found. This gives the expected value of the battery and genset power within each hour.

As mentioned the equation for the expected genset power is adjusted for the minimum run time, T_{min}. This affects the time steps in which the net load is positive so the genset is not needed yet it is forced to continue to run because it has been on for less than T_{min}. The probability that the net load is positive is:

$$p^+ = \int_0^\infty f_N(P)\,\mathrm{d}P \tag{4.44}$$

Assuming the net power is independent between the high resolution time steps within the hour, then the probability that the generator is forced to run at any time is:

$$p_{run} = 1 - (p^+)^{(T_{min}/T_{hr}-1)} \tag{4.45}$$

For example, if T_{min} is ten minutes and T_{hr} is one minute, then this probability is equal to the probability that the generator was not running in any of the previous nine minutes. Adding this factor to Equation 4.4 gives the new mean generator power output:

$$\mathrm{E}[\boldsymbol{G}] = -\int_{-\infty}^{-P_{min}} P f_N(P)\,\mathrm{d}P + P_{min}\int_{-Pmin}^{0} f_N(P)\,\mathrm{d}P + P_{min}p_{run}p^+ \tag{4.46}$$

Next, the fuel consumption is estimated in each hour, which are then summed over the entire year. Applying the linear relationship between power output and fuel consumption in Equation 2.13, the high resolution fuel consumption over the hour is:

$$V_f = F_1 P_{d,r} + [1 - p^+(1 - p_{run})]F_0\mathrm{E}[\boldsymbol{G}] \tag{4.47}$$

The second term accounts for the probability that the net power is positive and the generator is not forced to run so it can be shut off and can save the idling fuel consumption.

8. Estimate required E_b: The required battery capacity is estimated by assuming the batteries are initially fully charged and the energy in the batteries, E_b, is set to the datum point of zero. The required capacity is simply equal to the

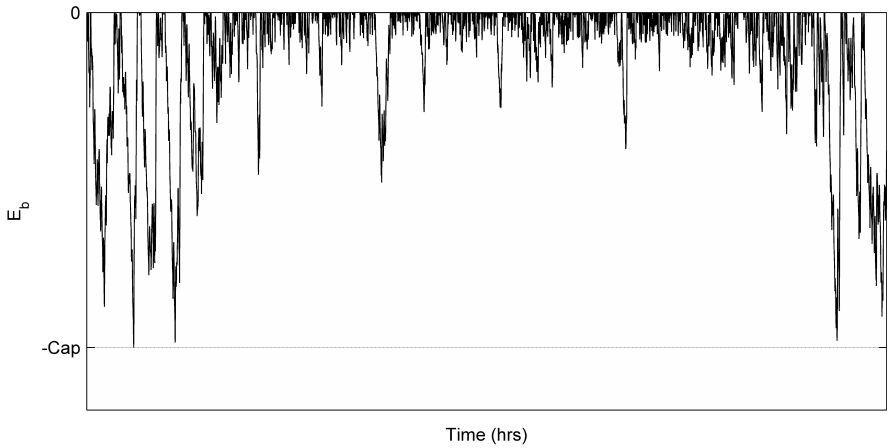

Figure 4.7: Determining battery capacity for time series/probabilistic simulation

minimum drop below zero over the course of the year with the constraint that E_b can never be positive (Figure 4.7).

What sets this type of model apart from the fully probabilistic model is that it accounts for the synoptic and diurnal trends of the resources and load. Also, since the PDFs of wind, solar, and load are defined within each hour, the assumption of independence between system elements is more valid. Though there are clearly dependencies between all three of these variables, they are mostly over longer time scales (seasonal and diurnal) and are likely negligible within the hour. The analysis in the next chapter will help determine the validity of this assumption and also whether it is necessary to capture the long-term trends in the data for the purposes of predicting the error from low temporal resolution.

The main disadvantage of this model is its slow speed. In each of the 8760 time steps, the net load distribution must be reconstructed from its cumulants and integrated to calculate the battery and generator power. For this reason, the maximum entropy method is impractical for PDF reconstruction since the computational time is significantly longer. Also, since PDF reconstruction occurs in each time step, there are more opportunities for errors such as a negative PDF using Gram-Charlier expansion or a problem during the minimization in the maximum entropy method.

4.8.2 Probabilistic Model

The algorithm for the fully probabilistic model is shown in Figure 4.8. Unlike the time series/probabilistic model, the input data is not binned. Instead the statistical

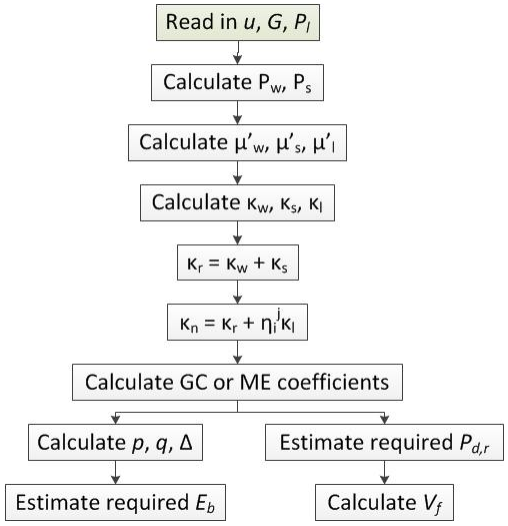

Figure 4.8: Fundamental algorithm for probabilistic model

moments are calculated from the high resolution data spanning the entire year. Again, the cumulants for wind power, solar power, and load are calculated from the moments and the net power cumulants are determined by cumulant arithmetic. Therefore, the resulting net power distribution reconstructed by Gram-Charlier expansion or the maximum entropy method includes information from the entire year.

Estimating the required battery capacity is difficult because any information regarding synoptic and diurnal trends is lost. The probabilistic method assumes that the wind, solar, and load power are independent random variables with no correlation between time steps or with one another. Of course, this assumption is not true. All of these variables have some dependence on the time and date and on each other [76]. The question being asked here is whether the validity of this assumption is important for getting a reasonable estimate of the temporal resolution error in a time series simulation. In this case, the battery capacity is estimated by using a two-event approximation for the battery power distribution and using random walk theory from Section 4.7.1 to determine the battery capacity required to meet a prescribed LOLP. Since random walk theory assumes that each step is independent, it is important to choose a step size, dt, that is not so short that each step is highly dependent on the last. For example, a 1-minute step would definitely give inaccurate results since wind, solar, and load power would all be highly correlated between time steps. In this thesis, dt was somewhat arbitrarily chosen to be six hours in order to divide each day into four equal parts (morning, midday, evening, night). The required generator

capacity was estimated by Equation 4.42 as in the time series/probabilistic model.

The advantage of this model is that it is faster than the time series/probabilistic model. Also, PDF reconstruction only happens once and it is therefore easy to identify when there is an issue. The next chapter will analyze results from the two models developed in this chapter for two particular case studies. This will help determine whether the simplest probabilistic model is suitable for predicting temporal resolution error despite its recognized flaws.

Chapter 5

Case Studies

Ideally, the models developed in the previous chapter could be implemented by a system designer with access to only hourly mean resource and load data. This would require the ability to accurately synthesize higher frequency data from the hourly means or to accurately model a PDF of the resources and load, which proved to be a difficult task in Section 4.3. The analysis of the models in this chapter will not attempt to measure the accuracy of synthesizing data or assuming particular distributions. Instead, it will model the resource and load distribution based on the moments of high frequency data. The ability to obtain an accurate estimate of these moments from only the hourly means, whether it be from data synthesis or more accurate assumed PDFs, is left for future work.

In particular, this analysis will investigate the estimated error in battery capacity and diesel fuel consumption from the time series/probabilistic and fully probabilistic models. The results will be compared with the results from time series simulations for two case studies. The final discussion will address the effectiveness of the probabilistic models and make general recommendations for future studies.

The highest resolution (1-second time step) time series simulation is assumed to provide the actual solution. The accuracy of any of the models using any time step could be calculated by comparing with this result. However, the purpose of the probabilistic models is to avoid running high resolution time series simulations. For this reason, temporal resolution error is measured relative to a higher frequency simulation from the same model. In a sense, this is a measurement of the precision of the model using different time steps. This precision is then compared alongside the precision of the time series model in order to evaluate the effectiveness of the model as a tool for measuring temporal resolution error.

The first case study is for the same system analyzed in the sensitivity analysis in Chapter 3. The purpose of this case is to investigate the capabilities and accuracies of the models developed in the previous chapter. The second case study is for an integrated multi-trophic aquaculture site on Vancouver Island, BC. This system is for the Kyuquot SEAFoods Ltd. site and was the initial inspiration for the analysis of temporal resolution in system models because of its highly variable load.

5.1 Model Overview

Five different models are used for the analysis in this chapter, including both models developed in the previous chapter. The fully probabilistic model is implemented with both Gram-Charlier expansion and the maximum entropy method.

- Full Time Series (FTS): This model is the same as was used for the sensitivity analysis in Chapter 3 but stripped down to remove unnecessary calculations such as the economics module. Detailed component models are included such as the 4.5 kW dynamic wind turbine Simulink model and temperature effects in the PV model. The required battery capacity is estimated by assuming the batteries are initially fully charged similar to Figure 4.7 for the time series/probabilistic method. The required genset capacity is equal to the largest net load deficit of all time steps.

- Simplified Time Series (STS): This is similar to the FTS model but ignores all turbine dynamics (i.e. there is a direct relationship between wind speed and power) and PV temperature effects. Wind and solar power are calculated by Equations 4.40 and 4.41, respectively. Also, the treatment of the inverter efficiency is slightly different than the FTS model. As evident from the schematic in Figure 2.1, power only flows through the inverter when it is required to meet the AC load. For example, excess renewable power is already DC and can directly charge the batteries while power discharging from the batteries must be converted to AC to meet the load. This is how the FTS models the system but the STS model immediately applies the inverter efficiency to any renewable power generated. This should be a reasonable assumption if the simulation covers an adequately long period of time and a one year simulation is expected to be adequate. All assumptions made in the STS model are also made by the

probabilistic models. The purpose of this model is to determine the validity of these assumptions.

- Time Series/Probabilistic (TSP): As described in Section 4.8.1. The first four moments are used for the reconstruction. However, as mentioned earlier, Gram-Charlier expansion can produce negative probabilities. Therefore, a check is included. If negatives are found, the number of moments is reduced until an acceptable distribution is created. The hourly LOLP is 0.1%.

- Probabilistic using Gram-Charlier reconstruction (PGC): As described in Section 4.8.2 using Gram-Charlier expansion for PDF reconstruction. The first five moments are used unless negative probabilities are found. The 6-hour LOLP is 2%.

- Probabilistic using Maximum Entropy reconstruction (PME): As described in Section 4.8.2 using the maximum entropy method for PDF reconstruction. The first five moments are used unless the optimization procedure crashes. The 6-hour LOLP is 2%.

5.2 Off-Grid Residential Power System

This case study is for the same system as in the sensitivity analysis. This included a residential load with a heat pump, a water heater, and several other appliances as well as wind and solar data from NREL's SRRL database [58]. It is used to evaluate the usefulness of the probabilistic methods by comparing the results with those from the time series method.

5.2.1 Battery Backup

Time Series Results

The metric for evaluating the accuracy of a 1-hour time series simulation will be the difference between the required capacity for the 1-hour simulation and the required capacity using a shorter time step. To evaluate the ability of the probabilistic models to estimate this error, the actual difference in capacities must be calculated first. For this comparison, the full time series (FTS) model was run for a range of wind and

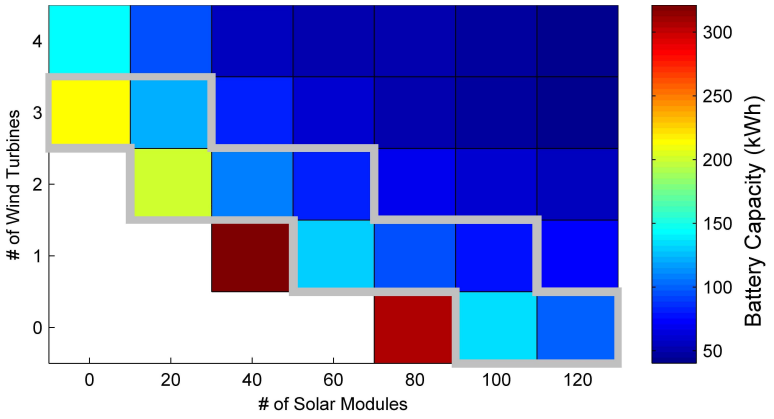

Figure 5.1: Required battery capacity for a 1h time series simulation

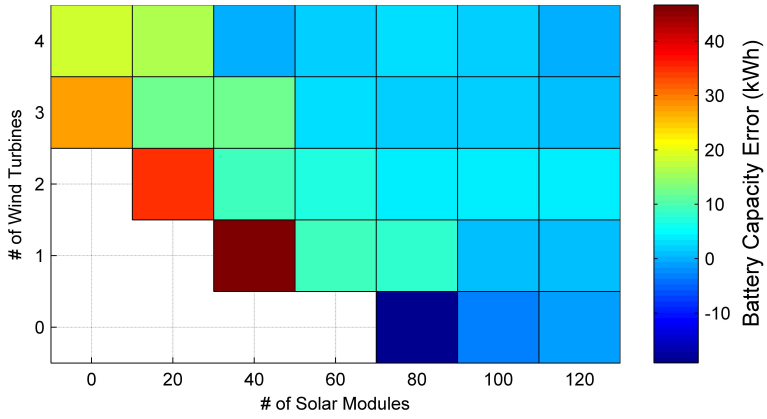

Figure 5.2: Battery capacity error in time series simulation, $E_{b,1\text{hr}} - E_{b,10\text{min}}$

solar component sizes. The number of wind turbines varied from 0 to 4 in increments of 1 and the number of solar modules varied from 0 to 120 in increments of 20.

The required battery capacity was determined for each combination of wind and solar component sizes and plotted in Figure 5.1. Some were omitted from the plot as they required extremely high capacities. The outlined region will be called the "feasible region" as it represents the component sizes that are most likely to be the optimal configuration based on the results from Chapter 3. It is this region that is of most concern when evaluating the ability of the probabilistic models to predict the accuracy of a 1-hour time series simulation.

If the same is done using shorter time steps, it is possible to calculate the battery capacity error of the 1-hour time series simulation relative to the higher resolution

simulation. For example, the error relative to a 10-minute simulation is plotted in Figure 5.2 over the range of component sizes. Negative errors mean the 1-hour capacity is less than the 10-minute capacity.

Model Comparison

Table 5.1 lists the battery capacity error between a 1-hour and 10-minute time step using each of the models defined in the previous section.

Comparing the simplified time series (STS) model with the FTS model, the reults are fairly close, though some differences are noted. Since this table is comparing a 1-hour time step with a 10-minute step, turbine dynamics should be insignificant. Also, the biggest discrepancy is for the configuration without any PV modules. Therefore, the PV temperature effects are not the most significant. It appears that any differences can be attributed to how the inverter efficiency is handled. Since the probabilistic models make the same assumptions, they cannot be expected to perform better than the STS model.

It is surprising therefore that, for most configurations, the time series/probabilistic (TSP) model did do a better job of predicting the error than the simplified time series model. There is no logical reason why this would be true. However, it clearly shows that this type of model is able to accurately estimate the higher frequency effects in the simulation. The information lost in the TSP model is the ordering of sub-hour data. The good agreement between the STS and TSP results suggest that

Table 5.1: Battery capacity error (kWh), $E_{b,1\text{hr}} - E_{b,10\text{min}}$

Configuration	FTS	STS	TSP	PGC	PME
0S-3W	27.2	21.9	22.8	-5.2	-13.0
20S-3W	12.2	11.1	12.4	-4.7	-11.3
20S-2W	35.3	29.9	32.6	-7.6	-12.1
40S-2W	9.0	7.0	8.0	-6.0	-8.6
60S-2W	7.0	6.6	6.9	-5.1	-7.8
60S-1W	9.6	9.1	6.8	-8.7	-10.8
80S-1W	7.7	7.2	4.8	-6.9	-9.3
100S-1W	0.9	1.5	2.7	-6.1	-8.5
100S-0W	-3.0	-0.1	-2.7	-11.9	-13.4
120S-0W	-1.3	-0.0	-1.1	-9.5	-13.8

S - 0.175kW solar module, W - 4.5kW wind turbine

the assumption that sub-hour wind, solar, and load power are independent random variables is reasonable.

Since the statistical moments of the sub-hour distributions were calculated directly from high resolution data sets, this result is a "best-case scenario" that could be obtained if accurate sub-hour distributions of solar, wind, and load data are known or if the high frequency data can be accurately synthesized. Section 4.3 showed that this can be difficult and that even widely accepted distributions, such as the Gaussian distribution for short-term wind speeds, are not always accurate enough (though these assumed distributions would be better than ignoring high resolution effects altogether).

Though it was not initially the intention, the time series/probabilistic model that has been developed could actually be used on its own for designing a system instead of merely predicting temporal resolution error. The fundamental concept is similar to that of Hybrid2 but it has some additional features, including the ability to add variability to the solar resource within the hour as well. By using the method of cumulants, distributions with higher order moments can be specified as opposed to the assumption of Gaussian distributions for wind speeds and loads in Hybrid2.

It is evident from the final two columns of Table 5.1 that the probabilistic model is not good at predicting the error. This is true regardless of the method of choice for PDF reconstruction. With this model, the 1-hour capacity was smaller than the 10-minute capacity for all configurations, as opposed to the opposite result found using the time series model for configurations with at least one wind turbine. The reason for this is because 10-minute data generally have a higher variance leading to a greater likelihood of large drops in power in the random walk portion of the probabilistic model.

The main reason for the poor performance of the probabilistic model is that it does not account for long-term trends. In fact, the required capacity is largely influenced by synoptic and diurnal variations. To be more accurate, some form of autocorrelation should be added to the model. Exactly how to determine this autocorrelation and how to implement such information into the probabilistic model was not within the scope of this thesis but could potentially make the model significantly more useful since the computational time is much lower than for the TSP model.

Results comparing the 1-hour time step with time steps shorter than 10 minutes are shown in Appendix D.1. The same general conclusions were found in all cases.

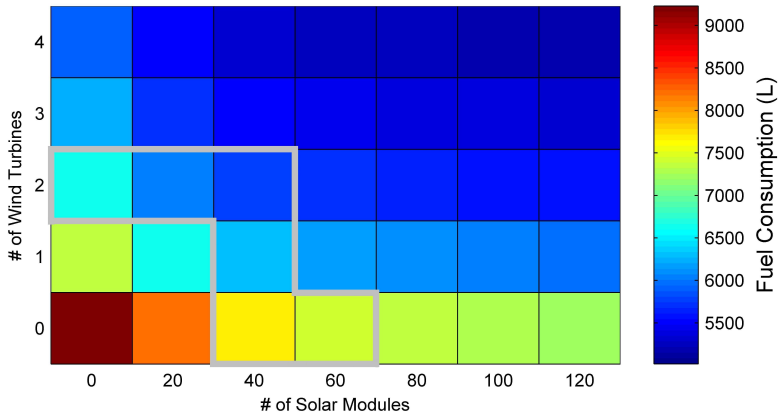

Figure 5.3: Annual fuel consumption for a 1h time series simulation

5.2.2 Diesel Backup

Time Series Results

In this case the evaluation metric is the difference in total fuel consumption over the year. The 1-hour fuel consumption for the FTS simulation is shown in Figure 5.3. Again, the outlined region is the "feasible region" that will be considered for the model comparison.

Model Comparison

The fuel consumption was estimated and compared using all five models for each of the configurations in the feasible region. Table 5.2 lists the estimated fuel consumption error between a 1-hour and 10-minute time step.

Table 5.2: Fuel consumption error (kL), $V_{f,1\text{hr}} - V_{f,10\text{min}}$

Config.	FTS	STS	TSP	PGC	PME
0S-2W	-4.3	-4.3	-18.0	-5.9	-5.9
20S-2W	-3.3	-3.4	-19.0	-6.0	-5.9
40S-2W	-3.0	-3.1	-19.4	-6.4	-6.5
40S-1W	-3.9	-3.9	-18.7	-5.5	-5.9
40S-0W	-6.5	-6.5	-17.3	-5.2	-7.8
60S-0W	-6.0	-6.0	-17.6	-5.9	-6.9

S - 0.175kW solar module, W - 4.5kW wind turbine

Again, the results from the STS model are very similar to the FTS model. Therefore, any major differences in the results from the probabilistic models cannot be attributed to the assumptions that ignore wind dynamics and the PV cell temperature.

The results from all three of the probabilistic models correctly show that the 1-hour simulation significantly underestimates the fuel consumption relative to the 10-minute simulation. However, they do not accurately estimate the magnitude of this error. The TSP model estimates an error up to more than six times greater than the actual error in the time series simulation. The estimated error from the probabilistic model (PGC and PME) is closer in magnitude but does not follow the same increasing/decreasing trend as the FTS results. Clearly, these models are not suitable for estimating the temporal resolution error of time series simulations of systems with diesel backup.

One reason for the large error in the TSP model results is that the net power distribution is not represented accurately enough by Gram-Charlier expansion. In particular, this method is only accurate if the distribution is roughly Gaussian. Of course, this is not always true, particularly with the residential load of this case study. This can lead to an overestimate of the fuel consumption. Consider one hour of the year in which there is steady renewable power from wind or solar power but the load fluctuates between very small and very large values because the heat pump operates for 20 minutes. The net power would be positive and steady for 40 minutes but drop significantly negative for 20 minutes. In a 1-minute time series simulation, the genset would turn on for 20 minutes to supply the heat pump. Now consider that the net load is approximated by a Gaussian distribution. The 20-minute heat pump operation will lower the mean and increase the variance of the net power significantly. But it cannot properly represent the large spikes in load. The largest probability will be around the mean net power which is less than the actual net power when the heat pump is not running but greater than the net power when it is. Since this mean is typically fairly close to zero, it will predict that the genset must run very inefficiently in order to meet a very small load far more often than it actually does. Since there is a constraint limiting the minimum generator power output, much more power will be dumped and more fuel consumed.

This is an inherent challenge with PDF reconstruction methods in general. Loads that are not Gaussian are typically not well represented, which motivates more complicated methods such as convolution, fast Fourier transforms, and point estimate

methods. For the method used in this thesis, some other PDF reconstruction method is necessary. Gram-Charlier expansion is only accurate for distributions that are roughly Gaussian. The maximum entropy method is too time-consuming for the TSP model and is severely limited by the number of input moments, meaning it cannot properly model this type of residential load either. For systems models of larger communities, multiple residences would smooth the load profile and could potentially provide better results.

The results for time steps less than 10 minutes are shown in Appendix D.2.

5.3 Integrated Multi-Trophic Aquaculture Site

The second case study is for the Kyuquot SEAFoods Ltd. aquaculture site that was the initial inspiration for the analysis of the temporal resolution in system models.

5.3.1 Project Background

With the recent growth of the global aquaculture industry [77], concerns have been rising regarding the social and environmental sustainability issues associated with it [78]. As with other animal husbandry practices, one such concern is the level of greenhouse gas (GHG) emissions associated with the production of farmed fish. Pelletier *et al.* [79] found that the production of one live-weight tonne of salmon in British Columbia results in GHG emissions of 2370 kg CO_2-e.

One method being developed to address some of these sustainability concerns is integrated multi-trophic aquaculture (IMTA). IMTA is a form of polyculture that combines the cultures of fed organisms (finfish or shrimp) with organisms that extract either dissolved inorganic nutrients (seaweeds) or particulate organic matter (shellfish). While the primary goals of IMTA are to reduce eutrophication and increase economic diversification [80], the sites have also been shown to reduce GHG emissions as well. Nobre *et al.* [81] found that an abalone and seaweed IMTA configuration, with a 240 ton/year yield, operating side-by-side with an abalone monoculture in South Africa reduced GHG emissions from 11.6 to 11.3 thousand tons CO_2-e per year. This improvement is fairly small and the level of GHG emissions remains significant.

For the average aquaculture salmon, feed accounts for 94% of its GHG emissions while farm-level energy use accounts for only 4% [79]. These numbers suggest that the level of GHG emissions is not a driving factor for incorporating clean power sources for

Figure 5.4: Location of Kyuquot SEAFoods Ltd.

the farm-level energy supply at aquaculture sites. Development of feed formulations with less environmental cost would be more effective at reducing GHG emissions. Therefore, for a renewable energy system to be justified, it must be advantageous for economical and logistical reasons. In fact, most aquaculture sites are far removed from the electrical grid and the cost of running power lines or transporting diesel fuel can often make renewable energy systems feasible in such locations. The slightly lower GHG emissions and improved social perception are additional benefits as well.

The proposed energy system is for Kyuquot SEAFoods Ltd., an IMTA site located in the northwest portion of Vancouver Island (Figure 5.4). The site is both a commerical farm and a research lab for developing the IMTA process.

On the cage system at this farm is a tram structure designed to move along the cages. The tram includes six winches that are used to lift scallop-filled nets out of the water for grading, maintenance, and harvest. Currently, these winches are hand-powered but are to be replaced by electric winches in the future to improve worker efficiency. The purpose of the proposed system is to power these electric winches. It can serve as a model test-case for future IMTA sites as well.

Load Data

A unique property of the power system is the spiky loads caused by the on/off schedule of the winches. Since the site was not yet in full operation at the time of this study, it was difficult to predict the magnitude and shape of the load profile. For this analysis,

a worst-case scenario was estimated in which each of the six winches would run three long lifts and twelve short lifts each hour for a ten hour work day. The long lift, assumed to be 12 m long, represented the initial lift to bring the nets out of the water. The short lift, assumed to be 0.3 m long, represented the small incremental lifts to access different layers of the net. A simple time step model balancing the forces of gravity, drag, buoyancy, and tension was created to determine the length of each lift.

In this model, the drag coefficient, C_d, was required. It was assumed that each scallop layer could be modelled as a flat disk. The C_d value for a thin disk is 1.17 [60]; however, no values are listed for the drag over multiple parallel disks and no study could be found that provided this information. A water tunnel experiment was completed to compare the drag over a single disk with the drag over multiple disks. The number of disks, spacing between disks, and water velocity were varied and the drag was measured using a counterweight by summing moments. The measured C_d for a single disk with a water velocity of 0.44 m/s was 1.18. This was only a 0.9% error from the theoretical value. However, when the velocity was increased to 0.52 and 0.60 m/s, the C_d values for one disk were 1.32 and 1.29 (13.2% and 9.9% errors). This discrepancy could have been caused by several factors including effects from the support structure for the experiment and human error. As the number of disks increased, the measured C_d values remained very similar. In total, 27 trials were completed that varied the number of disks (from 1 to 5), the spacing between disks, and the water velocity. The error relative to the theoretical C_d value for a thin

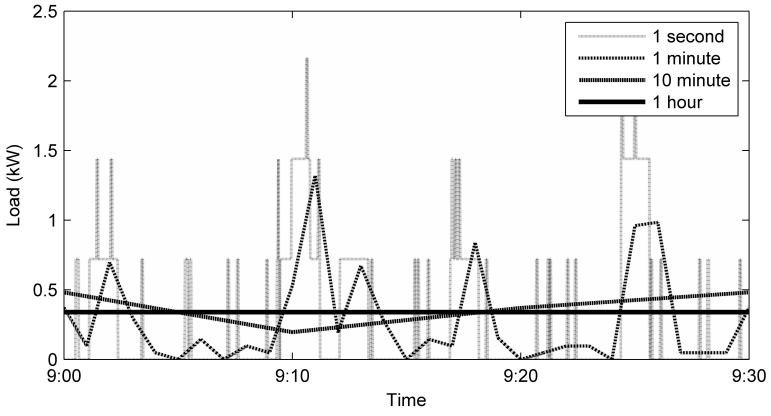

Figure 5.5: Half-hour sample from load profile

disk was between 0.5% and 17.1% for all trials and had an average error of 6.0%. Therefore, this experiment made it evident that additional disks in parallel did not significantly affect the total drag and a constant C_d of 1.17 could be assumed.

The winch was assumed to provide 720 W and have a maximum speed of 0.1778 m/s (35 ft/min). The total lift times of the long and short lifts were calculated to be 75 s and 4 s, respectively.

To add some variability, a load profile for each winch was created for each day of the year where the length of time between each long lift and short lift was taken at random from a normal distribution with the mean required to ensure the correct number of lifts per hour. A half-hour sample from a typical day is shown in Figure 5.5. It is clear the profile is artificially smoothed over the longer time steps.

Wind Data

The wind data used in this analysis was gathered from an instrument buoy located about 100 m from the cage system, where the potential wind turbine would be located. The anemometer on the buoy is approximately 1.5 m above the surface of the water. The average wind speed and direction has been recorded once every hour since 01 June 2007. For this analysis, data for one full year (January - December 2008) were used.

The wind speed was scaled to a 15 m rotor height using the logarithmic relationship [82]:

$$V(z_R) = V(z)\frac{\ln(z_R/z_0)}{\ln(z/z_0)} \tag{5.1}$$

where z_R is the rotor height, z is the height of the known velocity, and z_0 is the surface roughness height. Depending on the assumed roughness height, the adjusted wind speed can vary somewhat significantly because the height of the anemometer was so low. Because the terrain at the site was unusual (mountains, trees, a building, and the cage system), it was difficult to confidently estimate the surface roughness. To get a better idea, a meteorological tower was installed at the site with three anememoters, a wind vane, and a temperature sensor. However, the currently limited available data has not provided a conclusive result. In lieu of an accurate estimate of the surface roughness from the data, it is assumed to be 0.001 m, which is close to the value for blown sea. Sub-hour data was again synthesized from the Kaimal spectrum.

Solar Data

Solar radiation data for this analysis was obtained from HOMER at the site's coordinates (50°2' N, 127°17' W). HOMER synthesizes a typical meteorological year (TMY) using monthly averages of radiation data from the NASA Surface Solar Energy Data Set [83] and statistical properties that reflect global averages. Sub-hour data was simply interpolated. This was assumed to be reasonable since the actual sub-hour distribution of solar data has been shown to be less significant than the wind and load distributions.

5.3.2 Results

For several reasons, only batteries are considered for backup power at the aquaculture site. First, the load is such that the genset would be idling for a large majority of the time between lifts and it would therefore be wasteful and have a shorter lifetime. Also, eliminating the use of diesel fuel reduces emissions (especially since it must be transported to the site) and is likely beneficial from a marketing standpoint as it is an IMTA farm aiming for a more sustainable process. Finally, the previous case study showed that the probabilistic models were not effective for modelling systems with generator backup.

A 1-hour optimization using the time series model from Chapter 2 outputs an optimal system configuration of:

14 PV modules
0 Wind turbines
16 Batteries
NPC: $26,822.38

To estimate the effect of temporal resolution on this optimization, the time series/probabilistic model was run with this configuration of solar cells and load to determine the required battery capacity. The estimated error relative to several shorter time steps is shown in Table 5.3. The results using the fully probabilistic model (with both methods of PDF reconstruction) are included for reference despite being previously shown to be poor estimators of the temporal resolution error.

To understand the context, the 16 batteries in the optimal configuration have a capacity of 35.52 kWh. In order to keep the system voltage at 48 V, batteries can be added in increments of 8 (or 17.76 kWh). Therefore, the error using a 1-hour time

Table 5.3: Battery capacity error (kWh) relative to 1h optimal configuration

	10 Minute	**1 Minute**	**10 Second**	**1 Second**
TSP	-1.3	-4.8	-6.1	-1.2
PGC	-0.3	-2.5	-3.5	-4.1
PME	-0.5	-3.8	-5.0	-5.6

Table 5.4: Optimal configuration with different time steps

	S	**W**	**B**	**NPC**
1 Hour	14	0	16	$26,822
10 Minute	14	0	16	$26,822
1 Minute	15	0	16	$27,950
10 Second	15	0	16	$27,950

S - 0.175kW solar module; W - 400W wind turbine; B - 370Ah battery

step instead of a 10-second time step estimated with the TSP model is only 34% of the battery bank increment. The TSP model estimates the temporal resolution error but does not recommend a best course of action in order to account for this error. If the error is large, higher resolution data should be obtained and the time series model should be run with a shorter time step. If the error is small, a small addition of PV modules, a wind turbine, or batteries should be sufficient. There is no "right" answer for which is best but a designer is likely to get a better feel for this as she or he gains experience.

As for this system, the temporal resolution error is small enough that a system designer could be quite confident that a shorter time step is not required. The addition of a few additional PV modules, a small wind turbine, or 8 batteries to the 1-hour optimal configuration is recommended to account for the temporal resolution error. With two additional PV modules, the NPC increases to $29,077 using the time series model with a 1-hour time step. Alternatively, with a 400 W wind turbine, the NPC is $29,738. With 8 more batteries, it is $32,343.

Table 5.4 shows the optimal configuration from the time series model for each of the time steps. The 1-second time step is excluded for computational reasons.

Given these results, the optimal configuration includes 15 PV modules and 16 batteries. From the perspective of a system designer with only 1-hour data, the TSP model provided an estimate of the temporal resolution error. It accurately showed

that the 1-hour optimization likely undersized the system but that the error was less than the allowed incremental increases in storage capacity.

5.4 Summary of Findings

This chapter summarized two case studies intended to evaluate the probabilistic models and perform the preliminary system design for Kyuquot SEAFoods Ltd. This section provides a discussion of what was learned regarding the probabilistic models.

The time series/probabilistic model was developed in order to take advantage of the benefits of both time series and probabilistic models. Theoretically, by representing sub-hour data by probabilistic distributions, significant reductions in computational time could be made when trying to run a simulation that accounts for high temporal resolution features.

The results from this chapter have shown that modelling the sub-hour distributions based on moments calculated directly from the data provides an accurate representation of the temporal effects of a system with battery backup. This is important as it shows that exact knowledge of the sub-hour sequence of data is unnecessary. Therefore, if accurate sub-hour distributions can be determined based only on hourly data and site characteristics, the TSP model would be a very useful tool for estimating temporal resolution error.

Another contribution of this work is the method of cumulants that was used to do arithmetic of the random variables in the model. This technique makes it very simple to include many random variables that are not restricted to a particular form such as the Gaussian distribution. This is something unavailable in most other probabilistic models, including Hybrid2 which cannot model solar sub-hour distributions and limits wind speed and load data to the Gaussian form. Since wind speed distributions have been shown to be non-Gaussian at the tail ends and load distributions can take many forms depending on the location and application, this could be a useful next step for these types of models.

For systems with battery backup, the results from the first case study showed that the fully probabilistic model did not provide accurate estimates of the temporal resolution error. It can be concluded then that lower frequency trends such as synoptic and diurnal variations must be accounted for. Most probabilistic models ignore these. Gassner [17] assumed the distribution of the "storage period" mean wind speeds is Gaussian but the method assumes no correlation between the means based on month

or time of day. The Markov process used in this thesis also includes no autocorrelation or synoptic/diurnal correction factors. This is a topic that could benefit from future studies.

For systems with diesel backup, seasonal and diurnal trends do not affect the fuel consumption estimate. For example, there is no difference in fuel consumption whether the generator has to output 1 kW for 20 hours in January and 20 hours in August or for 40 hours in January and none in August. The end result is an output of 1 kW for 40 hours. There is no cumulative effect as there is with a battery being charged and discharged. The problem with the probabilistic models for estimating the fuel consumption is therefore different from the issues with battery backup. The main issue appears to be that the PDF reconstruction methods underestimate the tail ends of the distribution and overestimate the powers below the minimum allowable generator output, which leads to greater dump loads and fuel consumption. This is possibly due to the computational limitations of accurately reconstruction the net power PDFs based on higher moments of the distribution.

Chapter 6

Conclusions

In this thesis, the topic of temporal resolution in simulations and optimizations of renewable power systems was investigated. The optimizations considered were intended for component sizing in the overall system design. The main contributions were an analysis of the sensitivity of time series simulations to the chosen time step and progress towards a probabilistic model able to estimate the expected error due to the coarse temporal resolution of a 1-hour time step in a time series model.

A time series model with optimization capability was developed in Matlab. This model includes a dynamic wind turbine model capable of accounting for the turbine's inertia. The objective function of the optimization procedure was to minimize the net present cost with the constraint that the system must be autonomous with no unmet load over the 1-year simulation. A full-factorial algorithm was implemented to ensure a global minimum was found.

The sensitivity analysis first considered the individual components. Comparing a 1-second time step with a 1-hour time step, the energy output from the wind turbine dynamic model was found to increase by a maximum of 4.3% at wind speeds below the rated wind speed and decrease by a maximum of 7.0% at wind speeds close to the rated speed. There was a maximum decrease in fuel consumption of 5.6% in the genset simulation. The influence of the time step on the PV and battery simulations was negligible.

The time step sensitivity of the optimization was found to greatly depend on the system configuration. Systems with only diesel for backup were far more influenced by temporal resolution. With battery backup, the results showed better agreement between time step choices. With both diesel and batteries, the total system cost was less sensitive to the time step than the diesel-only systems. However, because of the

many factors that affect the reults of these systems, it was not possible to determine a general method for choosing an acceptable time step prior to a simulation. For this reason, probabilistic models were developed with the goal of estimating the temporal resolution error prior to the simulation.

Two probabilistic models were developed: a time series/probabilistic model and a fully probabilistic model. In the fully probabilistic model, first high resolution wind speed and solar radiation data are converted to wind power and solar power values based on simple relationships. The first m moments are calculated directly from these power values spanning an entire year and converted to cumulants. The cumulants of the net load are calculated using cumulant arithmetic and the probability density function is reconstructed using Gram-Charlier expansion or the maximum entropy method. In the time series/probabilistic model, wind speed, solar radiation, and load data are first binned by their hourly mean before being converted to power values. The moments and cumulants are calculated for each bin. Each hour of the year is treated like the fully probabilistic model such that the net power distribution is unique for each hour.

In developing these models, different methods of representing the variability of sub-hour data were investigated. One method is to assume a distribution shape and set the distribution parameters based on site characteristics or data. For wind speeds, it is common to assume a Gaussian distribution. The standard deviation is known if the turbulence intensity is known or assumed. However, the turbulence intensity is not typically constant at a particular location. Also, the Gaussian distribution does not properly fit the tail ends of real wind speed distributions and leads to an underestimate of the total wind energy generated. There is no widely accepted distribution for solar data within an hour and load distributions are highly variable depending on the application. Finally, the addition of two random variables with known probability density functions requires convolution which is computationally limiting because of the triple numerical integration required.

For these reasons, the method of cumulants is employed in this thesis. Moments are calculated directly from data so distribution shapes do not need to be assumed. Cumulant arithmetic greatly simplifies the addition of random variables, making computationally intensive convolution unnecessary. Theoretically, an infinite number of cumulants could be calculated to perfectly represent the data but only 4 or 5 were found to be practical. This is because of the methods of reconstructing a probability density function from a set of moments. Gram-Charlier expansion is not always

positive definite using higher order moments and the maximum entropy method has serious computational issues using anything more than about 4 moments.

The results of the first case study showed that the time series/probabilistic model provided a more accurate estimate of the temporal resolution error than the fully probabilistic model for systems with battery backup. This was an indication of the significance of accounting for synoptic and diurnal trends which the fully probabilistic model ignore. Neither model produced reliable results for systems with diesel backup. This appeared to be caused by the PDF reconstruction methods which were limited by the number of moments that could be included for computational reasons. They tended to underestimate the probabilities at the tail ends and overestimate the probabilities of small net loads which increased the calculated fuel consumption.

It is worth noting that the single household load is quite horrible for diesel genset operation. Multiple residences would smooth out the load profile, reduce fuel consumption per residence, and possibly improve the results from the probabilistic models. Also, if a lifetime degradation model of the diesel genset was available, the minimum run time constraint could be replaced with the alternative of having the genset turn on and shut down as necessary but with additional wear to the genset. For this type of load, the genset would need to be replaced sooner but would likely reduce fuel consumption enough to lower the total system cost.

The case study of the aquaculture site provided confirmation of the general results from the first case study. Again, the time series/probabilistic model produced a more accurate estimate of the temporal resolution error for the system with battery backup. The study resulted in a recommendation for the overall system design which included 15 PV modules each with a 175 W rated power output and 16 batteries with 370 Ah capacity each. The total NPC was estimated to be just under $28,000 over 25 years.

6.1 Future Work

A few key areas were identified for possible future work in order to further develop the probabilistic models into more effective tools. In this thesis the probabilistic models were run by calculating the moments from high resolution data. Since system designers often have access to data with only 1-hour resolution, the ideal tool would be able to estimate the temporal resolution error caused by ignoring higher resolution effects without actually requiring the higher resolution data. In order to make this possible, there needs to be improvements made towards developing more accurate PDF

shapes or data synthesis methods. Additionally, to be able to accurately estimate the required battery capacity, the fully probabilistic model must account for synoptic and diurnal trends. Likely, this could be accomplished by including some form of autocorrelation in the model but determining how to accomplish this is left for future work.

Morales *et al.* [66] characterized high resolution wind data by higher-order one-point and two-point statistics. It was concluded that higher-order statistics are required to properly represent the PDF, in particular to account for the probability of higher speeds and gusts. Further work in this direction will help discover a better overall representation of a generalized wind regime. Additionally, two-point statistics might be useful to account for autocorrelation in the fully probabilistic model. It is recommended that they are investigated further for the possibility of extending their application in order to model long-term trends such as synoptic and diurnal variations.

Finally, there is an opportunity to implement the method of cumulants in current time series/probabilistic models such as Hybrid2. Doing so would allow for the inclusion of a high resolution solar power distribution and would also allow higher-order moments to be accounted for, removing the assumption of Gaussianity.

Bibliography

[1] P. Fox-Penner, *Smart Power: Climate Change, the Smart Grid, and the Future of Electric Utilities*. Washington DC: Island Press, 2010.

[2] "Rationale for new ground-mounted microfit and fit program price category," tech. rep., Ontario Power Authority, July 2010.

[3] "HOMER." HOMER Energy. `http://www.homerenergy.com/`.

[4] T. Lambert, P. Gilman, and P. Lilienthal, "Micropower system modeling with HOMER," in *Integration of Alternative Sources of Energy* (F. A. Farret and M. G. Simões, eds.), ch. 15, pp. 379–418, Hoboken, New Jersey: Wiley, 2006.

[5] G. Bekele and B. Palm, "Feasibility study for a standalone solar-wind-based hybrid energy system for application in Ethiopia," *Applied Energy*, vol. 87, pp. 487–495, 2010.

[6] P. Balamurugan, S. Ashok, and T. L. Jose, "Optimal operation of biomass/wind/PV hybrid energy system for rural areas," *International Journal of Green Energy*, vol. 6, pp. 104–116, 2009.

[7] G. J. Dalton, D. A. Lockington, and T. E. Baldock, "Feasibility analysis of renewable energy supply options for a grid-connected large hotel," *Renewable Energy*, vol. 34, pp. 955–964, 2009.

[8] S. M. Shaahid and I. El-Amin, "Techno-economic evaluation of off-grid hybrid photovoltaic-diesel-battery power systems for rural electrification in Saudi Arabia - A way forward for sustainable development," *Renewable and Sustainable Energy Reviews*, vol. 13, pp. 625–633, 2009.

[9] Y. Himri, A. B. Stambouli, B. Draoui, and S. Himri, "Techno-economical study of hybrid power system for a remote village in Algeria," *Energy*, vol. 33, pp. 1128–1136, 2008.

[10] J. A. Razak, K. Sopian, M. Y. Y. Ali, M. A. Alghoul, and A. Zaharim, "Optimization of renewable energy hybrid system," in *8th WSEAS International Conference on Power Systems*, 2008.

[11] S. M. Shaahid and M. A. Elhadidy, "Technical and economic assessment of grid-independent hybrid photovoltaic-diesel-battery power systems for commercial loads in desert environments," *Renewable and Sustainable Energy Reviews*, vol. 11, pp. 1794–1810, 2007.

[12] M. J. Khan and M. T. Iqbal, "Pre-feasibility study of stand-alone hybrid energy systems for applications in Newfoundland," *Renewable Energy*, vol. 30, pp. 835–854, 2005.

[13] K. Wild, "Coupled operation of a wind farm and pumped storage facility: Techno-economic modelling and stochastic optimization," Master's thesis, University of Victoria, 2011.

[14] T. A. Niet, "Modelling renewable energy at race rocks," Master's thesis, University of Victoria, 2001.

[15] A. Gupta, R. Saini, and M. Sharma, "Steady-state modelling of hybrid energy system for off grid electrification of cluster of villages," *Renewable Energy*, vol. 35, pp. 520–535, 2010.

[16] J. P. Barton and D. G. Infield, "A probabilistic method for calculating the usefulness of a store with finite energy capacity for smoothing electricity generation from wind and solar power," *Journal of Power Sources*, vol. 162, pp. 943–948, 2006.

[17] A. Gassner, "Sizing storage and wind generation capacities in remote power systems," Master's thesis, University of Victoria, 2010.

[18] G. Tina, S. Gagliano, and S. Raiti, "Hybrid solar/wind power system probabilistic modelling for long-term performance assessment," *Solar Energy*, vol. 80, pp. 578–588, 2006.

[19] J. F. Manwell, A. Rogers, G. Hayman, C. T. Avelar, J. G. McGowan, U. Abdulwahid, and K. Wu, *HYBRID2- A Hybrid System Simulation Model: Theory Manual*. Renewable Energy Research Laboratory, 2006.

[20] G. Notton, M. Muselli, P. Poggi, and A. Louche, "Autonomous photovoltaic systems: Influences of some parameters on the sizing: Simulation timestep, input and output power profile," *Renewable Energy*, vol. 7, no. 4, pp. 353–369, 1996.

[21] G. Ambrosone, S. Catalanotti, U. Coscia, and G. Troise, "Comparison between power and energy methods of analyses of photovoltaic plants," *Solar Energy*, vol. 34, no. 1, pp. 1–8, 1985.

[22] A. Hawkes and M. Leach, "Impacts of temporal precision in optimisation modelling of micro-Combined Heat and Power," *Energy*, vol. 30, pp. 1759–1779, 2005.

[23] S. Diaf, G. Notton, M. Belhamel, M. Haddadi, and A. Louche, "Design and techno-economical optimization for hybrid PV/wind system under various meteorological conditions," *Applied Energy*, vol. 85, pp. 968–987, 2008.

[24] D. B. Nelson, M. H. Nehrir, and C. Wang, "Unit sizing and cost analysis of stand-alone hybrid wind/PV/fuel cell power generation systems," *Renewable Energy*, vol. 31, pp. 1641–1656, 2006.

[25] M. A. Elhadidy, "Performance evaluation of hybrid (wind/solar/diesel) power systems," *Renewable Energy*, vol. 26, pp. 401–413, 2002.

[26] M. Muselli, G. Notton, and A. Louche, "Design of hybrid-photovoltaic power generator, with optimization of energy management," *Solar Energy*, vol. 65, no. 3, pp. 143–157, 1999.

[27] H. G. Beyer and C. Langer, "A method for the identification of configurations of PV/wind hybrid systems for the reliable supply of small loads," *Solar Energy*, vol. 57, no. 5, pp. 381–391, 1996.

[28] M. H. Nehrir, B. J. LaMeres, G. Venkataramanan, V. Gerez, and L. A. Alvarado, "An approach to evaluate the general performance of stand-alone wind/photovoltaic generating systems," *IEEE Transactions on Energy Conversion*, vol. 15, no. 4, pp. 433–439, 2000.

[29] E. J. Hoevenaars and C. A. Crawford, "Implications of temporal resolution for modeling renewables-based power systems," *Renewable Energy*, vol. 41, pp. 285–293, 2012.

[30] E. Hoevenaars and C. Crawford, "Renewable energy feasibility and optimization at an aquaculture site," in *CSME Forum 2010*, (Victoria, Canada), June 2010.

[31] O. Ekren and B. Y. Ekren, "Size optimization of a PV/wind hybrid energy conversion system with battery storage using simulated annealing," *Applied Energy*, vol. 87, pp. 592–598, 2010.

[32] R. Dufo-López and J. L. Bernal-Agustín, "Multi-objective design of PV- wind-diesel- hydrogen- battery systems," *Renewable Energy*, vol. 33, pp. 2559–2572, 2008.

[33] H. Yang, W. Zhou, L. Lu, and Z. Fang, "Optimal sizing method for stand-alone hybrid solar-wind system with LPSP technology by using genetic algorithm," *Solar Energy*, vol. 82, pp. 354–367, 2008.

[34] R. Chedid and Y. Saliba, "Optimization and control of autonomous renewable energy systems," *International Journal of Energy Research*, vol. 20, pp. 609–624, 1996.

[35] B. S. Borowy and Z. M. Salameh, "Methodology for optimally sizing the combination of a battery bank and PV array in a wind/PV hybrid system," *IEEE Transactions on Energy Conversion*, vol. 11, no. 2, pp. 367–375, 1996.

[36] M. Deshmukh and S. Deshmukh, "Modeling of hybrid renewable energy systems," *Renewable and Sustainable Energy Reviews*, vol. 12, pp. 235–249, 2008.

[37] "IEC 61400-12-1 ed.1: Wind turbines - part 12-1: Power performance measurements of electricity producing wind turbines," 2005.

[38] S. McIntosh, *Wind Energy for the Built Environment*. PhD thesis, University of Cambridge, 2009.

[39] E. Muljadi, K. Pierce, and P. Migliore, "Control strategy for variable-speed stall-regulated wind turbines," in *American Controls Conference*, (Philadelphia, PA), National Renewable Energy Laboratory, June 1998.

[40] O. Perpiñan, E. Lorenzo, and M. A. Castro, "On the calculation of energy produced by a PV grid-connected system," *Progress in Photovoltaics: Research and Applications*, vol. 15, pp. 265–274, 2007.

[41] R. A. Gansler, S. A. Klein, and W. A. Beckman, "Investigation of minute solar radiation data," *Solar Energy*, vol. 55, no. 1, pp. 21–27, 1995.

[42] D. T. Reindl, W. A. Beckman, and J. A. Duffie, "Evaluation of hourly tilted surface radiation models," *Solar Energy*, vol. 45, no. 1, pp. 9–17, 1990.

[43] J. A. Duffie and W. A. Beckman, *Solar Engineering of Thermal Processes*. Hoboken, New Jersey: Wiley, 3rd ed., 2006.

[44] D. G. Erbs, S. A. Klein, and J. A. Duffie, "Estimation of the diffuse radiation fraction for hourly, daily and monthly-average global radiation," *Solar Energy*, vol. 28, pp. 293–302, 1982.

[45] G. Vijayakumar, M. Kummert, S. A. Klein, and W. A. Beckman, "Analysis of short-term solar radiation data," *Solar Energy*, vol. 79, pp. 495–504, 2005.

[46] R. Perez, P. Ineichen, R. Seals, J. Michalsky, and R. Stewart, "Modeling daylight availability and irradiance components from direct and global irradiance," *Solar Energy*, vol. 44, no. 5, pp. 271–289, 1990.

[47] J. F. Manwell and J. G. McGowan, "Lead acid battery storage model for hybrid energy systems," *Solar Energy*, vol. 50, no. 5, pp. 399–405, 1993.

[48] J. G. McGowan and J. F. Manwell, "Wind/diesel energy systems: Review of design options and recent developments," *Solar Energy*, vol. 41, pp. 561–575, 1988.

[49] D. G. Infield, G. W. Slack, N. H. Lipman, and P. J. Musgrove, "Review of wind/diesel strategies," *IEE Proceedings*, vol. 130, no. 9, pp. 613–619, 1983.

[50] A. G. Bhave, "Hybrid solar-wind domestic power generating system - a case study," *Renewable Energy*, vol. 17, pp. 355–358, 1999.

[51] R. Dufo-López and J. L. Bernal-Agustín, "Design and control strategies of PV-diesel systems using genetic algorithms," *Solar Energy*, vol. 79, pp. 33–46, 2005.

[52] E. L. Petersen, N. G. Mortensen, L. Landberg, J. Højstrup, and H. P. Frank, "Wind power meteorology. Part I: Climate and turbulence," *Wind Energy*, vol. 1, pp. 2–22, 1998.

[53] J. Mann, "Wind field simulation," *Probabilistic Engineering Mechanics*, vol. 13, no. 4, pp. 269–282, 1998.

[54] E. Branlard, "Generation of wind time series from the Kaimal spectrum," tech. rep., National Laboratory for Sustainable Energy, 2010.

[55] "GridLAB-D." `http://www.gridlabd.org/`.

[56] I. Van der Hoven, "Power spectrum of horizontal wind speed in the frequency range from 0.0007 to 900 cycles per hour," *Journal of Meteorology*, vol. 14, pp. 160–164, 1957.

[57] T. Barton, D. Sharpe, N. Jenkins, and E. Bossanyi, *Wind Energy Handbook*. Wiley, 2001.

[58] "Solar radiation research laboratory," May 2011. `http://www.nrel.gov/midc/srrl_bms/`.

[59] C. A. Crawford, *Advanced Engineering Models for Wind Turbines with Application to the Design of a Coning Rotor Concept*. PhD thesis, University of Cambridge, 2006.

[60] F. M. White, *Fluid Mechanics*. McGraw-Hill, 6th ed., 2008.

[61] C. D. Barley and C. B. Winn, "Optimal dispatch strategy in remote hybrid power systems," *Solar Energy*, vol. 58, no. 4-6, pp. 165–179, 1996.

[62] R. Edwards, J.-F. Larivé, V. Mahieu, and P. Rouveirolles, "Well-to-wheels analysis of future automotive fuels and powertrains in the European context," Tech. Rep. 3, EUCAR, CONCAWE, JRC/IES, 2008.

[63] L. Neij, "Cost dynamics of wind power," *Energy*, vol. 24, pp. 375–389, 1999.

[64] L. L. Bucciarelli Jr., "Estimating loss-of-power probabilities of stand-alone photovoltaic solar energy systems," *Solar Energy*, vol. 32, no. 2, pp. 205–209, 1984.

[65] A. D. Bagul, Z. M. Salameh, and B. Borowy, "Sizing of a stand-alone hybrid wind-photovoltaic system using a three-event probability density approximation," *Solar Energy*, vol. 56, no. 4, pp. 323–335, 1996.

[66] A. Morales, M. Wächter, and J. Peinke, "Characterization of wind turbulence by higher-order statistics," *Wind Energy*, 2011.

[67] J. Tovar, F. J. Olmo, and L. Alados-Arboledas, "One-minute global irradiance probability density distributions conditioned to the optical air mass," *Solar Energy*, vol. 62, no. 6, pp. 387–393, 1998.

[68] J. Tovar, F. J. Olmo, F. J. Batlles, and L. Alados-Arboledas, "Dependence of one-minute global irradiance probability density distributions on hourly irradiation," *Energy*, vol. 26, pp. 659–668, 2001.

[69] K. G. T. Hollands and R. G. Huget, "A probability density function for the clearness index, with applications," *Solar Energy*, vol. 30, no. 3, pp. 195–209, 1983.

[70] P. J. Smith, "A recursive formulation of the old problem of obtaining moments from cumulants and vice versa," *The American Statistician*, vol. 49, no. 2, pp. 217–218, 1995.

[71] P. Zhang and S. T. Lee, "Probabilistic load flow computation using the method of combined cumulants and Gram-Charlier expansion," *IEEE Transactions on Power Systems*, vol. 19, no. 1, pp. 676–682, 2004.

[72] A. Stuart and J. K. Ord, *Kendall's Advanced Theory of Statistics, Volume 1: Distribution Theory*. Arnold, 6th ed., 1994.

[73] D. E. Barton and K. E. Dennis, "The conditions under which Gram-Charlier and Edgeworth curves are positive definite and unimodal," *Biometrika*, vol. 39, no. 3/4, pp. 425–427, 1952.

[74] N. van Erp and P. van Gelder, "Introducing entropy distributions," in *Proceedings of the 6th International Probabilistic Workshop*, (Darmstadt), 2008.

[75] M. Rockinger and E. Jondeau, "Entropy densities with an application to autoregressive conditional skewness and kurtosis," *Journal of Econometrics*, vol. 106, pp. 119–142, 2002.

[76] Y. Li, V. G. Agelidis, and Y. Shrivastava, "Wind-solar resource complementarity and its combined correlation with electricity load demand," in *Industrial Electronics and Applications, 2009 (ICIEA 2009)*, (Xi'an), pp. 3623–3628, May 2009.

[77] "The state of world fisheries and aquaculture," tech. rep., Food and Agriculture Organization of the United Nations, Rome, 2010.

[78] M. Allsopp, P. Johnston, and D. Santillo, "Challenging the aquaculture industry on sustainability," tech. rep., Greenpeace, March 2008.

[79] N. Pelletier, P. Tyedmers, U. Sonesson, A. Scholz, F. Ziegler, A. Flysjo, S. Kruse, B. Cancino, and H. Silverman, "Not all salmon are created equal: Life Cycle Assessment (LCA) of global salmon farming systems," *Environmental Science and Technology*, vol. 43, pp. 8730–8736, 2009.

[80] T. Chopin, A. H. Buschmann, C. Halling, M. Troell, N. Kautsky, A. Neori, G. P. Kraemer, J. A. Zertuche-González, C. Yarish, and C. Neefus, "Integrating seaweeds into marine aquaculture systems: A key toward sustainability," *Journal of Phycology*, vol. 37, pp. 975–986, 2001.

[81] A. M. Nobre, D. Robertson-Andersson, A. Neori, and K. Sankar, "Ecological-economic assessment of aquaculture options: Comparison between abalone monoculture and integrated multi-trophic aquaculture of abalone and seaweeds," *Aquaculture*, vol. 306, pp. 116–126, 2010.

[82] S. Mathew, *Wind Energy: Fundamentals, Resource Analysis and Economics*. Springer, 2006.

[83] "Surface meteorology and solar energy," May 2011. NASA Atmospheric Science Data Center. `http://eosweb.larc.nasa.gov/sse/`.

[84] J. C. Kaimal, J. C. Wyngaard, Y. Izumi, and O. R. Coté, "Spectral characteristics of surface-layer turbulence," *Quarterly Journal of the Royal Meteorological Society*, vol. 98, pp. 563–589, 1972.

Appendix A

Photovoltaic Model Calculations

The tilted surface model and cell temperature calculation are described here. The methodologies for both were taken from HOMER [4].

A.1 Tilted Surface Model

Given the radiation on a horizontal surface, the calculation of the radiation on a tilted surface requires information on the location of the sun in the sky relative to the PV array, the orientation of the PV surface, and an estimate of the fraction of radiation that is diffuse. The general procedure is obtained from Duffie and Beckman [43].

The solar declination angle is:

$$\delta = 23.45^\circ \sin\left(360^\circ \frac{284+n}{365}\right) \tag{A.1}$$

where n is the day of the year, starting at 1 for January 1st.

The location of the sun depends on the time of day. For these calculations, the solar time, t_s, is of interest:

$$t_s = t_c + \frac{\text{Long.}}{15} - Z + E(n) \tag{A.2}$$

$$\begin{aligned} E(n) = \quad 3.82 \quad & (0.000075 + 0.001868\cos B - 0.032077\sin B \\ & -0.014615\cos 2B - 0.04089\sin 2B) \end{aligned} \tag{A.3}$$

$$B = 360^\circ \frac{n-1}{365} \tag{A.4}$$

where t_c is the civil time, Z is the time zone in hours east of GMT, and E is the equation of time which accounts for the obliquity and eccentricity of the earth's orbit. The sun moves across the sky at 15° per hour. The hour angle, ω, is defined such that it is negative before solar noon, zero at solar noon, and positive after solar noon:

$$\omega = (t_s - 12) \cdot 15 \tag{A.5}$$

The angle of incidence, θ, is the angle between the sun's beam radiation and the normal of the PV surface:

$$\begin{aligned} \cos\theta &= \sin\delta\sin(\text{Lat.})\cos\beta - \sin\delta\cos(\text{Lat.})\sin\beta\cos\gamma \\ &\quad + \cos\delta\cos(\text{Lat.})\cos\beta\cos\omega + \cos\delta\sin(\text{Lat.})\sin\beta\cos\gamma\cos\omega \\ &\quad + \cos\delta\sin\beta\sin\gamma\sin\omega \end{aligned} \tag{A.6}$$

where β is the slope of the PV surface, γ is the azimuth angle, and Lat. is the latitude. By setting $\beta = 0$ in the above equation, the zenith angle is calculated:

$$\cos\theta_z = \cos(\text{Lat.})\cos\delta\cos\omega + \sin(\text{Lat.})\sin\delta \tag{A.7}$$

The amount of radiation striking the top of the earth's atmosphere perpendicular to the sun's rays is called the extraterrestrial normal radiation:

$$G_{on} = G_{sc}\left(1 + 0.033\cos\frac{360n}{365}\right) \tag{A.8}$$

where G_{sc} is the solar constant (1.367 kW/m^2). The extraterrestrial horizontal radiation is the radiation striking a horizontal surface at the top of the atmosphere:

$$G_o = G_{on}\cos\theta_z \tag{A.9}$$

The average extraterrestrial horizontal radiation over a time step is found by integrating this equation over the time step:

$$\overline{G}_o = \frac{12}{\pi}G_{on}\left[\cos(\text{Lat.})\cos\delta(\sin\omega_2 - \sin\omega_1) + \frac{\pi(\omega_2 - \omega_1)}{180}\sin(\text{Lat.})\sin\delta\right] \tag{A.10}$$

where ω_1 and ω_2 are the hour angles at the beginning and end of the time step, respectively. The sunset hour angle, ω_{ss}, is found from Equation A.7 by solving for

ω when $\theta_z = 90°$. Then the sunrise hour angle is $\omega_{sr} = -\omega_{ss}$. If a time step includes sunrise or sunset, then ω_1 or ω_2 are adjusted to ω_{sr} or ω_{ss} as necessary in Equation A.10.

The clearness index is defined as the ratio of the measured horizontal radiation on the earth's surface to the extraterrestrial horizontal radiation:

$$k_T = \frac{G}{\overline{G}_o} \tag{A.11}$$

The correlation from Erbs *et al.* [44] is used to define the diffuse fraction of the measured radiation. The empirical regression gives the diffuse fraction as a function of the clearness index:

$$\frac{G_d}{G} = \begin{cases} 1.0 - 0.09k_T & : k_T \leq 0.22 \\ 0.9511 - 0.1604k_T + 4.388k_T^2 - 16.638k_T^3 + 12.336k_T^4 & : 0.22 < k_T \leq 0.80 \\ 0.165 & : k_T > 0.80 \end{cases} \tag{A.12}$$

The remaining radiation is then assumed to be beam radiation:

$$G_b = G - G_d \tag{A.13}$$

In some cases, k_T can be greater than unity. This can be caused by cloud reflection but generally only occurs in time steps that include sunrise or sunset because the theoretical extraterrestrial horizontal radiation is very small. Therefore, even a small amount of measured radiation can be many times greater than the extraterrestrial radiation. To prevent erroneous calculations in subsequent steps, the radiation is assumed to be all diffuse if k_T is calculated to be greater than unity.

Three more terms are defined as part of the HDKR tilted surface model developed by Reindl *et al.* [42]. The ratio of beam radiation on the tilted surface to beam radiation on the horizontal surface is:

$$R_b = \frac{\cos\theta}{\cos\theta_z} \tag{A.14}$$

In order to estimate the amount of circumsolar diffuse radiation, the anisotropy index is defined as a measure of the atmospheric transmittance of beam radiation:

$$A_i = \frac{G_b}{G_o} \tag{A.15}$$

A final term is introduced to account for horizon brightening:

$$f = \sqrt{\frac{G_b}{G}} \tag{A.16}$$

Finally, the total radiation on the tilted surface is:

$$G_T = (G_b + G_d A_i) R_b + G_d (1 - A_i) \left(\frac{1 + \cos\beta}{2} \right) \left[1 + f \sin^3 \left(\frac{\beta}{2} \right) \right] + G \rho_g \left(\frac{1 - \cos\beta}{2} \right) \tag{A.17}$$

where ρ_g is the ground reflectance or albedo.

A.2 Cell Temperature Calculation

An energy balance of the array of PV cells shows that the absorbed solar energy must be equal to the sum of the output electricity and the heat transfer to the surroundings [43]:

$$\tau \alpha G_T = \eta_c G_T + U_L (T_c - T_a) \tag{A.18}$$

where τ is the solar transmittance of the PV cover (%), α is the solar absorptance of the PV cells (%), G_T is the total solar radiation on the PV surface (kW/m^2), η_c is the cell efficiency, U_L is the coefficient of heat transfer to the surroundings (kW/m$^{2\circ}$C), T_c is the cell temperature (°C), and T_a is the ambient temperature (°C). Solving for the cell temperature:

$$T_c = T_a + G_T \left(\frac{\tau \alpha}{U_L} \right) \left(1 - \frac{\eta_c}{\tau \alpha} \right) \tag{A.19}$$

Measuring $(\tau\alpha/U_L)$ is difficult so manufacturers report the nominal operating cell temperature (NOCT), which is the cell temperature measured with an incident radiation of 0.8 kW/m^2, an ambient temperature of 20°C, and no load operation (i.e. $\eta_c = 0$). Therefore, from Equation A.18:

$$\frac{\tau \alpha}{U_L} = \frac{T_{c,NOCT} - T_{a,NOCT}}{G_{T,NOCT}} \tag{A.20}$$

Since it is assumed that a maximum power point tracker is always included, the cell efficiency is assumed to be equal to the efficiency at the maximum power point. However, this efficiency depends on the cell temperature. The relationship is assumed to be linear with a slope defined by the temperature coefficient of power specified by

the manufacturer. Therefore:

$$\eta_c = \eta_{PV}[1 + \alpha_P(T_c - T_{c,STC})] \tag{A.21}$$

where η_{PV} is the cell efficiency under standard test conditions, α_P is the temperature coefficient of power (%/°C) and is typically negative, and $T_{c,STC}$ is the cell temperature under standard test conditions (25°C). Substituting Equations A.20 and A.21 into Equation A.19:

$$T_c = \frac{T_a + (T_{c,NOCT} - T_{a,NOCT})\left(\frac{G_T}{G_{T,NOCT}}\right)\left[1 - \frac{\eta_{PV}(1-\alpha_P T_{c,STC})}{\tau\alpha}\right]}{1 + (T_{c,NOCT} - T_{a,NOCT}\left(\frac{G_T}{G_{T,NOCT}}\right)\left(\frac{\alpha_P \eta_{PV}}{\tau\alpha}\right)} \tag{A.22}$$

where $\tau\alpha$ is assumed to be 0.9. Note that a time-accurate thermal model of the PV panel would improve the accuracy for short time step simulations.

Appendix B

Net Present Cost Calculation

The NPC calculation is based on that in HOMER [4]. Two factors are used to convert cash flows. The capital recovery factor (CRF) is the ratio of a constant annuity over N years to its present value:

$$\mathrm{CRF}(i, N) = \frac{i(1+i)^N}{(1+i)^N - 1} \tag{B.1}$$

The sinking fund factor (SFF) is the ratio of a constant annuity to its future value:

$$\mathrm{SFF}(i, N) = \frac{i}{(1+i)^N - 1} \tag{B.2}$$

In these equations, i is the real interest rate which is used so that the terms can all be defined in constant dollars. It can be calculated by:

$$i = \frac{i' - f}{1+f} \tag{B.3}$$

where i' is the nominal interest rate and f is the annual inflation rate.

Therefore, the NPC is calculated by:

$$\mathrm{NPC} = \frac{C_{ann,tot}}{\mathrm{CRF}(i, N_{proj})} \tag{B.4}$$

where $C_{ann,tot}$ is the sum of all annualized costs including capital, replacement, operation, maintenance, and fuel.

For each component, the annualized capital cost is simply:

$$C_{ann,cap} = C_{cap} \times \mathrm{CRF}(i, N_{proj}) \tag{B.5}$$

where C_{cap} is the capital cost of the component.

The annualized replacement cost accounts for the cost of replacing components throughout the project as well as the revenue from salvage value at the end of the project. The salvage value is assumed to be proportional to its remaining life. The annualized replacement cost is:

$$C_{ann,repl} = C_{repl} f_{repl} \times \mathrm{SFF}(i, N_{comp}) - S \times \mathrm{SFF}(i, N_{proj}) \tag{B.6}$$

where C_{repl} is the component replacement cost, S is the salvage value, N_{comp} is the component lifetime, and f_{repl} is an additional factor accounting for the fact that the final replacement might not be at the end of the project lifetime. It is calculated by:

$$f_{repl} = \frac{\mathrm{CRF}(i, N_{proj})}{\mathrm{CRF}(i, N_{repl})} \tag{B.7}$$

Here N_{repl} is the total time until the last replacement:

$$N_{repl} = N_{comp} \left\lfloor \frac{N_{proj}}{N_{comp}} \right\rfloor \tag{B.8}$$

where $\lfloor \rfloor$ represents the "floor" function.

Appendix C

Wind Speed Data Synthesis

The method used for data synthesis in this thesis was based on the first approach by Branlard [54]. The Kaimal spectrum is used to approximate the wind spectrum since it provides a good empirical description of the observed spectra in the atmosphere [52]. In this method, the expression of the Kaimal spectrum is [54]:

$$S(\omega) = u_*^2 \frac{52.5z/U}{(1 + 33\omega z/U)^{5/3}} \tag{C.1}$$

where $S_u(\omega)$ is the autospectral density of the horizontal wind speed in the direction of the mean velocity, ω is the frequency (rad/s), u_* is the friction velocity (m/s), z is the height (m), and U is the mean wind speed (m/s). This definition of the Kaimal spectrum is slightly different than the more widely used definition that uses the frequency f, in Hz, in place of ω [84]. Though different, the -5/3 slope at high frequencies on a log-log plot is conserved.

Since a digitized time series signal of wind speeds is desired, a set of Fourier coefficients equal in length is required. The above spectrum represents the contribution to the total variance in wind speeds of each frequency component. The total variance of the signal is distributed amongst the Fourier coefficients by:

$$\sigma_{X_\omega}^2 = \frac{T}{2\pi} S_u(\omega) \tag{C.2}$$

where X_ω are the Fourier coefficients, $\sigma_{X_\omega}^2$ is the variance associated with the Fourier coefficient for a particular frequency, $T = N/f_s$ is the total length of time of the desired time series output with f_s being the sampling frequency, and N is the total number of data points. The 2π in the denominator is a scale factor since the Fourier

coefficients correspond to frequency bands in Hz rather than rad/s.

For synthesizing a random time series from the power spectrum, each of the N individual coefficients X_ω is selected from a normal distribution with mean 0 and standard deviation σ_{X_ω}. Since only the real parts of the Fourier coefficients are specified, the frequency components are all in phase. However, since the random amplitudes have a zero mean, they can add or cancel at random. The result is similar to what would be obtained if the phase of each frequency component was randomly varied.

The first Fourier coefficient (i.e. the DC component) is set equal to $TU/2\pi$. Finally, the time series is synthesized using Matlab's *ifft* function:

$$x(t) = 2\pi f_s \,\mathrm{ifft}(X) \tag{C.3}$$

Again, the output is scaled by 2π since the Fourier coeffients were defined from $S(\omega)$ instead of $S(f)$. Because the random Fourier coefficients are not conjugate symmetric, the output time series is complex and the imaginary part should be discarded.

Analyzing the above method, it appears unnecessary to define the spectrum as $S(\omega)$ instead of $S(f)$. In doing so, the original spectrum was altered since f was simply replaced by ω without accounting for the relationship $\omega = 2\pi f$.

To ensure that this method was acceptable, it was necessary to compare the total variance of the output time series with the output using the more widely accepted spectrum where ω is replaced by f in Equation C.1. For this comparison, the sample frequency was set to 1 second and the total length of the time series output was 5000 seconds. Several input parameters were varied (U = [6, 12, 18] m/s, z = [15, 30, 60] m, z_0 = [0.001, 0.01, 0.1] m) and each combination of parameters was run 100 times with each method. The ratio between the standard deviation using the Branlard method and that using the $S(f)$ spectrum was always between 0.972 and 1.062. Therefore, the method from Branlard was considered acceptable since the variance of the time series output, and subsequently the turbulence intensity, was very similar.

Appendix D

Case Study Results Tables

The results comparing a 1-hour time step with time steps shorter than 10 minutes are provided here for the off-grid residential power system case study.

D.1 Battery Backup

Table D.1: Battery capacity error (kWh), $E_{b,1\text{hr}} - E_{b,1\text{min}}$

Config.	FTS	STS	TSP	PGC	PME
0S-3W	38.8	34.2	38.7	-5.7	-15.4
20S-3W	16.6	15.2	20.8	-5.7	-13.9
20S-2W	57.0	50.5	54.2	-8.9	-14.4
40S-2W	11.5	9.4	13.6	-7.4	-10.8
60S-2W	8.8	8.4	11.8	-6.5	-9.6
60S-1W	12.2	11.5	11.1	-11.0	-13.3
80S-1W	10.4	9.1	7.8	-8.9	-11.6
100S-1W	1.7	2.2	4.6	-8.0	-10.6
100S-0W	-13.8	-10.4	-4.3	-16.3	-21.6
120S-0W	-2.1	-0.0	-1.5	-13.1	-17.4

S - 0.175kW solar module, W - 4.5kW wind turbine

Table D.2: Battery capacity error (kWh), $E_{b,1\text{hr}} - E_{b,10\text{sec}}$

Config.	FTS	STS	TSP	PGC	PME
0S-3W	37.7	33.3	36.9	-6.2	-15.8
20S-3W	16.9	15.2	20.1	-5.9	-14.1
20S-2W	54.0	48.5	51.7	-9.3	-14.7
40S-2W	11.7	9.4	13.1	-7.6	-10.9
60S-2W	9.1	8.4	11.4	-6.6	-9.8
60S-1W	12.2	11.5	10.7	-11.2	-13.5
80S-1W	10.4	9.2	7.5	-9.0	-11.7
100S-1W	1.7	2.2	4.4	-8.1	-10.6
100S-0W	-13.9	-10.5	-4.3	-16.3	-21.6
120S-0W	-2.1	-0.0	-1.5	-13.1	-17.4

S - 0.175kW solar module, W - 4.5kW wind turbine

Table D.3: Battery capacity error (kWh), $E_{b,1\text{hr}} - E_{b,1\text{sec}}$

Config.	FTS	STS	TSP	PGC	PME
0S-3W	38.6	34.7	37.1	-6.3	-9.2
20S-3W	16.9	15.5	20.3	-6.0	-14.2
20S-2W	56.0	51.6	52.0	-9.4	-14.8
40S-2W	11.8	9.6	13.3	-7.7	-11.0
60S-2W	9.1	8.6	11.5	-6.7	-9.8
60S-1W	12.6	12.0	10.9	-11.2	-13.6
80S-1W	10.6	9.2	7.6	-9.0	-11.7
100S-1W	1.8	2.3	4.5	-8.1	-10.7
100S-0W	-13.9	-10.5	-4.3	-16.3	-21.6
120S-0W	-2.1	-0.0	-1.5	-13.1	-17.4

S - 0.175kW solar module, W - 4.5kW wind turbine

D.2 Diesel Backup

Table D.4: Fuel consumption error (kL), $V_{f,1\text{hr}} - V_{f,1\text{min}}$

Config.	FTS	STS	TSP	PGC	PME
0S-2W	-6.1	-6.2	-25.1	-13.1	-11.9
20S-2W	-4.8	-5.0	-26.1	-13.4	-12.2
40S-2W	-4.5	-4.5	-26.3	-14.4	-13.2
40S-1W	-5.2	-5.3	-25.7	-11.9	-15.3
40S-0W	-7.3	-7.3	-24.0	-10.9	-15.1
60S-0W	-6.7	-6.7	-24.2	-13.1	-13.2

S - 0.175kW solar module, W - 4.5kW wind turbine

Table D.5: Fuel consumption error (kL), $V_{f,1\text{hr}} - V_{f,10\text{sec}}$

Config.	FTS	STS	TSP	PGC	PME
0S-2W	-7.1	-7.1	-25.7	-16.1	-14.4
20S-2W	-5.6	-5.7	-26.8	-16.6	-15.0
40S-2W	-5.2	-5.2	-27.1	-17.9	-16.5
40S-1W	-6.0	-6.0	-26.4	-14.5	-17.5
40S-0W	-7.3	-7.3	-24.6	-13.1	-16.2
60S-0W	-6.7	-6.7	-24.8	-15.9	-15.6

S - 0.175kW solar module, W - 4.5kW wind turbine

Table D.6: Fuel consumption error (kL), $V_{f,1\text{hr}} - V_{f,1\text{sec}}$

Config.	FTS	STS	TSP	PGC	PME
0S-2W	-10.3	-10.3	-26.0	-17.7	-17.4
20S-2W	-8.4	-8.5	-27.1	-18.3	-18.4
40S-2W	-7.8	-7.8	-27.5	-19.8	-20.4
40S-1W	-7.9	-7.9	-26.7	-15.9	-18.0
40S-0W	-7.3	-7.3	-24.8	-14.3	-16.5
60S-0W	-6.7	-6.7	-25.0	-17.5	-18.2

S - 0.175kW solar module, W - 4.5kW wind turbine